STUDY OF CP VIOLATION AND MASS HIERARCHY SENSITIVITIES AT LONG BASELINE NEUTRINO EXPERIMENTS

By

MEHEDI MASUD

PHYS08200905007

Harish-Chandra Research Institute, Allahabad

A thesis submitted to the

Board of Studies in Physical Sciences

In partial fulfillment of requirements

for the Degree of

DOCTOR OF PHILOSOPHY

of

HOMI BHABHA NATIONAL INSTITUTE

November, 2016

STATEMENT BY AUTHOR

This dissertation has been submitted in partial fulfillment of requirements for an advanced degree at Homi Bhabha National Institute (HBNI) and is deposited in the Library to be made available to borrowers under rules of the HBNI.

Brief quotations from this dissertation are allowable without special permission, provided that accurate acknowledgement of source is made. Requests for permission for extended quotation from or reproduction of this manuscript in whole or in part may be granted by the Competent Authority of HBNI when in his or her judgment the proposed use of the material is in the interests of scholarship. In all other instances, however, permission must be obtained from the author.

Mehedi Masud

DECLARATION

I, hereby declare that the investigation presented in the thesis has been carried out by me. The work is original and has not been submitted earlier as a whole or in part for a degree / diploma at this or any other Institution / University.

Mehedi Masud

List of Publications arising from the thesis

Journal

1. "Configuring the Long-Baseline Neutrino Experiment", Vernon Barger, Atri Bhattacharya, Animesh Chatterjee, Raj Gandhi, Danny Marfatia, Mehedi Masud, *Physical Review D*, **2014**, *89*, 011302.

2. "The impact of sterile neutrinos on CP measurements at long baselines",Raj Gandhi, Boris Kayser, Mehedi Masud, Suprabh Prakash, *Journal of High Energy Physics*, **2015**, *1511*, 039.

3. "Optimal configurations of the Deep Underground Neutrino Experiment", Vernon Barger, Atri Bhattacharya, Animesh Chatterjee, Raj Gandhi, Danny Marfatia, Mehedi Masud, *International Journal of Modern Physics A*, **2016**, *31*, 1650020.

4. "Probing the CP violation signal at DUNE in the presence of non-standard neutrino interactions", Mehedi Masud, Animesh Chatterjee, Poonam Mehta, *Journal of Physics G*, **2016**, *43*, 095005.

5. "Nonstandard interactions spoiling the CP violation sensitivity at DUNE and other long baseline experiments", Mehedi Masud, Poonam Mehta, *Physical Review D*, **2016**, *94*, 013014.

6. "Nonstandard interactions and resolving the ordering of neutrino masses at DUNE and other long baseline experiments", Mehedi Masud, Poonam Mehta, *Physical Review D*, **2016**, *94*, 053007.

7. "Capabilities of long-baseline experiments in the presence of a sterile neutrino", Debajyoti Dutta, Raj Gandhi, Boris Kayser, Mehedi Masud, Suprabh Prakash, *Journal of High Energy Physics*, **2016**, *1611*, 122.

Mehedi Masud

Dedicated to

My parents

ACKNOWLEDGMENTS

It is said that writing the acknowledgement is more challenging than writing the thesis itself. Because, there is always a risk of omission which can lead to friendly misunderstandings! So, accepting my inability to remember names and instances, I would like to thank all the people I have encountered in this significant journey of my life.

First and foremost, I owe a very special gratitude to my thesis advisor Prof. Raj Gandhi who provided excellent guidance to me both academically and non-academically throughout this significant journey of my life. Apart from providing me with very interesting and important problems to work on, he has helped me improve my way of thinking, showed proper direction whenever I am stuck and also boosted my confidence in moments of frustration. I am indebted to Prof. Gandhi in a great many ways.

It gives me immense pleasure to thank my collaborators. I would like to give a very special thanks to Prof. Poonam Mehta for all the collaborative works, support and the frequent, intense and very fruitful discussions that immensely helped me in learning the nitty-gritties of neutrino physics. I will always be grateful to Dr. Atri Bhattacharya for his support and help and for the excellent and unconventional teaching of the basics of computer programming, an essential skill for working in high energy physics. I must express my deepest gratitude to Dr. Animesh Chatterjee, Dr. Suprabh Prakash and Dr. Debajyoti Dutta for providing me with helping hands whenever needed. I thank Prof. Boris Kayser, Prof. Danny Marfatia, Prof. Vernon Barger who have given their enormous support and suggestions all the time.

I would like to thank the members of my thesis committee Prof. Sandhya Choubey, Prof. Biswarup Mukhopadhyaya and Prof. Anshuman Maharana. I sincerely express my gratitude to Prof. Ashoke Sen, Prof. Tirthankar Roychowdhury, Prof. Rajesh Gopakumar, Prof. Pinaki Majumdar and Prof. Jayanta Kumar Bhattacharjee, for the excellent teaching and discussions. I am also thankful to Prof. Pomita Ghoshal, Dr. Sushant Raut, Dr. Anushree Ghosh for the long and patient discussions.

I spent a few months during my PhD at IGCAR, Kalpakkam and at VECC, Kolkata for doing experimental projects. I would like to thank Prof. K.G.M. Nair, Prof. P. Gangopadhyay, Prof. A.K. Dubey, Dr. Sachin Srivastava for the continuous help during my stay at these places.

Next, the turn for HRI, where I spent one of the most beautiful times of my life and

which thus has become a "Home away from home" for me during the past seven years. My wholehearted thanks goes to Subhroneel, Swapnamay, Atri-da, Godfather(Animesh-da), Dibya, Nilay-da, Subha-da, Gupta, Baccha (Titas), Avijit, Sauri, Arindam-da for all the intensive and enjoyable "adda"s/ gossips/ discussions and what not!, thereby making my stay at HRI a forever memorable one. Thanks Landau (Nabarun), Arijit, Shrobona, Raghunath, Dharmadas, Akansha, Mohan, Arif, Khorshed, Bedo-da (Arghya-da), Urmi-di, Debajyoti, Suprabh, Avishake-da, Shamik-da, Ipsita-di, Ramlal, Sanjoy(Dutta)-da, Biswajit, Ratul, Samrat, Juhi, Bhocha, Nyayabanta, Sandeep, Samiran, Vuru-da (Sourav), Manimala-di, JD (Joydeep-da), Mama (Arjun-da), Sanjay(Biswas)-da, Anirban (Basu)-da, Sudipto, Baby, Harshant, Namrata, Uttam, Krishna Mohan, Avishek, Jonthu-da, Avinanda-di, Soumyarup, Joyee, Sayantan, Maguni, Papon (Satadal), Siddharth, Samya-da, Sunando-da, Niyogi-da, Rana, Taushif, Hochi-da, Dhiraz-da, Shankha, Debashis, Anushree-di, Ushoshi, Samiran, Mrityunjay, Sitender, Sandeep, Ajanta, Arpita, Sushovan, Ritabrata, Sreetama, Sneh, Eshita, Anindita, Sumona, Dipyaman, Shouvik, Chiranjeeb, Anirban (Biswas)-da, Gautam, Sarif, Arpan, Pallab, Bibek, Tarat-da, Paromita-di, Abhas, Deepak, Satya-da, Fuchu (Arnab), Biswas, Upayan, Manoj-da, Jaydip, Jogesh, Sayanti, Rumu, Nandini, Panchali whom I interacted with at various times during my PhD and became friends. I also thank my very good friends Trisha, Avik and my childhood friends Abir, Aniket, Shamimah who always remained by my side during the whole time. I am also thankful to the numerous story books, the active movie club of HRI and a large set of classic rock music which kept me afloat and immensely helped me move through this sometimes difficult journey!

I am grateful to the people in the administration and technical section of HRI. In particular, I would like to mention Amit Khulve, Chandan Kanaujiya, Sanjay Verma, Archana Tandon and Ravindra Singh, the registrar of HRI.

Last but not the least, I am forever grateful to my loving parents and my sister for the patience and the support whenever I needed them.

Contents

SYNOPSIS

Neutrino physics offers the potential for insight into physics beyond the Standard Model (BSM). The first and foremost signature of nonzero neutrino mass is given by neutrino oscillations, which have by now been conclusively established by several pioneering experiments. The mixing between the three standard neutrino flavors is governed by the PMNS mixing matrix (containing the three mixing angles $\theta_{12}, \theta_{13}, \theta_{23}$ and the CP phase δ_{cp}) and the mass squared differences $\Delta m^2_{31} = m^2_3 - m^2_1$ and $\Delta m^2_{21} = m^2_2 - m^2_1$. While the first two mixing angles and the mass squared differences were determined by the solar and the atmospheric neutrino experiments, the third mixing angle θ_{13} has recently been measured by reactor experiments. The values determined by the experiments are expected to be rendered more precise by the current and the upcoming neutrino experiments.

There are however, some important questions which have not been answered. The focus of neutrino oscillation experiments has now shifted to the measurement of the phase, δ_{cp}, that determines whether or not the lepton sector violates CP. Another important question for model building purposes is whether the neutrinos are arranged in a normal hierarchy ($\Delta m^2_{31} > 0$) or inverted hierarchy ($\Delta m^2_{31} < 0$). Also, the question of whether the mixing angle θ_{23} is greater or smaller than $\pi/4$ (called the *octant degeneracy*) bears on models based on lepton symmetries. Apart from these, there are questions about whether the presence of some new physics such as sterile neutrinos or Non Standard Interaction (NSI) can substantially affect the measurements of the standard oscillation parameters.

Motivated by these open challenges, I have worked on aspects of the above questions using neutrino oscillation studies in the context of long baseline experiments. Below, I briefly summarise my work.

DUNE (or the erstwhile LBNE,- Long Baseline Neutrino Experiment), the Deep Underground Neutrino Experiment is an upcoming long baseline (1300 km) oscillation experiment (with a 35 kt liquid argon far detector) which has the potential to resolve the issues mentioned above. We compared various detector configurations of this experiment and evaluated their sensitivities to CP violation (CPV), mass hierarchy (MH) and the octant of θ_{23}. We made extensive use of the GLoBES (General Long baseline Experiment Simulator) software to simulate the various detector configurations. In particular, we compared the

scenario of a surface far detector (FD) augmented with a near detector (ND) to the case of an underground FD with no ND. In the latter case, the data from the atmospheric neutrinos was also incorporated. We have written our own C++ code to simulate the effect of the atmospheric neutrinos. We also studied the effect of adding data from currently ongoing long baseline experiments such as T2K and NOνA. We also discussed how the sensitivities depend on the precision with which θ_{13} is measured by reactor experiments (so called "θ_{13} prior"), on the detector size, beam power, exposure time and on detector magnetization.

We found that CP can be resolved to more than 5σ for a small portion of the δ_{cp} parameter space (around $\pm\pi/2$) with a 35 kt FD augmented with an ND and with (5+5) years of $(\nu + \bar{\nu})$ beam running. We have observed that the presence of a near detector is crucial as it significantly increases the sensitivity and takes it above 5σ (as mentioned). The contribution from the atmospheric neutrinos to the CP sensitivity is very small, as expected. Although the sensitivities to CP violation for other long baseline experiments such as NOvA and T2K are small on their own, they can serve in significantly improving the CPV sensitivity for DUNE and increases the portion of δ_{cp} space for which CP can be resolved above 5σ. The mass hierarchy can be resolved above 3σ for the entire δ_{cp} space with beam data alone (with the usual 35 kt FD) with just about 1 to $1\frac{1}{2}$ year of running. And with the full (5+5) years of $(\nu + \bar{\nu})$ beam runtimes, the hierarchy can be resolved well above 5σ for all δ_{cp} values. Although the information from the atmospheric neutrinos and from other long baseline experiments are not small as far as sensitivity to hierarchy is concerned, the data from beam alone is sufficient to determine hierarchy. We also found that the presence of an ND as well as the data from atmospheric neutrinos can significantly help to resolve octant degeneracy. Our eventual conclusion is that a 35 kt FD with an ND will resolve the eight-fold degeneracy that is intrinsic to long baseline experiments and will meet the primary goals of oscillation physics that it is designed for.

A major aim of the present and the future long baseline experiments is to determine whether or not oscillating neutrinos violate CP by measuring the phase δ_{cp}. Usually these experiments assume the standard paradigm with three neutrino flavors (so called 3+0 scenario). But, there is evidence (from the anomalies in LSND, MiniBooNE, GALEX, SAGE) suggesting the possibility of the existence of one (or possibly more) generation(s) of sterile neutrino(s) (of mass ~ 1 eV) which may have small mixings with the standard model neutrinos. We showed that the presence of even one such sterile neutrino (3+1 scenario)

of mass ~ 1 eV can significantly impact the measurements of CP violation (CPV) in long baseline experiment such as DUNE.

We have derived a probability expression for the appearance channel in the 3+1 paradigm in vacuum and discussed the modifications brought in by matter effects. Thus, using probability level analysis and neutrino-antineutrino asymmetry calculations, we discussed, in our work, the large magnitude of these effects, and showed how they translated into significant event rate deviations at DUNE. Our results demonstrated that measurements which, when interpreted in the context of the standard three family paradigm, indicate CP conservation at long baselines, may, in fact hide large CP violation if there is a sterile state. Similarly, any data indicating the violation of CP cannot be properly interpreted within the standard paradigm unless the presence of sterile states of mass O(1 eV) can be conclusively ruled out.

In the level of χ^2, we have observed that if one $\sim$ 1 eV sterile neutrino is indeed present, it can both potentially reduce or increase the CP sensitivity significantly (compared to the standard 3+0 sensitivity) depending upon the magnitude of the mixing angles ($\theta_{14}, \theta_{24}, \theta_{34}$). Consequently, it may so happen that the CPV sensitivity is quite high ($\sim 3\sigma$) even for the CP conserving values $(0, \pi)$. Conversely, the sensitivity might be very small even for the maximally CP violating values ($\pm\pi/2$). Our work thus underscores the need for a parallel and linked short baseline oscillation program and a highly capable near detector for DUNE, in order that its highly anticipated results on CP violation in the lepton sector may be correctly interpreted. Our paper[3] on this work has recently been published in JHEP, and has generated significant interest within the DUNE collaboration.

For long baseline experiments such as DUNE, where the baseline is $O(\sim 1000)$ km, the earth matter effects during the propagation of neutrinos is not negligible. Hence the additional CPV effects introduced by the matter complicates the extraction of the intrinsic CP phase. New physics in neutrino interactions can, in principle, allow for flavour changing interactions thereby allowing for additional CP violating effects, making the measurement of the intrinsic CP phase even more difficult. In this work, we showed that the appearance channel is significantly affected by the presence of two propagation Non-standard Interaction (NSI) parameters such as $\varepsilon_{e\mu}$ and $\varepsilon_{e\tau}$ due to the non trivial interplay between the moduli and the phases introduced by the NSI parameters.

In one more set of works we consider another new physics phenomenon-which can phenomenologically be described by Non standard Interaction (NSI) during the neutrino propagation through matter. The additional CP phases which are in general associated with the NSI parameters can complicate the extraction of the Dirac CP phase in the standard interaction (SI) scenario,-giving rise to the SI-NSI degenracy. Using probability and event level analyses, we showed the existence of NSI-SI degeneracies (similar to the case of sterile neutrinos) where it is difficult to ascribe the observed CP signal to standard (SI) or NSI scenario alone. We have illustrated this degeneracy by showing the probability and the asymmetry bands (due to variation of the associated CP phases) as a function of energy and pointing out the significantly large overlapping regions between SI and the NSI. For DUNE, which mainly looks at the $\nu_\mu \rightarrow \nu_e$ appearance channel, the most relevant NSI parameters are $\varepsilon_{e\mu}$, $\varepsilon_{e\tau}$ and to some extent ε_{ee} (The parameters $\varepsilon_{\mu\mu}$ and $\varepsilon_{\mu\tau}$ are very strongly constrained and hence have negligible effect). From the point of view of statistics, we have shown that if NSI is present (and even if we restrict ourselves very conservatively within the present global bounds on $\varepsilon_{e\mu}$, $\varepsilon_{e\tau}$, ε_{ee}) it can drastically increase or decrease the CPV sensitivity, similar to the sterile neutrino case. We have also found a clear explanation of the mechanism which increases/decreases the sensitivity in the presence of NSI. We have also illustrated how NSI can bring about a change in the choice of optimized baseline at DUNE.

Thus, in order to ascribe any result on the CP phase to the lone CP phase in the standard three neutrino paradigm, it is crucial to rule out or put stronger new constraints on new physics scenarios that can contribute to the signal.

List of Figures

List of Tables

Chapter 1

Introduction

Neutrinos are some of the most elusive Standard Model (SM) particles even though they are the most abundant particles in the universe after photon. They are neutral, interact only through the weak interaction and therefore, do not readily interact with other particles. As a result, neutrinos are particularly difficult to study. Neutrino experiments require extremely massive detectors in order to produce statistically significant results. With so little knowledge about neutrinos, neutrino experiments are integral to understanding of the weak interaction and are an important probe of new physics. Neutrino physics has now entered an exciting era in which we are in the process of getting precession measurements of neutrino masses and mixings. It also offers great potential for understanding physics beyond the standard model (BSM). A number of present and future experiments are expected to yield more precise knowledge regarding the many unresolved questions. In this chapter, we will first briefly summarize the history of neutrinos. Then, after describing the sources of neutrinos, we will talk about the phenomenology of neutrino mixing and neutrino oscillations. We will then mention the present status of the neutrino oscillations and then briefly discuss physics beyond oscillations. Finally, we describe the content of the thesis concisely.

1.1 History of neutrinos

The history of the neutrinos started with the famous letter by Wolfgang Pauli on 4th December, 1930 [17], addressed to "Dear Radioactive Ladies and Gentlemen"! In 1914, Chadwick demonstrated that the β-spectrum was continuous, in contrast to α- and γ-rays which were unique in energy. Meitner later demonstrated that the missing energy could not be ascribed to neutral γ-rays, which led to the idea that the missing energy could be

explained by the existence of a new particle. In order to propose a solution to this problem and also as a remedy to the problem of spin statistics in β-decay, Pauli presented in his open letter, the idea of the existence of a neutral weakly interacting fermion emitted in β-decay. The term *neutrino* was given to this new particle later by Enrico Fermi [18]. Later Fermi expanded upon his idea to publish a groundbreaking theory on β-decay [19, 20], -known as *Fermi theory*.

After the remarkable success of Fermi Theory, in 1956 F. Reines and C.L.Cowan discovered the neutrino by observing the inverse β-decay reaction in a nuclear reactor experiment for the first time [21]. The muon neutrino was discovered in 1962 by Lederman, Schwartz and Steinberger [22] in the first ever accelerator neutrino experiment and the tau neutrino was detected later in 2000 by the direct observation of the Nu-Tau (DONuT) collaboration [23]. In 1957 Pontecorvo first conceptualized [24, 25] the possibility of neutrino oscillations by generalizing the notions related to kaon mixing. As only one flavour of neutrino had been discovered at that time, Pontecorvo's hypothesis focused on mixing between ν and $\bar{\nu}$. In 1962, with the knowledge that multiple flavours of neutrinos existed in nature, Maki, Nakagawa and Sakata proposed oscillations between ν_e and ν_μ [26]. This framework was later extended to tau neutrino.

In 1967, the Homestake experiment, pioneered by Davis and Bahcall uncovered the first indication that supported the neutrino oscillation theory. They sought to measure the rate at which solar neutrinos were captured by chlorine nuclei. They had observed a deficit between the measurement and the prediction, but the source of the discrepancy remained unclear. Many pointed towards an inadequate understanding of the solar model or errors in the neutrino experiments. The deficit phenomenon, however, was not limited to solar neutrino observations. Atmospheric neutrino experiments also reported a deviation from the approximately 2:1 ratio between muon and electron neutrinos that were produced through the $\pi \rightarrow \mu\nu_\mu, \mu \rightarrow e\nu_e\nu_\mu$. IMB [27] experiment, MACRO [28], and Kamiokande collaboration [29] found significant deficits in ν_μ fluxes. In 1998, Super-Kamiokande [30, 31] explained the shortfall by fitting their results with $\nu_\mu \rightarrow \nu_\tau$ oscillation framework. The debate in the solar neutrino sector ended in 2001 when the Sudbury Neutrino Observatory (SNO) [32] experiment provided conclusive evidence that roughly two-thirds of the solar neutrino flux was related to non ν_e flavours. This result supported the notion of neutrino oscillations and reconciled the total flux measurement with the standard solar model (SSM) prediction. by the Mikheev-Smirnov-Wolfenstein (MSW) resonance conversion effects [33, 34]. The confirmation of the phenomenon of neutrino oscillation by Super-Kamiokande and SNO has been honoured by awarding the Nobel

Prize in Physics in 2015 [35]. This shows that neutrinos have mass and has opened up promising avenue for probing beyond standard model physics.

1.2 Source of neutrinos

- **Solar neutrinos:** According to the Standard Solar Model (SSM) developed by Bahcall *et. al.* [36–38], these are mainly produced through the following two chain reaction inside the sun:

  1. *pp chain:* The primary reaction (with 86% branching ratio) in this chain is,

     $$p + p \rightarrow (H^2)^+ + e^+ + \nu_e,$$

     where the neutrinos can have kinetic energy in the range 0 to 0.42 MeV.

  2. *CNO cycle:* In the CNO (Carbon-Nitrogen-Oxygen) cycle, neutrinos are produced through the following reactions:

     $$(N^{13})^+ \rightarrow C^{13} + e^+ + \nu_e,$$
     $$(O^{15})^+ \rightarrow N^{15} + e^+ + \nu_e,$$
     $$(F^{17})^+ \rightarrow O^{17} + e^+ + \nu_e,$$

     where the neutrinos have energy approximately in the range $0 - 2.7$ MeV. The C, N,O thus produced act as catalysts in the fusion process stated below.

  The net effect of each of the chain reactions above is the following fusion process,

  $$4p \rightarrow (He^4)^{++} + 2\nu_e + n\gamma, \tag{1.1}$$

  where n depends on the particular reaction. We note that there is a high expectation of ν_e flux generated according to SSN. The calculation of the total solar neutrino flux on earth has been done in [39] and is about $5.94 \times 10^{10} cm^{-2} s^{-1}$.

- **Atmospheric neutrinos:** Primary cosmic rays interact with the nuclei in the atmosphere to produce secondary particles pions and kaons. Pions and kaons subsequently decay to muon neutrino, electron neutrino and the corresponding anti-neutrinos:

  $$\pi^+, K^+ \rightarrow \nu_\mu \mu^+ \rightarrow \nu_\mu e^+ \nu_e \bar{\nu}_\mu,$$
  $$\pi^-, K^- \rightarrow \bar{\nu}_\mu \mu^- \rightarrow \bar{\nu}_\mu e^- \bar{\nu}_e \nu_\mu, ,$$

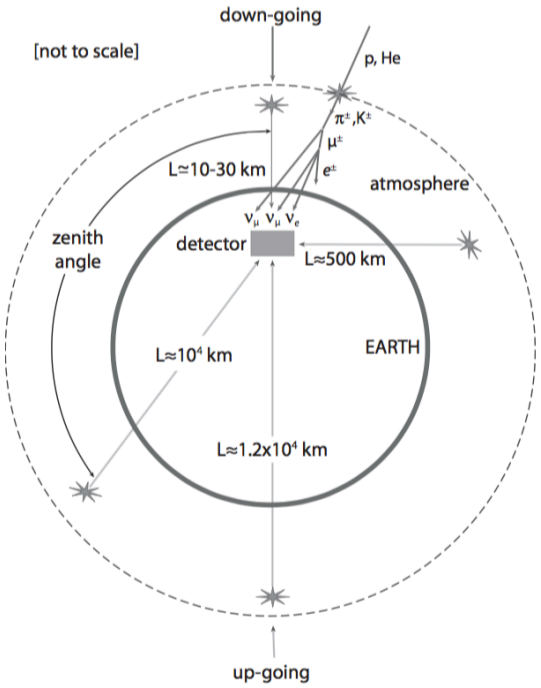

Figure 1.1: A schematic view of different zenith angles of atmospheric neutrinos and the different distances they travel before detection [1].

The ratio of ν_μ to ν_e flux becomes roughly 2:1 since ν_e gets produced in the secondary step above. Energy range of the atmospheric neutrinos is from a few hundred of MeV to 10^8 GeV. Atmospheric neutrino flux falls steeply as $E^{2.7}$ for energies above 1 GeV and the flux becomes undetectably small after about 100 TeV (See [40] for a detailed review). Atmospheric neutrino flux peaks at zenith angle $\approx 90^\circ$, i.e near the horizon, due to the larger length of atmosphere available in that direction. Atmospheric neutrinos observed at different zenith angles have different path lengths:- from $\sim 10 - 30$ km for downward going neutrinos to $\sim 10^4$ km for upward going neutrinos. See fig. 1.1 for a schematic (not to scale) of the atmospheric neutrinos (taken from [41]). Atmospheric neutrinos have long energy range and oscillation length, and hence are very useful to study neutrino oscillations as well as new physics.

- **Accelerator neutrinos:** Here the beams of neutrinos are produced by decay of pions, kaons, and muons created by a proton beam hitting a target. They can be of the following three categories.

  1. *Pion Decay In Flight (DIF):* Neutrino beam is produced by the decay of pions

and kaons initially produced by a proton beam hitting a target. The pions and kaons are allowed to decay in a decay tunnel of length of the order of 100 m. The beam is mainly composed of ν_μs or $\bar{\nu}_\mu$s. The typical energy of the neutrinos is of the order of a few GeV, but can be much larger, depending on the energy of the proton beam.

2. *Muon Decay At Rest (DAR):* In this process lower energy beam composed of muon antineutrinos coming from the decay

$$\mu^+ \rightarrow e^+ + \nu_e + \bar{\nu}_\mu$$

of the μ^+ produced in the pion decay:

$$\pi^+ \rightarrow \mu^+ + \nu_\mu \tag{1.2}$$

(the π^- are mostly absorbed by nuclei) are produced. The energy of neutrinos thus produced can be several tens of MeV.

3. *Beam Dump:* a proton beam with very high energy, of the order of some hundreds of GeV, is completely stopped in a thick target, called the beam dump, where the proton nucleon interactions generate heavy hadrons. The charmed heavy hadrons decay promptly with practically equal branching ratios into electrons and muons, emitting equal fluxes of electron and muon neutrinos with energies of the order of 10^2 GeV.

- **Reactor neutrinos:** Nuclear reactors are the major sources of artificially produced neutrinos. Power generation in nuclear reactors take place through the fission of neutron-rich isotopes like $U^{235}, U^{238}, Pu^{239}$. Electron antineutrinos are produced by the chain of inverse β-decays ($\bar{\nu}_e + p \rightarrow n + e^+$) of the fission products in the energy range of 0.1 to 10 MeV. The calculation of a reactor antineutrino spectrum is a difficult task, since the decay of each isotope produces a different neutrino spectrum. The qualitative features of the existing calculations are reviewed in [42, 43].

- **Core collapse supernova neutrinos:** Stars more massive than about $8M_\odot$ undergo gravitational collapse that leads to the production of a neutron star or a black hole. Among them Stars with mass $\gtrsim 10M_\odot$ have iron cores that exceed the Chandrasekar limit of about $1.44M_\odot$; they can no longer be supported against gravitational collapse by electron degeneracy pressure and catastrophic collapse ensues. Once the core of the star becomes constituted primarily of iron, further compression

of the core does not ignite nuclear fusion and the star is unable to thermodynamically support its outer envelope. As the surrounding matter falls inward under gravity, the temperature of the core rises and iron dissociates into α particles and nucleons. Electron capture on protons becomes heavily favored and electron neutrinos are produced[1]. The collapse continues until $3-4$ times nuclear density is reached, after which the inner core rebounds, sending a shock-wave across the outer core and into the mantle. This shock-wave loses energy as it heats the matter it traverses and incites further electron capture on the free protons left in the wake of the shock. During the few milliseconds in which the shock-wave travels from the inner core to the neutrinosphere, electron neutrinos are released in a pulse. This neutronization burst carries away approximately 10^{51} ergs of energy.However, 99% of the binding energy $Eb \sim 10^{53}$ ergs of the protoneutron star (which is about 10% of the star's rest mass energy) is released in the following $\sim 10s$. The primary processes are beta decay (providing a source of electron antineutrinos), $\nu_e\ \bar{\nu}_e$ annihilation, e^+e^- annihilation, and nucleon bremsstrahlung ($N+N \rightarrow N+N+\nu+\bar{\nu}$, which give all flavors of neutrinos: $\nu_e\bar{\nu}_e, \nu_\mu\bar{\nu}_\mu, \nu_\tau\bar{\nu}_\tau$), in addition to electron capture.

- **Astrophysical neutrinos:** Very high energy neutrino fluxes from cosmologically distant sources are generally expected in association with the production of cosmic-rays (CR), whose energy spectrum can extend to even 10^{20} eV and is likely dominated above $\sim 3\times10^{17}$ eV by protons, neutrons, and nuclei of extragalactic origin. Source candidates include galactic sources like supernova remnants (SNR) and extragalactic sources like Active Galactic Nuclei (AGN) and Gamma Ray Bursts (GRB). This Ultra High-energy (UHE) neutrino production is thought to be associated with the interactions of high-energy protons that produce energetic charged pions by $p\gamma$ or by $p\bar{p}$ interactions. In sources that are optically thin to meson-nucleon interactions, the $\pi^+ \rightarrow \mu^+\nu_\mu$ decays and subsequent $\mu^+ \rightarrow e^+\nu_e\bar{\nu_\mu}$ decays (and corresponding π^- decay chain) lead to ultra high-energy neutrinos. The decays of neutral pions, $\pi^0 \rightarrow \gamma\gamma$, may be observed as gamma ray signals in experiments such as observations by the Fermi Gamma-ray Space Telescope (FGST).

- **Relic neutrinos:** Relic neutrinos are an important product of the standard hot Big Bang. Neutrinos were in thermal equilibrium in the hot plasma which filled the early Universe through weak interactions with the other particles. As the universe

[1]This process is known as neutronization.

expanded and cooled, the rates of weak interaction processes decreased and neutrinos decoupled when these rates became smaller than the expansion rate. Since for the three known light neutrinos with masses smaller than about 1 eV the decoupling occurred when they were relativistic, these neutrinos are hot relics. Relic neutrinos pervade space, but their temperature T_ν^0 is extremely small, being of the order of 10^4 eV. Their weak interaction cross-section with matter is thus extremely small and hence the direct detection of relic neutrinos is a very difficult task with present experimental techniques.

1.3 Standard derivation of neutrino oscillation

Before proceeding to derive the neutrino oscillation in the standard framework, we first make the following assumptions:

- Neutrinos produced or detected in charged current weak interaction processes are described by *flavor states* (see eq. 1.3.).
- Flavor neutrinos have a definite momentum $\vec{p}$, i.e. all the massive neutrino components have the same momentum. However, there is an alternative method[2] of deriving the neutrino oscillation probability where this equal momentum assumption is irrelevant.
- The propagation time t is equal to the distance L traveled by the neutrino between production and detection[3]

a neutrino with flavor α and momentum $\vec{p}$, created in a charged-current weak interaction process from a charged lepton ℓ_α^- or together with a charged antilepton ℓ_α^+, is described as the flavor state,

$$|\nu_\alpha\rangle = \sum_k U_{\alpha k}^* |\nu_k\rangle \quad (\alpha = e, \mu, \tau; \langle\nu_k|\nu_j\rangle = \delta_{kj}). \tag{1.3}$$

, where the unitary matrix $U_{\alpha k}^*$ is known as the mixing matrix or the Pontecarvo-Maki-Nakagawa-Sakata (PMNS) matrix [26,49]. In general for an $N \times N$ unitary mixing matrix,

[2] known as *wave packet analysis* in which the wave packet nature of propagating neutrinos are taken into into account. See, for *e.g.* [44–48]

[3] It can be shown in the so called *wave packet analysis* of neutrino oscillation phenomena that neutrinos are described by wave packets that are localized in the production process at the production time and propagate between the production and the detection processes with a group velocity close to the velocity of light, justifying the assumption 3 above.

there are $N(N-1)/2$ mixing angles and $N(N+1)/2$ phases. But $2N-1$ phases can be absorbed by the redefinition of the fields. Hence, in case of N flavours the leptonic mixing matrix $U_{\alpha k}$ depends on $(N-1)(N-2)/2$ Dirac CP- violating phases. For the standard 3 flavor scenario, $N=3$ and there is only one CP violating phase known as $\delta_{\rm CP}$. If the neutrinos are Majorana particles, there are $(N-1)$ additional Majorana phases. The unitarity of the mixing matrix implies that the flavor states are orthonormal:

$$\langle \nu_\alpha | \nu_\beta \rangle = \delta_{\alpha\beta}. \tag{1.4}$$

The massive neutrino states $|\nu_k\rangle$ are eigenstates of the Hamiltonian:

$$\mathcal{H} \, |\nu_k\rangle = E_k \, |\nu_k\rangle \, , \tag{1.5}$$

with energy eigenvalues $E_k = \sqrt{|\vec{p}|^2 + m_k^2}$. The Schrödinger equation

$$i \frac{d}{dt} \, |\nu_k(t)\rangle = \mathcal{H} \, |\nu_k(t)\rangle \tag{1.6}$$

implies that the massive neutrino states evolve in time as plane waves:

$$|\nu_k(t)\rangle = e^{-iE_k t} \, |\nu_k\rangle \, . \tag{1.7}$$

Let us consider now a flavor state $|\nu_\alpha(t)\rangle$ which describes a neutrino created with a definite flavor α at time t = 0. So using eqs. 1.3-1.7, we can now write the time evolution of the flavor state,

$$|\nu_\alpha(t)\rangle = \sum_k U^*_{\alpha k} e^{-iE_k t} \, |\nu_k\rangle \, , \tag{1.8}$$

such that $|\nu_\alpha(t=0)\rangle = |\nu_\alpha\rangle$. Now, using the unitarity relation,

$$\sum_\alpha U^*_{\alpha k} U_{\alpha j} = \delta_{jk}, \tag{1.9}$$

and inverting eq. 1.3, the massive neutrino states can be expressed in terms of the flavor states as,

$$|\nu_k\rangle = \sum_\alpha U_{\alpha k} \, |\nu_\alpha\rangle \, . \tag{1.10}$$

Using the relation 1.10 in eq. 1.8, we can write,

$$|\nu_\alpha(t)\rangle = \sum_{\beta=e,\mu,\tau} \left(\sum_k U^*_{\alpha k} U_{\beta k} e^{-iE_k t} \right) |\nu_\beta\rangle \, . \tag{1.11}$$

The amplitude of the neutrino flavor transition $\nu_\alpha \to \nu_\beta$ as a function of time is given by,

$$A_{\nu_\alpha \to \nu_\beta}(t) = \langle \nu_\beta | \nu_\alpha(t) \rangle \sum_k U^*_{\alpha k} U_{\beta k} e^{-iE_k t}, \tag{1.12}$$

and the probability of the flavor transition $\nu_\alpha \to \nu_\beta$ is given by,

$$P_{\nu_\alpha \to \nu_\beta}(t) = |A_{\nu_\alpha \to \nu_\beta}(t)|^2 = \sum_{k,j} U^*_{\alpha k} U_{\beta k} U_{\alpha j} U^*_{\beta j} e^{-i(E_k - E_j)t}. \tag{1.13}$$

For ultrarelativistic neutrinos, the dispersion relation $E_k = \sqrt{\vec{p}^2 + m_k^2}$ can be written as (using the equal momentum assumption),

$$E_k \approx E + \frac{m_{k^2}}{2E} \implies E_k - E_j \approx \frac{\Delta m^2_{kj}}{2E}, \tag{1.14}$$

where $\Delta m^2_{kj} = m^2_k - m^2_j$, is the mass squared difference. Also $E = |\vec{p}|$, neglecting the mass contribution. In an actual neutrino oscillation experiment the neutrino propagation length L between the source and the detector is measured instead of the propagation time t. Since neutrinos are ultrarelativistic, we use the assumption $t \approx L$ and the oscillation probability in eq. 1.13 as a function of energy,

$$P_{\nu_\alpha \to \nu_\beta}(t) = |A_{\nu_\alpha \to \nu_\beta}(L, E)|^2 = \sum_{k,j} U^*_{\alpha k} U_{\beta k} U_{\alpha j} U^*_{\beta j} e^{-i\frac{\Delta m^2_{kj}}{2E} L}. \tag{1.15}$$

Using the unitarity of the mixing matrix (eq. 1.9), it can be shown that the probabilities add up to unity,

$$\begin{aligned} \sum_\beta P_{\nu_\alpha \to \nu_\beta}(L, E) &= 1 \\ \sum_\alpha P_{\nu_\alpha \to \nu_\beta}(L, E) &= 1. \end{aligned} \tag{1.16}$$

From relation 1.9, one can show that

$$\sum_k |U_{\alpha k}|^2 |U_{\beta k}|^2 = \delta_{\alpha\beta} - 2 \sum_{k>j} Re\left[U^*_{\alpha k} U_{\beta k} U_{\alpha j} U^*_{\beta j}\right], \tag{1.17}$$

which allows us to write the oscillation probability in the following form:

$$\begin{aligned} P_{\nu_\alpha \to \nu_\beta} = \delta_{\alpha\beta} \quad &- \quad 4 \sum_{k>j} Re\left[U^*_{\alpha k} U_{\beta k} U_{\alpha j} U^*_{\beta j}\right] \sin^2(\phi_{kj}) \\ &+ \quad 2 \sum_{k>j} Im\left[U^*_{\alpha k} U_{\beta k} U_{\alpha j} U^*_{\beta j}\right] \sin(2\phi_{kj}), \text{where, } \phi_{kj} = \frac{\Delta m^2_{kj} L}{4E} \end{aligned} \tag{1.18}$$

Eq. 1.18 is known as the transition probability when $\alpha \neq \beta$[4]

For the case of antineutrinos, one starts with

$$|\bar{\nu}_\alpha\rangle = \sum_k U_{\alpha k} |\bar{\nu}_k\rangle \quad (\alpha = e, \mu, \tau; \langle \nu_k | \nu_j \rangle = \delta_{kj}), \tag{1.20}$$

and gets the following expression for oscillation probability of antineutrinos,

$$\begin{aligned} P_{\bar{\nu}_\alpha \to \bar{\nu}_\beta} = \delta_{\alpha\beta} \quad &- \quad 4 \sum_{k>j} Re\left[U^*_{\alpha k} U_{\beta k} U_{\alpha j} U^*_{\beta j}\right] \sin^2(\phi_{kj}) \\ &- \quad 2 \sum_{k>j} Im\left[U^*_{\alpha k} U_{\beta k} U_{\alpha j} U^*_{\beta j}\right] \sin(2\phi_{kj}). \end{aligned} \tag{1.21}$$

1.4 Neutrino oscillation in vacuum

Neutrino oscillation in vacuum is simple to derive because the mass eigenstates evolve exactly as shown in the previous section (eq. 1.5). We give a brief description of it below both in the context of 2 flavour and 3 flavours.

1.4.1 Two flavour oscillation

In this case there is only one mixing angle θ and only one mass squared difference namely $\Delta m^2 = m_2^2 - m_1^2$. The two flavor neutrino states are linear superpositions of the two massive neutrinos ν_1 and ν_2 with coefficients given by the elements of the two-neutrino effective mixing matrix,

$$U = \begin{pmatrix} \cos\theta & \sin\theta \\ -\sin\theta & \cos\theta \end{pmatrix}, \quad \text{where } 0 \leqslant \theta \leqslant \pi/2. \tag{1.22}$$

Now using eq. 1.18 we can write,

$$P_{\nu_\alpha \to \nu_\beta}(L, E) \quad = \quad \sin^2 2\theta \sin^2\left(\frac{\Delta m^2 L}{4E}\right), \quad (\alpha \neq \beta). \tag{1.23}$$

It is convenient for practical purposes to write the probability expression after unit conversions, in the following form,

$$P_{\nu_\alpha \to \nu_\beta}(L, E) = \sin^2 2\theta \sin^2 1.27\left(\frac{\Delta m^2[ev^2] L[km]}{E[GeV]}\right) \tag{1.24}$$

[4]When $\alpha = \beta$,it is known as the survival probability and can be written as,

$$P_{\nu_\alpha \to \nu_\alpha} = 1 - 4 \sum_{k>j} Re|U_{\alpha k}|^2 |U_{\alpha j}|^2 \sin^2(\phi_{kj}) \tag{1.19}$$

1.4.2 Three flavor oscillation:

For three generation, one has 3 mixing angles ($\theta_{12}, \theta_{13}, \theta_{23}$), 2 mass squared differences and one Dirac CP phase (δ_{cp}). The PMNS matrix U can be conveniently parameterized as,

$$\begin{aligned} U &= R_{23}W_{13}R_{12} \\ &= O(\theta_{23})O(\theta_{13},\delta_{13})O(\theta_{12}) \\ &= \begin{pmatrix} 1 & 0 & 0 \\ 0 & c_{23} & s_{23} \\ 0 & -s_{23} & c_{23} \end{pmatrix} \begin{pmatrix} c_{13} & 0 & s_{13}e^{-i\delta_{cp}} \\ 0 & 1 & 0 \\ -s_{13}e^{-i\delta_{cp}} & 0 & c_{13} \end{pmatrix} \begin{pmatrix} c_{12} & s_{12} & 0 \\ -s_{12} & c_{12} & 0 \\ 0 & 0 & 1 \end{pmatrix} \\ &= \begin{pmatrix} c_{12}c_{13} & s_{12}c_{13} & s_{13}e^{-i\delta_{\rm CP}} \\ -s_{12}c_{23} - c_{12}s_{13}s_{23}e^{i\delta_{\rm CP}} & c_{12}c_{23} - s_{12}s_{13}s_{23}e^{i\delta_{\rm CP}} & c_{13}s_{23} \\ s_{12}s_{23} - c_{12}s_{13}c_{23}e^{i\delta_{\rm CP}} & -c_{12}s_{23} - s_{12}s_{13}c_{23}e^{i\delta_{\rm CP}} & c_{13}c_{23} \end{pmatrix}, \end{aligned} \tag{1.25}$$

where $s_{ij} = \sin\theta_{ij}, c_{ij} = \cos\theta_{ij}$ *etc.* The expression for 3 flavor in vacuum can be written in useful form in the approximation that the solar mass squared difference (Δm^2_{21}) and the mixing angle θ_{13} is small and neglected beyond 2 orders of magnitude.

$$\begin{aligned} P_{\mu e} &= \alpha^2 \sin^2 2\theta_{12} c_{23}^2 \left(\frac{\lambda L}{2}\right)^2 + 4 s_{13}^2 s_{23}^2 \sin^2\left(\frac{\lambda L}{2}\right) \\ &+ 2\alpha s_{13} \sin 2\theta_{13} \sin 2\theta_{23} \left(\frac{\lambda L}{2}\right) \sin\left(\frac{\lambda L}{2}\right) \cos\left(\delta_{\rm CP} + \frac{\lambda L}{2}\right), \end{aligned} \tag{1.26}$$

where $\lambda = \frac{\Delta m^2_{31}}{2E}$, $\alpha = \frac{\Delta m^2_{21}}{\Delta m^2_{31}}$. The discussion regarding the probability expressions for all other channels can be found in [50].

1.5 Neutrino oscillation in matter

Neutrinos propagating in matter are subject to coherent forward scattering with the particles present in the matter. The resulting potential changes the neutrino propagation through matter significantly than the vacuum, thereby changing the oscillation probability expressions in. The flavor changing mechanism in neutrino oscillation in presence of matter is given by the Mikheev-Smirnov-Wolfenstein (MSW) effect. The basis of the MSW effect is that the electron neutrinos have different interactions with matter than the neutrinos of other flavors. When the neutrino traverses the Earth, the oscillation probability is calculated taking into account earth's matter potential due to the forward scattering amplitude of charged current interactions with electrons. Neutral current interactions are

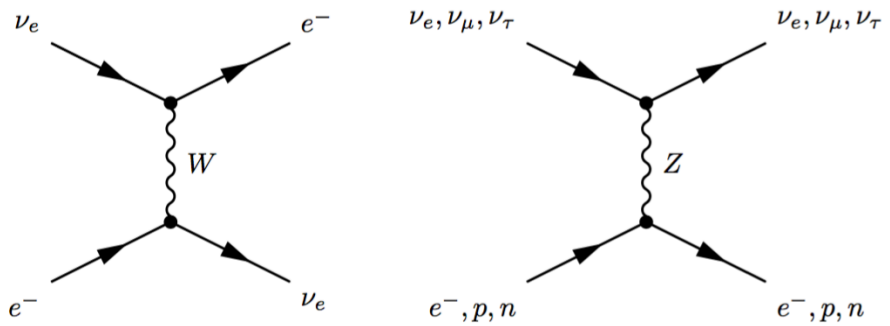

Figure 1.2: Feynman diagrams of coherent forward scattering processes that generate the CC potential though W exchange (left) and the NC potential through the Z exchange (right).

neglected here because they lead to flavour-independent terms which are irrelevant for the oscillation probabilities. The effective CC Hamiltonian for coherent forward elastic scattering (see fig. 1.2) can be written as,

$$\begin{aligned}\mathcal{H}^{CC}_{eff}(x) &= \frac{G_F}{\sqrt{2}}\Big[\bar{\nu}_e(x)\gamma^\rho(1-\gamma^5)e(x)\Big]\Big[\bar{e}(x)\gamma_\rho(1-\gamma^5)\nu_e(x)\Big] \\ &= \frac{G_F}{\sqrt{2}}\Big[\bar{\nu}_e(x)\gamma^\rho(1-\gamma^5)\nu_e(x)\Big]\Big[\bar{e}(x)\gamma_\rho(1-\gamma^5)e(x)\Big] \quad \text{(using Fierz Transformation).}\end{aligned}$$

Averaging over the electron background in the rest frame of the medium gives

$$\bar{\mathcal{H}}^{CC}_{eff}(x) = V_{CC}\bar{\nu}_{eL}(x)\gamma^0\nu_{eL}(x), \tag{1.27}$$

with the charged current potential given by,

$$V_{CC} = \sqrt{2}G_F N_e, \quad N_e \text{ being the electron no. density of the medium.} \tag{1.28}$$

For antineutrinos, $V_{CC} \to -V_{CC}$, because of the anti-commutation relation between the creation and the annihilation operators. Similarly starting with the effective NC Hamiltonian (the right one in fig. 1.2)

$$\mathcal{H}^{NC}_{eff}(x) = \frac{G_F}{\sqrt{2}}\sum_{\alpha=e,\mu,\tau}\Big[\bar{\nu}_\alpha(x)\gamma^\rho(1-\gamma^5)\nu_\alpha(x)\Big]\sum_f\Big[\bar{f}(x)\gamma_\rho(g^f_V - g^f_A\gamma^5)f(x)\Big], \tag{1.29}$$

one can see that the neutral current potential of any flavor neutrino due to coherent scattering with the fermions of the medium is given by[5],

$$V^f_{NC} = -\frac{1}{\sqrt{2}}G_F N_n. \tag{1.30}$$

[5]In an electrically neutral astrophysical environment with low temperature and density.

Summarizing, the effective neutrino potential is then given by,

$$\bar{\mathcal{H}}_{eff}(x) = \sum_{\alpha=e,\mu,\tau} V_\alpha \bar{\nu}_{\alpha L}(x)\gamma^0 \nu_{\alpha L}(x), \tag{1.31}$$

with the potential

$$V_\alpha = \sqrt{2} G_F \left(N_e \delta_{\alpha e} - \frac{1}{2} N_n \right). \tag{1.32}$$

Now, let us see how the potential affects neutrino oscillation. Going back to the evolution equation we see,

$$i\frac{d}{dt}\left|\nu_\alpha(t)\right\rangle = \mathcal{H}\left|\nu_\alpha(t)\right\rangle, \quad \text{with, } \left|\nu_\alpha(0)\right\rangle = \left|\nu_\alpha\right\rangle, \tag{1.33}$$

where $\mathcal{H}$ is the sum of the vacuum and the matter interaction Hamiltonian:

$$\mathcal{H} = \mathcal{H}_0 + \mathcal{H}_I. \tag{1.34}$$

The massive neutrino eigenstates ν_k with momentum $\vec{p}$ is an eigenstate of the vacuum Hamiltonian:

$$\mathcal{H}_0\left|\nu_k\right\rangle = E_k\left|\nu_k\right\rangle, \quad \text{with} \quad E_k = \sqrt{\vec{p}^2 + m_k^2}, \tag{1.35}$$

and the flavor states are the eigenstates of the interaction Hamiltonian:

$$\mathcal{H}_I\left|\nu_\alpha\right\rangle = V_\alpha\left|\nu_\alpha\right\rangle \quad \text{with } V_\alpha \text{ given by eq. 1.32} \tag{1.36}$$

If $\psi_\alpha(t) = \langle\nu_\beta|\left|\nu_\alpha(t)\right\rangle$ is the amplitude of the transition $\nu_\alpha \to \nu_\beta$ after a time t, then its evolution can be written by (using eq. 1.33 and using the approximation $t \sim x$)

$$i\frac{d}{dx}\Psi_\alpha = \mathcal{H}_F \Psi_\alpha, \tag{1.37}$$

where,

$$\mathcal{H}_F = \frac{1}{2E}(UM^2U^\dagger + A), \tag{1.38}$$

$$\Psi_\alpha = \begin{pmatrix} \psi_{\alpha e} \\ \psi_{\alpha\mu} \\ \psi_{\alpha\tau} \end{pmatrix}, \quad M^2 = \begin{pmatrix} 0 & 0 & 0 \\ 0 & \Delta m^2_{21} & 0 \\ 0 & 0 & \Delta m^2_{31} \end{pmatrix}, \quad A = \begin{pmatrix} A_{CC} & 0 & 0 \\ 0 & 0 & 0 \\ 0 & 0 & 0 \end{pmatrix},$$

$$A_{CC} = 2EV_{CC} = 2\sqrt{2}EG_F N_e$$

1.5.1 Two flavor oscillation:

For the two flavor scenario, eq.1.37 can be written as,

$$i\frac{d}{dx}\begin{pmatrix}\psi_{ee}\\ \psi_{e\mu}\end{pmatrix} = \mathcal{H}_F\begin{pmatrix}\psi_{ee}\\ \psi_{e\mu}\end{pmatrix}, \tag{1.39}$$

where

$$\mathcal{H}_F = \begin{pmatrix}-\Delta m^2\cos 2\theta + A_{CC} & \Delta m^2\sin 2\theta\\ \Delta m^2\sin 2\theta & \Delta m^2\cos 2\theta - A_{CC}\end{pmatrix}. \tag{1.40}$$

$\Delta m^2 = m_2^2 - m_1^2$ and the only mixing angle is defined as,

$$\nu_e = \nu_1\cos\theta + \nu_2\sin\theta, \quad \nu_\mu = -\nu_1\sin\theta + \nu_2\cos\theta. \tag{1.41}$$

In order to solve eq. 1.39, $\mathcal{H}_F$ is diagonalised by the following orthogonal transformation:

$$U_M^T\mathcal{H}_F U_M = \mathcal{H}_M. \tag{1.42}$$

Here the unitary matrix U_M is the effective mixing matrix in matter:

$$U_M = \begin{pmatrix}\cos\theta_M & \sin\theta_M\\ -\sin\theta_M & \cos\theta_M\end{pmatrix}, \tag{1.43}$$

and the effective squared mass difference is

$$\Delta m_M^2 = \sqrt{(\Delta m^2\cos 2\theta - A_{CC})^2 + (\Delta m^2\sin 2\theta)^2}. \tag{1.44}$$

The effective mixing angles in matter θ_M is given by,

$$\tan 2\theta_M = \frac{\tan 2\theta}{1 - \frac{A_{CC}}{\Delta m^2\cos 2\theta}}. \tag{1.45}$$

Note that, there is a resonance when $A_{CC} = \Delta m^2\cos 2\theta$ and at the resonance the effective mixing angle is maximal *i.e.*$\pi/4$. This implies that if the resonance region is wide enough it may induce total flavor transition of neutrinos. This is the famous MSW effect [33, 34]. Proceeding further, it can now be shown that the appearance probability in presence of matter is given by (by solving eq. 1.39 in a constant density *i.e.*, $d\theta_M/dx = 0$),

$$P(\nu_\mu \to \nu_e) = |\psi_{\mu e}|^2 = \sin^2 2\theta_M\sin^2\left(\frac{\Delta m_M^2 x}{4E}\right). \tag{1.46}$$

We note that, this probability expression has the similar form as in vacuum (eq. 1.23) with the mixing angle and the mass squared difference replaced by their matter counterparts.

1.5.2 Three flavor oscillation:

For the case of three neutrinos, the mixing matrix in the standard parametrization is (from eq. 1.25)

$$U = R_{23}W_{13}R_{12}. \tag{1.47}$$

Now, since the matrix A in eq. 1.38 commutes with R_{23},

$$R_{23}^{\dagger}AR_{23} = A. \tag{1.48}$$

Redefining $\Psi_\alpha \to R_{23}^{\dagger}\Psi_\alpha$ in eq. 1.37 we can write,[6]

$$\begin{aligned} \mathcal{H}_F &= \frac{1}{2E}\left(W_{13}R_{12}M^2R_{12}^{\dagger}W_{13}^{\dagger} + A\right) \\ &\approx \frac{1}{2E}\left(W_{13}M^2W_{13}^{\dagger} + A\right) \end{aligned} \tag{1.49}$$

Now one can follow the usual procedure (see subsec. 1.5.1) by diagonalising $\mathcal{H}_F$ and obtain the effective mixing angle and mass squared differences in matter as,

$$\begin{aligned} \tan 2\theta_{13}^m &= \frac{\tan 2\theta_{13}}{1 - \frac{A_{CC}}{\Delta m_{31}^2 \cos 2\theta_{13}}} \\ \Delta m_{m31}^2 &= \sqrt{(\Delta m_{31}^2 \cos 2\theta_{13} - A_{CC})^2 + (\Delta m_{31}^2 \sin 2\theta_{13})^2}. \end{aligned} \tag{1.50}$$

In the OMSD approximation, the expression for $P_{\mu e}$ in matter in given by,

$$P_{\mu e}^m = \sin^2\theta_{23}\sin^2 2\theta_{13}^m \sin^2\left[\Delta m_{m31}^2 L/4E\right] \tag{1.51}$$

For an expression upto the second order of $\frac{\Delta m_{21}^2}{\Delta m_{31}^2}$ and some more discussions about the implication of matter effect, please see sec. 2.1.

1.6 CPT transformation in the context of neutrino oscillation

CPT transformation, being the symmetry of any local quantum field theory, is a symmetry for oscillation probabilities also. Under CPT symmetry,

$$P_{\nu_\alpha \to \nu_\beta} = P_{\bar{\nu}_\alpha \to \bar{\nu}_\beta}, \tag{1.52}$$

[6] We also make use of the One Mass Squared Dominance (OMSD) approximation $\Delta m_{31}^2 >> \Delta m_{21}^2$ and $M \approx diag(0, 0, \Delta m_{31}^2)$

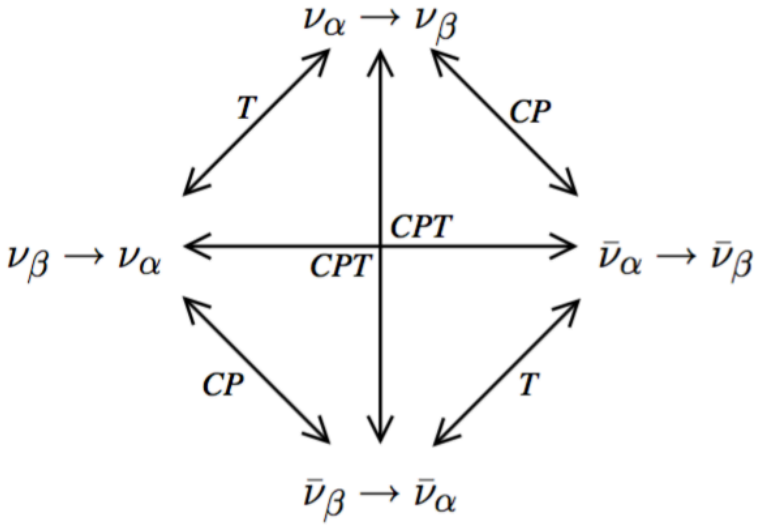

Figure 1.3: A schematic view of CPT, CP and T transformations that relate different flavor transition channels (reproduced from [1]).

which can be verified from eqs. 1.18 and 1.19, first using a CP transformation ($\bar{\nu}_\beta \to \bar{\nu}_\alpha \implies \nu_\beta \to \nu_\alpha$) which changes $U \rightleftarrows U^*$, followed by a T transformation ($\nu_\beta \to \nu_\alpha \implies \nu_\alpha \to \nu_\beta$) which changes $\alpha \rightleftarrows \beta$. See fig. 1.3 for a schematic of these various transformations.

1.7 Current status of oscillation parameters

Standard neutrino oscillation is governed by three mixing angles ($\theta_{12}, \theta_{13}, \theta_{23}$), two mass squared differences ($\Delta m^2_{31}, \Delta m^2_{21}$) and one Dirac CP phase (δ_{CP}). Combined analyses of KamLAND [51] and the solar neutrino experiments [52] have determined the parameters θ_{12} and Δm^2_{21}. The atmospheric neutrino experiments such as Super-Kamiokande (SK) [30], MINOS [30, 53] have measured $\sin^2 2\theta_{23}$ and $|\Delta m^2_{31}|$. The short baseline reactor neutrino experiments Daya Bay [54], RENO [55] and Double Chooz [56] have recently measured the non-zero value of θ_{13} very precisely. The ongoing and the upcoming accelerator long baseline neutrino experiments (T2K [10], NOvA [9, 57], DUNE [7, 13], T2HK [15]) are expected to probe the precise value of Δm^2_{31} (with correct sign), δ_{CP} and θ_{23}. The present status of the oscillation parameters are shown in table 1.7.

Table 1.1: Current status of oscillation parameters [5].

Oscillation parameter	Best fit value	3σ range
$\theta_{12}/^\circ$	$33.72^{+0.79}_{-0.76}$	$31.52 \rightarrow 36.18$
$\theta_{23}/^\circ$ (NH)	$49.3^{+1.5}_{-8.3}$	$38.6 \rightarrow 53.1$
$\theta_{23}/^\circ$ (IH)	$49.6^{+1.3}_{-1.7}$	$39.2 \rightarrow 53.0$
$\theta_{13}/^\circ$ (NH)	$8.47^{+0.24}_{-0.20}$	$7.86 \rightarrow 9.11$
$\theta_{13}/^\circ$ (IH)	$8.54^{+0.19}_{-0.20}$	$7.93 \rightarrow 9.12$
$\delta_{CP}/^\circ$ (NH)	272^{+61}_{-64}	$0 \rightarrow 360$
$\delta_{CP}/^\circ$ (IH)	256^{+43}_{-43}	$0 \rightarrow 360$
$\Delta m^2_{21}/10^{-5}eV^2$	$7.49^{+0.19}_{-0.17}$	$7.02 \rightarrow 8.08$
$\Delta m^2_{31}/10^{-3}eV^2$ (NH)	$+2.484^{+0.045}_{-0.048}$	$+2.351 \rightarrow +2.618$
$\Delta m^2_{31}/10^{-3}eV^2$ (IH)	$-2.467^{+0.041}_{-0.042}$	$-2.595 \rightarrow -2.341$

1.8 Neutrino oscillation: outstanding questions

After the discovery of the non-zero and not too small value of θ_{13}, the focus of neutrino oscillation has shifted to the following three questions, all of which are expected to be resolved by the promising upcoming accelerator long baseline experiments:

1.8.1 Neutrino mass hierarchy (MH):

Neutrinos have 3 mass eigenstates (say, ν_1, ν_2, ν_3). So far only the absolute value of the mass squared difference Δm^2_{31} has not been determined but not its sign. So there exists two possibilities in which the mass eigenstates are arranged: a) $m_3 > m_2 > m_1$ (called normal hierarchy or NH) or b) $m_2 > m_1 > m_3$ (called inverted hierarchy or IH). These are schematically shown in fig. 1.4. Non-zero value of θ_{13} will enhance the matter effect when neutrinos pass through matter. Because of the enhanced matter effect, the different interactions that neutrinos and antineutrinos undergo while passing through the earth matter will be more detectable. This will help to resolve the mass hierarchy.

The resolution of mass hierarchy will help distinguish between models based on lepton flavor symmetries. Models exhibiting a softly broken $L_e - L_\mu - L_\tau$ lepton number produce only an inverted hierarchy [58]. On the other hand, all of the successful grand unified models in the literature employing a conventional type I see-saw mechanism (see subsection 1.9.7 for the see-saw mechanism of neutrino mass generation) appear to prefer a normal hierarchy (see, for *e.g.*, [59–63]). With this in background, it can be

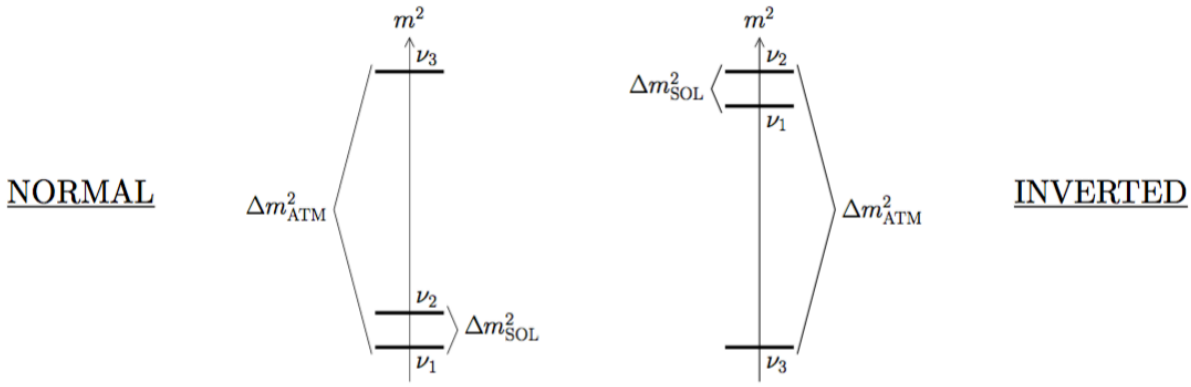

Figure 1.4: A schematic view of normal and inverted mass hierarchy allowed by $|\Delta m^2_{21}| << |\Delta m^2_{31}|$ [2].

shown [64] that for every successful normal neutrino mass hierarchy solution to a grand unified model, there exists an inverted hierarchy solution with exactly the same PMNS mixing matrix. Hence a future determination of the inverted hierarchy would tend to rule out grand unified models based on conventional type-I see-saw and would largely favor models based on type-II and type-III see-saw and models based on a conserved $L_e - L_\mu - L_\tau$ lepton number. In contrast, a determination of the normal hierarchy would rule out the conserved $L_e - L_\mu - L_\tau$ lepton number models in favor of the grand unified models.

1.8.2 Leptonic CP Violation (CPV):

CP Violation has so far only been observed in the quark sector of the Standard Model (SM). Whether CP is violated in the leptonic sector (*i.e.*, $\delta_{\rm CP} \neq 0$ or π) too is of fundamental importance because it will shed light on the observed baryonic asymmetry of the universe through an elegant natural process known as leptogenesis. In 1967, Sakharov first put forward [65] the three necessary conditions which could dynamically generate the presently observed baryon asymmetry in the universe through baryogenesis: i)Baryon number violation, ii) C and CP violation and iii) departure from thermal equilibrium. Among the viable baryogenesis scenario, leptogenesis [66] is the simplest and the most elegant, well-motivated mechanism[7]. In leptogenesis, the estimate of baryon asymmetry depends on the product of the three factors: (the leptonic CP asymmetry ε produced in heavy particle decays) $\times$ (an efficiency factor η due to washout processes in scattering,

[7]For reviews of leptogenesis, see [67, 68]

decays, and inverse decays) $\times$ (a reduction factor due to chemical equilibrium, charge conservation, and the redistribution of the asymmetry among different particle species by fast processes)[8]. The presence of the leptonic CP violation in the leptogenesis scenario, inevitably invites us to do new studies on the direct link between leptonic CPV and the latter. More specifically, if the strength of CP violation at low energies in neutrino oscillations is measured, what can one infer about the viability or nonviability of leptogenesis? Already there exists a few model dependent studies on this in literature [72–75]. Nevertheless, the discovery of leptonic CP violation will take us a massive step further to test leptogenesis. The upcoming long baseline experiments (such as DUNE, T2HK) have the potential to measure the value of the leptonic CPV phase $\delta_{\rm CP}$. Intrinsic CPV in the SM requires $\theta_{13} \neq 0$ (which has recently been discovered) and $\delta_{\rm CP} \neq 0, \pi$. Furthermore, earth matter effects[9] and possible sub-leading new physics effects (sterile neutrinos, Non Standard neutrino Interactions)[10] can induce fake CPV which must be taken into consideration into any measurement of $\delta_{\rm CP}$.

1.8.3 Octant degeneracy:

A look at the interference term of the expression for neutrino oscillation (eq. 1.26) tells us that it contains the term $\sin 2\theta_{23}$,- which is the same for θ_{23} and $\pi/2 - \theta_{23}$. So there is an ambiguity as to which octant the angle θ_{23} lies in. Atmospheric neutrino experiments like SK have measured the value of $\sin 2\theta_{23}$, but it still remains to be determined whether θ_{23} lies in the higher ($\pi/4 < \theta_{23} < \pi/2$) or the lower ($0 < \theta_{23} < \pi/4$) octant.

1.9 Beyond standard 3ν neutrino oscillation

In addition to the standard three neutrino phenomenology, there exists some experimental evidences, although not conclusive and some theoretical models which may indicate to some exotic phenomena that go beyond the standard framework. These different possibilities are briefly described below.

[8] The 2nd and the 3rd factor can be calculated by solving the full Boltzman equations describing the out of equilibrium dynamics, utilising the models describing the departure of thermal equilibrium provided by the expansion of the universe. For details, see for *e.g.*, [67, 69–71].

[9] Please see section 2.1 for more details on CPV and MH in the context of long baseline experiments.

[10] We discuss these issues in great details in chapters 3 and 4.

1.9.1 Sterile neutrinos:

The possibility of the existence of a fourth neutrino mass eigenstate (called *sterile* neutrino) originates from some anomalous neutrino experiment results. The LSND experiment [76] found evidence for $\bar{\nu}_\mu \rightarrow \bar{\nu}_e$ oscillation at 3.3σ significance (oscillation probability is $(2.64 \pm 0.67 \pm 0.45) \times 10^{-3}$). The evidence for $\nu_\mu \rightarrow \nu_e$ oscillation was found at much less significance with oscillation probabilities $(2.6 \pm 1.0 \pm 0.5) \times 10^{-3}$) (in the 1993-95 data) and $(1.0 \pm 1.6 \pm 0.4) \times 10^{-3}$) in the 1996-98 data. The mass squared difference which can successfully explain this LSND $\bar{\nu}_e$ excess (LSND anomaly) is $\Delta m^2_L \sim 1\ ev^2$. Since this mass scale is very different from the existing solar ($\Delta m^2_{21} \sim 10^5\ ev^2$) and the atmospheric ($\Delta m^2_{31} \sim 10^3\ ev^2$) mass differences, this suggests that there may exist a fourth neutrino mass eigenstate, called sterile neutrino, participating in neutrino oscillation[11].The so called *LSND anomaly* has also been observed by the MiniBooNE [79] experiment. The somewhat lower than expected event rate at the Gallium solar neutrino experiments SAGE and GALLEX also points to the hypothesis of ν_e disappearance due to oscillations with a $\Delta m^2 \gtrsim 1\ eV^2$ [80, 81] (*Gallium anomaly*). A recent re-evaluation of the neutrino flux emitted from the reactors has resulted in a somewhat increased fluxes compared to the previous calculation (*reactor anomaly*) and this is also consistent with a sterile neutrino with $\Delta m^2 \sim 1\ ev^2$ [82]. Sterile neutrinos can have a rather significant impact on the measurement of mass hierarchy and CP violation, among other things (see chapter 3).

1.9.2 Non Standard neutrino Interactions (NSI)

Although neutrino mass and mixing will require some new physics beyond the minimal Standard Model, most neutrino oscillation analyses are done assuming Standard Model neutrino interactions. However, in many cases new physics[12] will also introduce additional terms to the neutrino interaction Lagrangian. The usual ansatz is to parameterize these nonstandard interactions (NSI) of neutrinos [33, 85, 86] in terms of dimension-6 operators in an effective Lagrangian. NSI's can affect the oscillation probabilities as a subleading effect and can bring about significant changes on the observable results in the experiments (see chapter 4).

In general, the NSI can impact the neutrino oscillation signals via two kinds of interactions : (a) charged current (CC) interactions (b) neutral current (NC) interactions.

[11] measurements of the invisible Z width indicate that there are only three light active neutrinos [77], a fourth light neutrino must be sterile, i.e., it does not participate in the weak interactions [78].

[12] Supersymmetry could give rise to NSI of neutrinos; in the MSSM with right-handed neutrinos NSI are suppressed [83], but they may be observable in SUSY with R-parity violation [84].

However, CC interactions affect processes only at the source or the detector and these are clearly discernible at near detectors. On the other hand, the NC interactions affect the propagation of neutrinos. In principle NSI of neutrinos could affect the production, propagation, and detection of neutrinos, and in practice can be difficult to disentangle from other effects, such as neutrino oscillations due to neutrino masses and mixing. An important aspect of any future neutrino program will be to identify or constrain these interactions[13].

1.9.3 CPT violation/ Lorentz violation

In local field theories, operators that break CPT invariance are intimately related with those that break Lorentz symmetry [89, 90]. The CPT violating term contributes to the hamiltonian describing the neutrino flavor evolution. CPT violation will manifest itself via $P_{\nu_\alpha \to \nu_\beta} \neq P_{\bar{\nu}_\beta \to \bar{\nu}_\alpha}$. However, when neutrinos and antineutrinos propagate through matter, the matter effect gives rise to fake CP and CPT violating effects[14] which need to be accounted for properly to search for intrinsic CPT violation in neutrino oscillation. Possible origin of CPT violation in the neutrino sector has been studied in literature: in the context of Lorentz violation [91, 92], Extra dimensions [93, 94], in the context of NSI [95].

1.9.4 Neutrino decoherence

Neutrino states are more accurately described by means of wave packets with momentum and spatial uncertainty. Different mass eigenstates propagate with different group velocities; and when the wave packets of different mass eigenstates no longer overlap, coherence is lost. The degree of coherence depends upon both the production and the detection sizes. The possibility of observing decoherence effects and the bounds on decoherence related parameters in a reactor neutrino experiment has been studied in [96]. A different kind of decoherence can also arise from quantum gravity effects, in which the pure states can evolve into mixed states over time [97]. Many studies of possible neutrino decoherence effects has been made: for solar neutrinos [98], atmospheric neutrinos [99], long baseline neutrino experiments [100] and in a general context too [101].

[13] A few experiments have already attempted to put bounds on NSI parameters [87, 88].

[14] This is because matter itself is CP and CPT asymmetric,- neutrinos and antineutrinos interact differently with matter.

1.9.5 Neutrino decay

In the enhanced standard model with massive neutrinos, a heavier neutrino can decay into lighter neutrinos [102]. For lighter neutrinos the lifetime is extremely compared to the age of the universe. Fast neutrino decays may occur at the tree level due to a massless, spinless scalar $J : \nu_i \to \bar{\nu}_j + J$, where i, j are mass eigenstates that may be mixtures of active and the sterile flavors. The couplings of J to ν_μ and ν_e are experimentally constrained by π and K meson decays [103], but these bounds still allow for fast decays. Possible candidates for J include a Majoron [104–106] or a flavor changing axion [107, 108]. The modification in the oscillation probability due to neutrino decay has been treated in literature, for *e.g.*, in [109].

1.9.6 Are the neutrinos Dirac or Majorana particles?

Massive neutrinos can be of either Dirac or Majorana nature. Dirac particles are distinguishable from their anti-particles due to lepton number conservation. On the other hand, Majorana particles are identical with their own antiparticles and they participate in the lepton number violating processes. In the Standard Model the charge-neutral fermion neutrino is the only probable candidate to be of Majorana nature. As noted already in [110], since a Majorana spinor has only two independent components, the Majorana theory is simpler and more economical than the Dirac theory. Hence, the Majorana nature of massive neutrinos may be more natural than the Dirac nature. Determining whether the neutrinos are Dirac or Majorana particles is important to better understand the underlying symmetry of particle interactions and to probe the origin of neutrino masses. If the neutrinos are Majorana, two further CP phases enter into play. These two additional Majorana phases do not appear in a lepton number conserving process like neutrino oscillation [111, 112]. But the Majorana phases enter into the calculation of neutrinoless double beta decay ($0\nu\beta\beta$) [113]. Hence, only the $0\nu\beta\beta$ experiments (see for *e.g.*, [3, 114, 115] for more details) are the probable candidates to explore the Dirac/ Majorana nature of neutrinos.

1.9.7 Neutrino mass generation: *See-saw* mechanism

The most important mechanism for neutrino mass generation is the *see-saw* mechanism. This can explain the smallness of the neutrino mass. The renormalizable SM Lagrangian does not allow neutrino mass terms because there are no right-handed neutrino fields. Consequently, beyond the SM physics is mandated in the neutrino sector. A

simple scheme for neutrino mass generation is to use the SM fields to construct a non-renormalizable addition to the Lagrangian. We know the left handed chiral field ν_L exists and the Lagrangian contains the corresponding Majorana mass term,

$$\mathcal{L}^{L}_{mass} = \frac{1}{2} m_L \nu_L^T \mathcal{C}^\dagger \nu_L + h.c. \tag{1.53}$$

Now assuming the existence of the right handed chiral field ν_R, the neutrino Lagrangian can contain the Dirac mass term,

$$\mathcal{L}^{D}_{mass} = -m_D \bar{\nu_R} \nu_L + h.c. \tag{1.54}$$

However, in addition to the Dirac mass term, the Lagrangian will also contain the right handed Majorana mass term now.

$$\mathcal{L}^{R}_{mass} = \frac{1}{2} m_R \nu_R^T \mathcal{C}^\dagger \nu_R + h.c. \tag{1.55}$$

Therefore, in general it is possible to have a Dirac-Majorana neutrino mass term[15],

$$\begin{aligned} \mathcal{L}^{D+M}_{mass} &= \mathcal{L}^{D}_{mass} + \mathcal{L}^{L}_{mass} + \mathcal{L}^{R}_{mass} \\ &= \frac{1}{2} N_L^T \mathcal{C}^\dagger M N_L + h.c., \end{aligned} \tag{1.56}$$

where $N_L = \begin{pmatrix} \nu_L \\ \nu_R^C \end{pmatrix} = \begin{pmatrix} \nu_L \\ \mathcal{C}\bar{\nu_R}^T \end{pmatrix}$ and M is the mass matrix, $M = \begin{pmatrix} m_L & m_D \\ m_D & m_R \end{pmatrix}$. Note that among all the known elementary particles, all of which have both chiral left-handed and right-handed chiral field components, only neutrinos can have the Majorana mass terms $\mathcal{L}^{L}_{\rm mass}$ and $\mathcal{L}^{R}_{\rm mass}$. This possibility implies that neutrinos are very special particles that can generate new physics through the lepton number violating Majorana mass terms. The right handed neutrino field ν_R is assumed to be a field with a heavy mass m_R (mass scale at which new physics such as lepton no. violation occurs). So, in the limit

$$m_D << m_R, \quad m_L = 0, \tag{1.57}$$

if the mass matrix M is diagonalized, one will obtain the eigenvalues as,

$$m_1 \approx \frac{m_D^2}{m_R}, \quad m_2 \approx m_R. \tag{1.58}$$

[15]The Majorana mass term for ν_L in eq. 1.53, is not allowed by the symmetries and renormalizability of the SM (it is not invariant under $SU(2)_L \times U(1)_Y$ transformations). However, this can be generated by new physics beyond SM. The Majorana mass term in eq. 1.55 for ν_R is allowed by the symmetries of the SM, since ν_R is a singlet of $SU(3)_C \times SU(2)_L \times U(1)_Y$.Therefore, the Dirac-Majorana mass term in eq. 1.56 with $m_L = 0$ is allowed in the framework of the SM with the only addition of the right-handed chiral field ν_R.

Therefore, ν_2 is as heavy as m_R (the new physics mass scale) and ν_1 is very light, because its mass is suppressed with respect to m_D (close to the electroweak mass scale) by the small ratio $\frac{m_D}{m_R}$. This is the famous *see-saw* mechanism[16] [116–119]: the heavy mass of ν_2 is responsible for the light mass of ν_1. There has been extensive study in literature with the see-saw mechanism. For *e.g.*, it is also possible to investigate the viability of the see-saw mechanism when the left-handed Majorana mass (m_L) is small but nonzero in so called *type-II see-saw* [120–124]. In *type-III see-saw* [125, 126], the implication of adding right-handed lepton triplets to the SM fields in the adjoint representation of $SU(2)_L$ has been studied. A direct consequence of the seesaw mechanism is thermal leptogenesis [66] which is needed to understand the observed baryon asymmetry of the universe. There exist other mechanisms also in literature for the generation of neutrino mass: for *e.g.*, Zee model [127], models with $\mu - \tau$ symmetries [128–130], models with specific textures for the mass matrix [131–133], models with low energy new physics such as supersymmetry with R-parity violation [134–136], models with extra dimensions [93, 137–139] *etc.*

1.9.8 Absolute scale of neutrino mass

Constraints on the absolute neutrino mass can be obtained from beta decay, neutrinoless double beta decay ($0\nu\beta\beta$) experiments and from cosmological probes. The present limit on the absolute neutrino mass from the Troitsk [140] and Mainz [141] tritium beta decay experiments is $m_\beta \leq 2.2$ eV at 2σ. The upcoming experiment KATRIN [142] will be able to probe neutrino mass down to as small as 0.35 eV. In the SM, with massive neutrinos and no other new physics, $0\nu\beta\beta$ experiments probe the absolute neutrino masses. Extensive analyses of the past, ongoing and future $0\nu\beta\beta$ experiments have been reviewed in [143]. The best sensitivity was achieved in the Heidelberg-Moscow Ge^{76} experiment [144]. Recent study [145] shows the strongest upper limit on $m^{0\nu}_{\beta\beta}$ ranges from 0.115 to 0.339 eV depending on different choices of nuclear matrix elements. The Planck collaboration [146] provides the cosmological upper bound on neutrino mass to be 0.23 eV [147] and it is consistent with that obtained from $0\nu\beta\beta$ experiments.

The observation of $0\nu\beta\beta$ decay, apart from showing that the neutrinos are massive Majorana particle, will also have interesting implications in determining neutrino mass hierarchy. The spectrum of the effective Majorana mass (see Fig. 1.5) at high value of the lightest neutrino mass is quasi-degenerate and the hierarchy bands are not resolved. For a minimum neutrino mass of about $\lesssim 50$ meV, the degenerate band splits into two, rep-

[16] the so called *type-I see-saw* mechanism

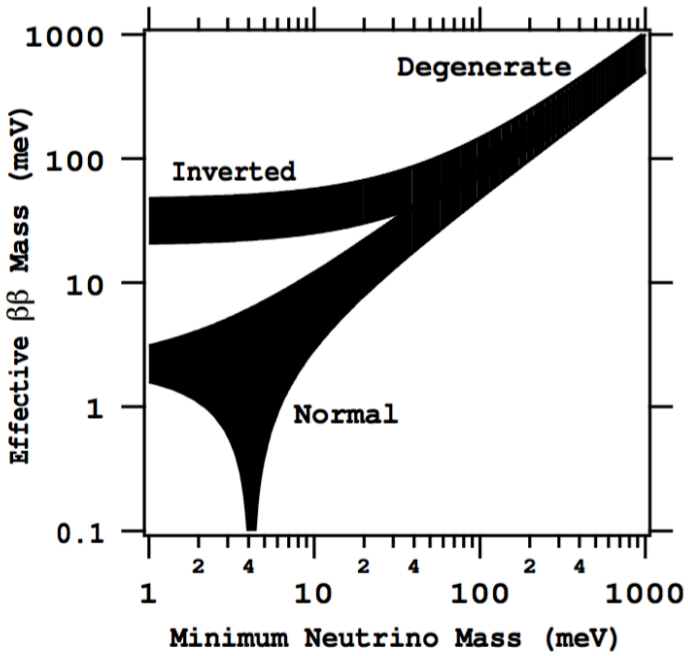

Figure 1.5: Effective Majorana mass $\left(\langle m_{\beta\beta}\rangle = \sum_j m_j U_{ej}^2\right)$ as a function of the lightest neutrino mass (reproduced from [3].

resenting the normal (m_1 lightest) and inverted (m_3 lightest) hierarchies. Fig. 1.5 appears to imply that it would be straight-forward to identify the appropriate band at these low mass values[17].

1.10 An overview of the thesis

To resolve the interesting issues discussed above, a large no. of ambitious neutrino experiments have been designed. This thesis addresses the capabilities of the long baseline neutrino experiments to resolve the issues such as leptonic CPV and mass hierarchy. The main focus is on the upcoming Deep Underground Neutrino Experiment (DUNE) and also on other experiments such as T2K, NOvA and T2HK.

We discuss in chapter 2, how the CP and the mass hierarchy ambiguity arises and the capability of DUNE to resolve these questions. We take into account many possible configurations (such as the presence of a near detector in addition to a far detector, taking the far detector underground to collect the atmospheric neutrino data, changing the exposure

[17]However, there are uncertainties in the oscillation parameters and the matrix elements that have to be considered for a thorough analysis [3].

etc..) of DUNE and compare their capabilities.

In chapter 3, we discuss how the presence of even one eV sterile neutrino can substantially compromise the CPV and hierarchy sensitivities at DUNE and other long baseline experiments. In particular, we illustrate how the additional CP phases can affect the measurement of the standard CP phase depending on the value of the active-sterile mixing angles.

In chapter 4, we discuss about another new physics called Non Standard Neutrino Interaction (NSI) and show how this can potentially affect CPV and mass hierarchy in the probability, event and also on the level of statistical sensitivities.

Chapter 2

Mass hierarchy and CP violation studies at long baseline for standard neutrino oscillation

Neutrino oscillations have by now been conclusively established by several pioneering experiments. It is now understood that the mixing between the three neutrino flavors is governed by the so-called PMNS mixing matrix,

$$U_{\text{PMNS}} = \begin{pmatrix} c_{12}c_{13} & s_{12}c_{13} & s_{13}e^{-i\delta_{\text{CP}}} \\ -s_{12}c_{23} - c_{12}s_{13}s_{23}e^{i\delta_{\text{CP}}} & c_{12}c_{23} - s_{12}s_{13}s_{23}e^{i\delta_{\text{CP}}} & c_{13}s_{23} \\ s_{12}s_{23} - c_{12}s_{13}c_{23}e^{i\delta_{\text{CP}}} & -c_{12}s_{23} - s_{12}s_{13}c_{23}e^{i\delta_{\text{CP}}} & c_{13}c_{23} \end{pmatrix}, \tag{2.1}$$

and the mass-squared differences: $\Delta m^2_{31} = m^2_3 - m^2_1$ and Δm^2_{21}. Here, c_{ij} and s_{ij} are $\cos\theta_{ij}$ and $\sin\theta_{ij}$ respectively, for the three mixing angles θ_{12}, θ_{23} and θ_{13}, and δ_{CP} is a (Dirac) CP phase. While solar and atmospheric neutrino experiments have determined the first two mixing angles quite precisely, reactor experiments have made remarkable progress in determining θ_{13} [54,55,148,149]. (See Table 2.1 for the values of the oscillation parameters used in our work.)

Now that θ_{13} has been conclusively shown to be non-zero and not too small [54, 55, 148–150], the focus of neutrino oscillation experiments has shifted to the measurement of δ_{CP}

that determines whether or not oscillating neutrinos violate CP. Leptonic CP violation is a necessary ingredient to explain the observed baryon asymmetry of the Universe via leptogenesis (for a review, see [68]). Neutrino oscillations at long baselines offer a promising option to infer leptonic CP violation [151–159]. [1]

[1] For more recent status reviews see [160–171].

Table 2.1: Best fit values of the oscillation parameters [6].

Parameter	**Best fit value**
$\sin^2\theta_{12}$	0.307
$\sin^2\theta_{13}$	0.0241
$\sin^2\theta_{23}$ (lower octant)	0.427
$\sin^2\theta_{23}$ (higher octant)	0.613
Δm^2_{21}	7.54×10^{-5} eV^2
$\lvert\Delta m^2_{31}\rvert$	2.43×10^{-3} eV^2
δ_{CP}	0

A second important unanswered question for model building is whether the mass hierarchy is *normal* with $\Delta m^2_{31} > 0$, or *inverted* with $\Delta m^2_{31} < 0$. Finally, the question of whether θ_{23} is larger or smaller than $\pi/4$ bears on models based on lepton symmetries.

An effort towards resolving the above issues and thereby taking us a step closer to completing our knowledge of the neutrino mass matrix, is the Deep Underground Neutrino Experiment (DUNE) [13, 14, 172–174].[2] DUNE will employ a large liquid argon far detector (FD). It is expected to be placed underground in the Homestake mine at a distance of 1300 km from Fermilab, from which a neutrino beam will be directed towards the detector. Large-mass Liquid Argon Time Projection Chambers (LAr-TPCs) have unprecedented capabilities for the detection of neutrino interactions due to precise and sensitive spatial and calorimetric resolution. However, the final configuration of the experiment is still under discussion [176]. The sensitivity of DUNE to the mass hierarchy, to CP violation and to the octant of θ_{23} depends on, among other things, how well other oscillation parameters are known, on the amount of data that can be taken in a reasonable time frame, on the systematic uncertainties that compromise the data, and on the charge discrimination capability of the detector.

The various considerations of our work [176, 177] are motivated by possible configurations for DUNE in the initial phase of its program. The initial stage of DUNE will, at the very least, permit the construction of an unmagnetized 10 kt FD underground. Several improvements upon this basic configuration are under consideration. These might include

[2]The inputs we use, and the corresponding references, pertain to the erstwhile Long Baseline Neutrino Experiment (LBNE) [7, 175], which has undergone a new phase of internationalisation and expansion. This has led to a change in the name of the experiment, to DUNE. Nonetheless, it is expected that the configuration we assume here vis a vis fluxes, baseline and energies will remain largely intact.

- upgrading the FD to 35 kt for improved statistics,
- having a precision near detector (ND) for better calibration of the initial flux and reducing the involved systematic uncertainties,
- magnetizing the FD to make it possible to distinguish between particles and antiparticles in the atmospheric neutrino flux.[3]

It must be noted that some of the above upgrades would also have supplementary benefits –an ND, for example, will also allow precision studies of the involved neutrino nucleon cross sections, thereby reducing present uncertainties.

Since it might not be feasible to combine all of the above upgrades into an initial DUNE configuration, we evaluate which combination would be most beneficial as far as the physics of neutrino oscillations is concerned. Specifically, we study the following experimental configurations:

1. A beam experiment with and without an ND.
2. An atmospheric neutrino experiment.
3. An experiment with and without an ND that combines beam and atmospheric neutrino data collected at the FD.
4. A global configuration that combines DUNE data (with and without ND) with NOνA [9] and T2K [10] data.

Other recent studies of some of the standard physics capabilities of DUNE can be found in Ref. [178–186].

2.1 Mass hierarchy ambiguity and CP violation at the probability level

We consider appearance ($\nu_\mu \to \nu_e$) and disappearance ($\nu_\mu \to \nu_\mu$) channels that are relevant in the context of accelerator-based neutrino oscillation experiments considered in the present work [176, 177]. For the case of matter with standard 3ν scenario (as well as

[3]The beam experiment would have the neutrino and antineutrino runs happen asynchronously. Thus, the events from the two would be naturally distinguished and magnetization of the FD would not affect its results.

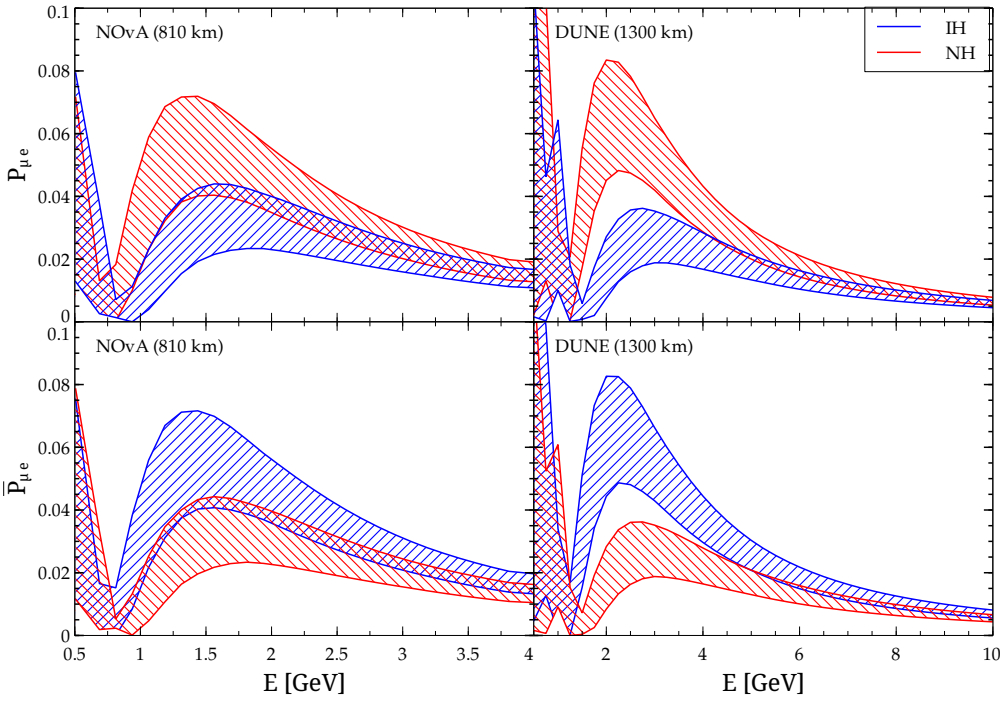

Figure 2.1: The probability ($\nu_\mu \to \nu_e$) bands (due to the variation of $\delta_{CP} \in [-\pi : \pi]$) for both hierarchy have been shown for both NOvA and DUNE. The top (bottom) row is for neutrino (antineutrino) probability. Note the different energy scales for NOvA and DUNE.

in vacuum with $r_A \to 0$) and for normal hierarchy (NH) we can express the probabilities in a compact form as follows [50]:

$$\begin{aligned} P_{\mu e} &= x^2 + y^2 + 2xy\cos(\delta + \lambda L/2) \\ &= x^2 + y^2 + 2xy\cos\delta\cos(\lambda L/2) - 2xy\sin\delta\sin(\lambda L/2) \end{aligned} \tag{2.2}$$

where,

$$\begin{aligned} \lambda = \frac{\Delta m^2_{31}}{2E} \quad ; \quad r_\lambda = \frac{\Delta m^2_{21}}{\Delta m^2_{31}} \quad ; \quad r_A = \frac{A(x)}{\Delta m^2_{31}} \quad ; \quad A(x) = 2\sqrt{2}EG_F n_e(x) \\ x = s_{2\times 13}s_{23}\frac{\sin\{(1-r_A)\lambda L/2\}}{(1-r_A)} \quad ; \quad y = r_\lambda s_{2\times 12}c_{23}\frac{\sin(r_A\lambda L/2)}{r_A} \end{aligned} \tag{2.3}$$

(where n_e is the electron number density and we have used the notation: $s_{2\times 13} = \sin 2\theta_{13}, s_{23} = \sin\theta_{23}$ *etc.*)

For the anti-neutrino channel, we need the following substitutions : $\delta \to -\delta$ and $r_A \to -r_A$. Among the oscillation parameters, $\theta_{12}, \theta_{13}, \Delta m^2_{21}$ have already been measured so far.

Apart from the octant of θ_{23}, the Dirac CP phase $\delta_{\rm CP}$ and the sign of the atmospheric mass squared difference Δm^2_{31} are yet to be determined. When the sign of Δm^2_{31} is positive it is referred to as normal hierarchy (NH) and for negative Δm^2_{31} it is inverted hierarchy (IH). For IH, we need to substitute : $r_A \to -r_A$, $\lambda \to -\lambda$ and $r_\lambda \to -r_\lambda$.

Fig. 2.1 illustrates the hierarchy determination capacities of NOvA and DUNE. The red (blue) band is due to the variation of the standard Dirac CP phase $\delta_{\rm CP} \in [-\pi, \pi]$ for the normal (inverted) mass hierarchy. We mention here that the maximum (minimum) value of $P_{\mu e}$ occurs when $\delta_{\rm CP} = -\pi/2$ $(\pi/2)$ both for NH and IH. For $P_{\bar{\mu}\bar{e}}$, the values of $\delta_{\rm CP}$ are the opposite for max/min[4]. In fig. 2.1, we see that the NH and IH bands overlap for some energy regions,- the degree of overlap being more pronounced for shorter baseline baseline experiments. So if the measured probability happens to have those values lying in the overlapping regions, it may come from either a) NH and some value of the CP violating phase $\delta_{\rm CP}$, or b) IH and some other value of $\delta_{\rm CP}$. This is the hierarchy-$\delta_{\rm CP}$ degeneracy. We observe that for longer baseline experiment like DUNE (right panels fig. 2.1), the less overlap between NH and IH tends to lift the hierarchy-$\delta_{\rm CP}$ ambiguity and in fact, around the energy 2.5 GeV, the NH and IH bands are apart from each other. This indicates that DUNE by itself has a higher capability to lift this degeneracy and resolve the hierarchy ambiguity. We have illustrated this from a detailed statistical point of view in sec. 2.4.

For the discussion of the CP violation, let us briefly review the parameterization of the PMNS mixing matrix $\mathcal{U}$. It is parameterized by three angles $\theta_{12}, \theta_{23}, \theta_{13}$ and one phase δ

$$\mathcal{U}(\{\theta_{ij}\}, \delta) \equiv \mathcal{U}_{23}(\theta_{23}) \cdot \mathcal{W}_{13}(\theta_{13}, \delta) \cdot \mathcal{U}_{12}(\theta_{12}) \tag{2.4}$$

with $\mathcal{W}_{13} = \mathcal{U}_\delta \, \mathcal{U}_{13} \, \mathcal{U}_\delta^\dagger$ and $\mathcal{U}_\delta = \mathrm{diag}\{1, 1, \exp(i\delta)\}$ [5] In the commonly used Pontecorvo-Maki-Nakagawa-Sakata (PMNS) parametrization [187], $\mathcal{U}$ is given by

$$\mathcal{U} = \begin{pmatrix} 1 & 0 & 0 \\ 0 & c_{23} & s_{23} \\ 0 & -s_{23} & c_{23} \end{pmatrix} \begin{pmatrix} c_{13} & 0 & s_{13}e^{-i\delta} \\ 0 & 1 & 0 \\ -s_{13}e^{i\delta} & 0 & c_{13} \end{pmatrix} \begin{pmatrix} c_{12} & s_{12} & 0 \\ -s_{12} & c_{12} & 0 \\ 0 & 0 & 1 \end{pmatrix}, \tag{2.5}$$

where $s_{ij} = \sin\theta_{ij}, c_{ij} = \cos\theta_{ij}$. If neutrinos are Majorana particles, there can be two additional Majorana-type phases in the three flavour case but they are of no consequence

[4]This behaviour can be easily understood from eqn. 2.2

[5]In the general case of n flavors the leptonic mixing matrix $U_{\alpha i}$ depends on $(n-1)(n-2)/2$ Dirac-type CP-violating phases. If the neutrinos are Majorana particles, there are $(n-1)$ additional, so called Majorana-type CP-violating phases.

in neutrino oscillations.. In this parameterization of the PMNS mixing matrix, the mixing between $\nu 1$ and $\nu 3$ mass states contains the CP phase δ. This phase appears twice in the $P(\nu_\mu \to \nu_e)$ (eq. 2.2),- in the CP-odd term ($\sin\delta$-term) and in the CP-even term ($\cos\delta$-term). It is the presence of the nonzero CP-odd term (*i.e.*, $\delta \neq 0$ or π) which induces an asymmetry in the neutrino versus antineutrino oscillation [6]. For detecting the presence of CP, the mixing between $\nu 1$ and $\nu 3$ thus needs to be maximal [175] *i.e.*, $\sin(\lambda L/2) = \pm 1$, which translates to the peak condition for the probability (in eq. 2.2),

$$\frac{L(\text{km})}{E(GeV)} \approx (2n-1)\ 510\ \text{km/ GeV} \tag{2.6}$$

For DUNE ($L = 1300$ km), for the 1st oscillation maxima ($n = 1$) this gives $E \approx 2.5$ GeV. We also note that (see fog. 2.1), this is the position of the peak of the probabilities and the two hierarchies are farthest apart around 2.5 GeV. Hence, while determining both the mass hierarchy and the CP violation with DUNE, the dominant contribution is expected to come from around 2.5 GeV. The incident ν_μ beam used by the collaboration [175] has also been engineered to utilise this energy(see fig. 2.3). For the shorter baseline experiments this energy is calculated to be ~ 1.5 GeV (NOvA, $L = 810$ km) and ~ 0.6 GeV (T2K, $L = 295$ km).

A measurement of the value of $\delta_{\text{CP}} \neq 0$ or π the standard three-flavor model, would imply CP violation in the leptonic sector. If CP is conserved, $\delta_{\text{CP}} = 0$ and $P(\nu_\mu \to \nu_e) = P(\bar{\nu}_\mu \to \bar{\nu}_e)$. In order to quantify effects due to CP violation, one can define the following observable CP asymmetry

$$A_{\mu e}^{CP}(\delta) \;=\; \frac{P(\nu_\mu \to \nu_e)\delta - P(\bar{\nu}_\mu \to \bar{\nu}_e)\delta}{P(\nu_\mu \to \nu_e)\delta + P(\bar{\nu}_\mu \to \bar{\nu}_e)\delta} = \frac{\Delta P_{\mu e}(\delta)}{\sum P_{\mu e}(\delta)}\,. \tag{2.7}$$

In the 3-flavor model, the asymmetry can be approximated to leading order in Δm^2_{21} as [158],

$$A_{\mu e}^{CP}(\delta_{\text{CP}}) \sim \frac{\cos\theta_{23}\ \sin 2\theta_{12}\ \sin\delta_{\text{CP}}}{\sin\theta_{23}\ \sin\theta_{13}} \left(\frac{\Delta m^2_{21}\ L}{4E}\right) + \text{matter effects} \tag{2.8}$$

In the context of long baseline experiments where matter can induce fake CP effects, a nonzero value of $A_{\mu e}^{CP}(\delta)$ does not unequivocally imply intrinsic CP violation arising due to the Dirac CP phase (see eq. 2.8). It is clear from both eq. 2.8 and the corresponding fig. 2.2 that a zero δ_{CP} implies a zero CP asymmetry for vacuum. But, if matter effect is not

[6] Note that the disappearance channel (see eq. 2.22) contains only the CP-even term and thereby induces no CP asymmetry (assuming CPT is conserved). Hence asymmetries in neutrino versus antineutrino oscillations arising for CP violation effects can only be accessed by appearance experiments.

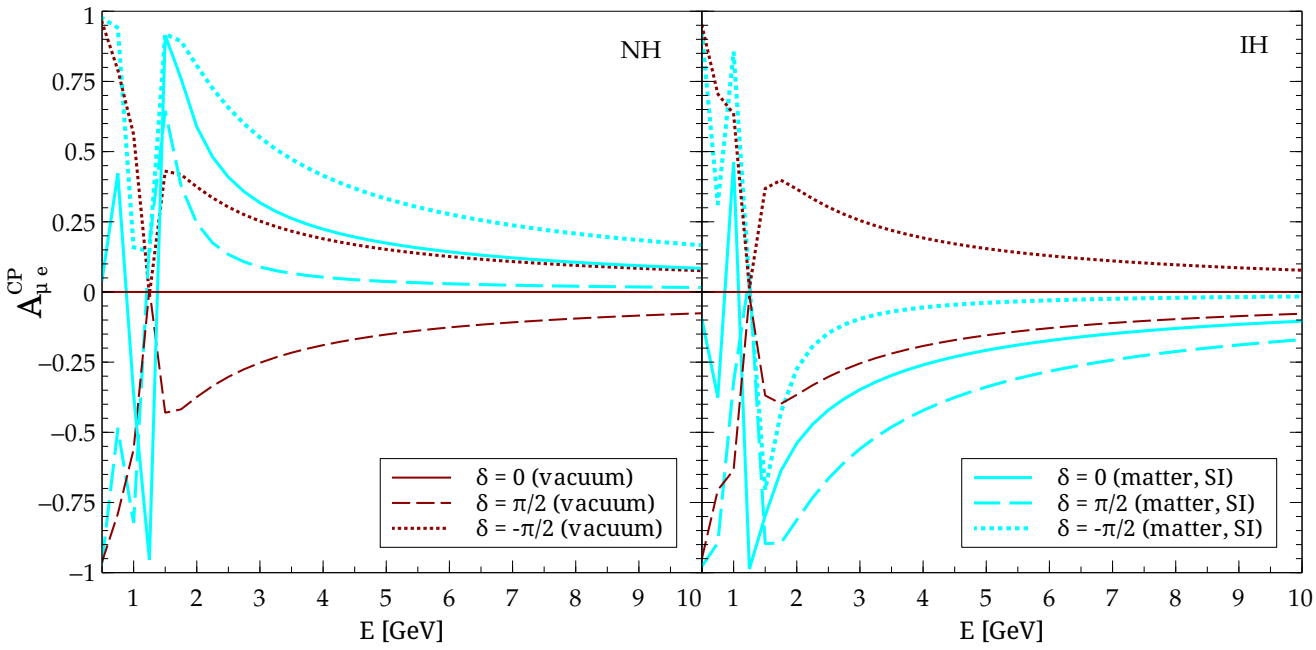

Figure 2.2: $A^{\mu e}_{cp}$ is shown as a function of energy for both matter (cyan) and vacuum (brown) for three fixed values of the standard Dirac CP phase $\delta_{\rm CP}$. The left (right) panel is for the true normal (inverted) hierarchy.

negligible, even a vanishing $\delta_{\rm CP}$ still gives nonzero CP asymmetry arising due to purely matter effect (*i.e.*, a fake CP violating effect). So for long baseline experiments such as DUNE, where the neutrino beam propagates through the earth's mantle, the leptonic CP violation effects must be disentangled from the matter effect. [7]

2.2 Simulation

The far detector (FD) in DUNE is most likely to be built underground so that it is sensitive to the atmospheric neutrinos, in addition to accelerator neutrinos. Additionally, there is a proposal to build a near detector (ND) as well. We have studied the experiment by simulating the FD and the ND for both these scenarios (accelerator and atmospheric neutrino).

[7] To get over the problem of differentiating between the case of CP violation due to intrinsic CP phase and CP violation arising due to the matter effect, other observables have been introduced [188] which can prove useful not only to establish whether CP violation effects arise purely due to the Dirac type CP phase or a combination of the intrinsic and extrinsic CP phases but also to distinguish between the cases based on spectral differences.

2.2.1 Simulation of long baseline experiment

The theoretically expected differential event rate is given by [14],

$$\frac{dN_{\nu_e}^{app}(E,L)}{dE} = R_{det} \times \Phi_{\nu_\mu}(E,L) \times P_{\mu e}(E,L) \times \sigma_{\nu_e}(E)\,, \tag{2.9}$$

where, R_{det} is the detector response function containing the detector energy resolution, fiducial mass of the detector and the detection efficiency;
$P_{\mu e}(E,L)$ is the appearance probability for $\nu_\mu \to \nu_e$ in matter, $\Phi_{\nu_\mu}(E,L)$ is the flux of ν_μ;
$\sigma_{\nu_e}(E)$ is the charged current (CC) cross section of ν_e given by

$$\sigma_{\nu_e} = 0.67 \times 10^{-42}(m^2/GeV/N) \times E\,, \quad \text{for} \quad E > 0.5\ \text{GeV}. \tag{2.10}$$

For the disappearance channel, $P_{\mu e}$ is to be replaced by $P_{\mu\mu}$ and $\sigma_{\nu_e} \to \sigma_{\nu_\mu}$. Note that $\sigma_{\nu_\mu} \sim \sigma_{\nu_e}$ for the considered energy range. For antineutrinos, $\nu_\mu \to \bar{\nu}_\mu$ and $\nu_e \to \bar{\nu}_e$ and $P_{\mu e} \to \bar{P}_{\mu e}$.

For the simulation of the long baseline neutrino experiments (DUNE, NOvA, T2K), we have used the GLoBES (General Long Baseline Experiment Simulator) [189,190] software where the events have been simulated by taking eq. 2.15 into consideration. For studying the CP violation and the mass hierarchy capability of DUNE in the standard 3 neutrino scenario in our papers [176,177] , we simulated neutrinos resulting from a 120 GeV proton beam from Fermilab with a beam power of 700 kW and an uptime of 1.65×10^7 seconds per year (or equivalently 6×10^{20} protons on target (POT) per year) incident at a LAr FD at a baseline of 1300 km; an upgrade to a 2.3 MW beam is a possibility. We assume that the beam is run in the neutrino mode for a period of five years, and thereafter in the antineutrino mode for five more years.

In our simulation of the DUNE beam experiment we employ the signal and background systematics for ν_e appearance and ν_μ disappearance channels from Refs. [7, 8]. [8] For the energy resolutions, we have used the method of bin-based automatic energy smearing with $\frac{\sigma}{E} = \frac{0.20}{\sqrt{E}}$ for ν_μ events and $\frac{\sigma}{E} = \frac{0.15}{E}$ for ν_e events; see the appendix of Ref. [7]. An alternative is to use migration matrices [7, 191]. The flux files for DUNE were obtained from the collaboration [192] and for the cross sections [193, 194] were consulted. We show the flux and the crosssections used for GLoBES simulation in fig. 2.3.

[8] Our ND analysis represents the most obvious benefit that the beam experiment will reap with an ND, *viz.*, improvement in systematics for the signal and background events. In addition, an ND will also improve our understanding of the fluxes and cross sections, thereby reducing shape-related uncertainties in the analysis. We do not attempt an exploration of this facet of the ND because the exact nature of the improvement would depend to a large extent on the specifics of the ND, which for the DUNE is yet in the planning stage. Our ND analysis represents a worst-case scenario for improvement in the systematics.

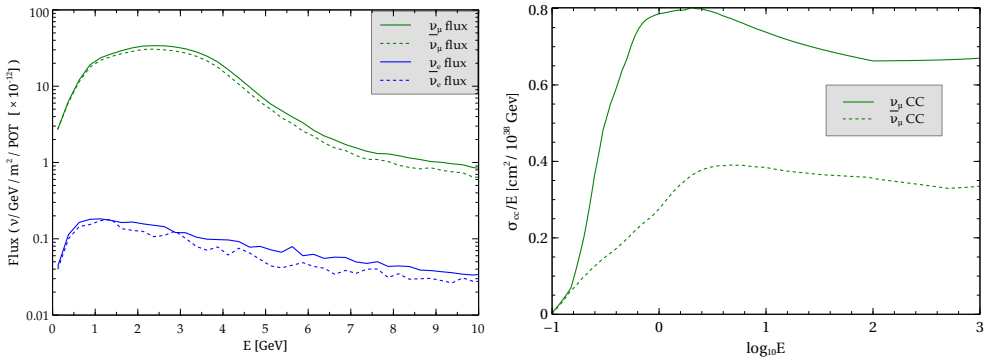

Figure 2.3: The neutrino and antineutrino fluxes are shown in the left panel. The right panel shows the ν and $\bar{\nu}$ charged current cross sections.

Table 2.2: Systematic uncertainties for signal and background channels in DUNE [7,8].

Detector configuration	Systematics	
	Signal	Background
With ND	ν_e: 1% ν_μ: 1%	ν_e: 1% ν_μ: 5%
Without ND	ν_e: 5% ν_μ: 5%	ν_e: 10% ν_μ: 45%

For modelling the matter effect, the PREM (Preliminary Reference Earth Model) density profile [195] was used in GLoBES. The systematics values used for DUNE are listed in table 2.2.

The simulation details for NOvA [9] and T2K [10,196,197] are given in tables 2.3 and 2.4 respectively.

Table 2.3: Systematic uncertainties for NOνA [9].

Detector configuration	Systematics	
	Signal	Background
15 kt TASD 3 yrs. ν + 3 yrs. $\bar{\nu}$ 6×10^{20} POT/yr with a 700 kW beam	ν_e: 5% ν_μ: 2%	ν_e: 10% ν_μ: 10%

Table 2.4: Systematic uncertainties for T2K [10].

Detector configuration	Systematics	
	Signal	Background
22.5 kt water Cherenkov 5 yrs. ν 8.3×10^{20} POT/yr with a 770 kW beam	ν_e: 5% ν_μ: 5%	ν_e: 5% ν_μ: 5%

2.2.2 Simulation of atmospheric neutrinos

For the simulation of the atmospheric neutrinos at DUNE, we have written a C++ code and we briefly describe the method below.

The total number of CC events is obtained by folding the relevant incident neutrino fluxes with the appropriate disappearance and appearance probabilities, relevant CC cross sections, and the detector efficiency, resolution, mass, and exposure time. For our analysis, we consider neutrinos with energy in the range $1-10$ GeV in 10 uniform bins, and the cosine of the zenith angle θ in the range -1.0 to -0.1 in 18 bins. The μ^- event rate in an energy bin of width dE and in a solid angle bin of width $\mathrm{d}\Omega$ is,

$$\frac{\mathrm{d}^2\mathrm{N}_\mu}{\mathrm{d}\Omega\ \mathrm{dE}} = \frac{1}{2\pi}\left[\left(\frac{\mathrm{d}^2\Phi_\mu}{\mathrm{d}\cos\theta\ \mathrm{dE}}\right)\mathrm{P}_{\mu\mu} + \left(\frac{\mathrm{d}^2\Phi_\mathrm{e}}{\mathrm{d}\cos\theta\ \mathrm{dE}}\right)\mathrm{P}_{\mathrm{e}\mu}\right]\sigma_{\mathrm{CC}}\mathrm{D}_{\mathrm{eff}}\,. \tag{2.11}$$

Here Φ_μ and Φ_e are the ν_μ and ν_e atmospheric fluxes, $P_{\mu\mu}$ and $P_{e\mu}$ are disappearance and appearance probabilities in obvious notation, σ_{CC} is the total CC cross section and $\mathrm{D}_{\mathrm{eff}}$ is the detector efficiency. The μ^+ event rate is similar to the above expression with the fluxes, probabilities and cross sections replaced by those for antimuons. Similarly, the e^- event rate in a specific energy and zenith angle bin is

$$\frac{\mathrm{d}^2\mathrm{N}_\mathrm{e}}{\mathrm{d}\Omega\ \mathrm{dE}} = \frac{1}{2\pi}\left[\left(\frac{\mathrm{d}^2\Phi_\mu}{\mathrm{d}\cos\theta\ \mathrm{dE}}\right)\mathrm{P}_{\mu\mathrm{e}} + \left(\frac{\mathrm{d}^2\Phi_\mathrm{e}}{\mathrm{d}\cos\theta\ \mathrm{dE}}\right)\mathrm{P}_{\mathrm{ee}}\right]\sigma_{\mathrm{CC}}\mathrm{D}_{\mathrm{eff}}\,, \tag{2.12}$$

with the e^+ event rate being expressed in terms of antineutrino fluxes, probabilities and cross sections.

We take into account the smearing in both energy and zenith angle, assuming a Gaussian form for the resolution function, R. For energy, we use,

$$\mathrm{R}_\mathrm{E}(\mathrm{E_t}, \mathrm{E_m}) = \frac{1}{\sqrt{2\pi}\sigma}\exp\left[-\frac{(\mathrm{E_m}-\mathrm{E_t})^2}{2\sigma^2}\right]. \tag{2.13}$$

Here, $\mathrm{E_m}$ and $\mathrm{E_t}$ denote the measured and true values of energy respectively. The smearing width σ is a function of $\mathrm{E_t}$.

The smearing function for the zenith angle is a bit more complicated because the direction of the incident neutrino is specified by two variables: the polar angle θ_t and the azimuthal angle ϕ_t. We denote both these angles together by Ω_t. The measured direction of the neutrino, with polar angle θ_m and azimuthal angle ϕ_m, which together we denote by Ω_m, is expected to be within a cone of half angle $\Delta\theta$ of the true direction. The angular smearing is done in a small cone whose axis is given by the direction $\theta_\mathrm{t}, \phi_\mathrm{t}$. The set of directions within the cone have different polar angles and azimuthal angles. Therefore, we need to construct a smearing function which takes into account the change in the azimuthal coordinates as well. Such an angular smearing function is given by,

$$\mathrm{R}_\theta(\Omega_\mathrm{t}, \Omega_\mathrm{m}) = \mathrm{N} \exp\left[-\frac{(\theta_\mathrm{t} - \theta_\mathrm{m})^2 + \sin^2\theta_\mathrm{t}\,(\phi_\mathrm{t} - \phi_\mathrm{m})^2}{2(\Delta\theta)^2}\right], \tag{2.14}$$

where N is a normalisation constant.

Now, the ν_μ event rate with the smearing factors taken into account is given by,

$$\frac{\mathrm{d}^2\mathrm{N}_\mu}{\mathrm{d}\Omega_\mathrm{m}\,\mathrm{dE_m}} = \frac{1}{2\pi}\int\int \mathrm{dE_t}\,\mathrm{d}\Omega_\mathrm{t}\,\mathrm{R_{EN}}(\mathrm{E_t}, \mathrm{E_m})\,\mathrm{R}_\theta(\Omega_\mathrm{t}, \Omega_\mathrm{m})\left[\Phi^\mathrm{d}_\mu\,\mathrm{P}_{\mu\mu} + \Phi^\mathrm{d}_\mathrm{e}\,\mathrm{P}_{\mathrm{e}\mu}\right]\sigma_\mathrm{CC}\mathrm{D_{eff}}\,, \tag{2.15}$$

and similarly for the ν_e event rate. We have introduced the notation,

$$(\mathrm{d}^2\Phi/\mathrm{d}\cos\theta\;\mathrm{dE})_{\mu,\mathrm{e}} \equiv \Phi^\mathrm{d}_{\mu,\mathrm{e}}.$$

Since $\mathrm{R_{EN}}(\mathrm{E_t}, \mathrm{E_m})$ and $\mathrm{R}_\theta(\Omega_\mathrm{t}, \Omega_\mathrm{m})$ are Gaussian, they can easily be integrated over the true angle Ω_t and the true energy $\mathrm{E_t}$. Then, integration over the measured energy $\mathrm{E_m}$ and measured angle Ω_m is carried out using the VEGAS Monte Carlo Algorithm.

For the atmospheric neutrino analysis, and consequently the combined beam and atmospheric analysis, it becomes important to consider both a magnetized and an unmag-

Table 2.5: Detector parameters used for the analysis of atmospheric neutrinos [11].

Rapidity (y)	0.45 for ν 0.30 for $\bar{\nu}$
Energy Resolution (ΔE)	$\sqrt{(0.01)^2 + (0.15)^2/(yE_\nu) + (0.03)^2}$
Angular Resolution ($\Delta\theta$)	3.2° for ν_μ 2.8° for ν_e
Detector efficiency ($\mathcal{E}$)	85%

netized LAr detector. In the former case, the detector sensitivity, especially for the resolution of the mass hierarchy, is significantly improved over the latter, due to its ability to distinguish between particles and antiparticles. This, however, is only partly applicable to the ν_e events, because for a 10 kt volume detector, it is difficult to distinguish between the tracks arising from of ν_e and $\bar{\nu}_e$ interactions. This difficulty arises because pair-production and bremsstrahlung sets in with increasing energies, and above ≈ 5 GeV, the detector completely loses its ability to distinguish between these CP conjugate pairs. On the other hand, due to their tracks being significantly longer, ν_μ and $\bar{\nu}_\mu$ events are clearly distinguishable at all accessible energies. We implement this in our detector simulation for the atmospheric neutrino and combined analysis.

For our simulation of atmospheric neutrino data, the energy and angular resolutions of the detector are as in table 2.5 [11]. The atmospheric fluxes are taken from Ref. [198] and the flux and systematic uncertainties from Ref. [12].

The charge identification capability of the detector is incorporated as discussed in Ref. [11] . For electron events, we conservatively assume a 20% probability of charge identification in the energy range $1 - 5$ GeV, and no capability for events with energies above 5 GeV. Since the muon charge identification capability of a LAr-TPC is excellent for energies between 1 and 10 GeV, we have assumed it to be 100%.

2.3 Method of χ^2 analysis

The calculation of χ^2 gives a measure of the validity of some theoretical hypothesis against a set of experimental data. To put it simply, χ^2 measures the amount of *deviation* between following two datasets,-
a) The dataset produced by the actual experiment,- called the *true* or simply *data*.
b) The dataset assuming the theoretical hypothesis, - called the *test* or *fit*.

The computation of χ^2 for a fixed set of parameters (test) is performed using the method of pulls. This method allows us to take into account the various statistical and systematic uncertainties in a straightforward way. The flux, cross sections and other systematic uncertainties are included by allowing these inputs to deviate from their standard values in the computation of the expected (test) event rate in the i-j$^{\text{th}}$ bin, $\mathrm{N}_{\mathrm{ij}}^{\mathrm{test}}$. Let the k^{th} input deviate from its standard value by $\sigma_{\mathrm{k}}\ \xi_{\mathrm{k}}$, where σ_{k} is its uncertainty. Then the value

of N_{ij}^{test} with the modified inputs is

$$N_{ij}^{test} = N_{ij}^{test}(std) + \sum_{k=1}^{npull} c_{ij}^{k}\, \xi_k \,, \tag{2.16}$$

where $N_{ij}^{test}(std)$ is the expected (test) event rate in the i-jth bin calculated with the standard values of the inputs and npull is the number of sources of uncertainty, which is 5 in our case. The ξ_k's are called the *pull* variables and they determine the number of σ's by which the k^{th} input deviates from its standard value. In Eq. (2.16), c_{ij}^{k} is the change in N_{ij}^{test} when the k^{th} input is changed by σ_k (*i.e.* by 1 standard deviation). Since the uncertainties in the inputs are not very large, we only consider changes in N_{ij}^{test} that are linear in ξ_k. Thus we have the modified χ^2 [9] defined as,

$$\chi^2(\xi_k) = \sum_{i,j} \frac{\left[\, N_{ij}^{true} - (N_{ij}^{test}(std) \;+\; \sum_{k=1}^{npull} c_{ij}^{k}\, \xi_k) \,\right]^2}{N_{ij}^{true}} + \sum_{k=1}^{npull} \xi_k^2 \,, \tag{2.17}$$

where the additional ξ_k^2-dependent term is the penalty imposed for moving the value of the k^{th} input away from its standard value by $\sigma_k\, \xi_k$. The calculation of χ^2 takes into account the contribution from all the channels. So, for the beam analysis where the neutrino and antineutrino can be distinguished (see footnote 3), the χ^2 with pulls, which includes the effects of all theoretical and systematic uncertainties, is obtained by minimizing with respect to all the pulls ξ_k:

$$\chi^2_{pull}(beam) = Min_{\xi_k} \left[\chi^2_{\mu e}(\xi_k) + \chi^2_{\mu\mu}(\xi_k) + \chi^2_{\bar{\mu}\bar{e}}(\xi_k) + \chi^2_{\bar{\mu}\bar{\mu}}(\xi_k)\right] . \tag{2.18}$$

where, $\chi^2_{\mu e}(\xi_k)$ is for the channel $\nu_\mu \to \nu_e$ *etc.*.

For the atmospheric neutrinos, the corresponding expression is (if FD is not magnetized):

$$\chi^2_{pull}(atmos) = Min_{\xi_k} \left[\chi^2_{\mu e+\bar{\mu}\bar{e}}(\xi_k) + \chi^2_{\mu\mu+\bar{\mu}\bar{\mu}}(\xi_k)\right] . \tag{2.19}$$

where, $\chi^2_{\mu e+\bar{\mu}\bar{e}}(\xi_k)$ takes into account the sum of the events for the channels $\nu_\mu \to \nu_e$ and $\nu_{\bar{\mu}} \to \nu_{\bar{e}}$ (since the sign of the particle cannot be distinguished for an unmagnetized FD).

[9] Throughout our work $\Delta\chi^2 = \chi^2$ as no fluctuations in simulated data was included [199]. This is the Pearson's definition of χ^2 [200], which is what GLoBES actually uses by considering systematics too. For other types of χ^2 analysis (using frequentist or Bayesian approach) see [200–204]. For large no. of samples, both of these methods of calculating χ^2 give very similar results.

Table 2.6: Uncertainties for various quantities [12].

Quantity	**Value**
Flux normalization uncertainty	20%
Zenith angle dependence uncertainty	5%
Cross section uncertainty	10%
Overall systematic uncertainty	5%
Tilt uncertainty	$\Phi_\delta \approx \Phi_0(E)\left[1+\delta\log\left(\frac{E}{E_0}\right)\right]$ with $E_0 = 2$ GeV, $\sigma_\delta = 5\%$ (see, *e.g.*, [206])

For a magnetized FD, taking into consideration the limited charge distinguishing capability of LAr detector (see subsection 2.2.2) the corresponding expression is [205],

$$\begin{aligned}\chi^2_{\text{pull}}(\text{atmos}) &= \text{Min}_{\xi_k}\Bigg[\chi^2_{\mu\mu}(\xi_k)+\chi^2_{\bar{\mu}\bar{\mu}}(\xi_k)+0.2\Big(\chi^2_{\mu e}(\xi_k)+\chi^2_{\bar{\mu}\bar{e}}(\xi_k)\Big)_{\text{1-5 GeV}} \\ &+ 0.8\chi^2_{\mu e+\bar{\mu}\bar{e}}(\xi_k)_{\text{1-5 GeV}}+\chi^2_{\mu e+\bar{\mu}\bar{e}}(\xi_k)_{\text{5-10 GeV}}\Bigg]. \end{aligned} \tag{2.20}$$

In the calculation of χ^2_{pull}, we consider uncertainties in the flux, cross sections etc. (as in table 2.6), keeping the values of the oscillation parameters fixed while calculating $\text{N}^{\text{true}}_{\text{ij}}$ and $\text{N}^{\text{test}}_{\text{ij}}$. However, in general, the values of the mass-squared difference Δm^2_{31} and the mixing angles θ_{23} and θ_{13} can vary over a range corresponding to the actual measurements of these parameters. Holding them fixed at particular values is equivalent to knowing the parameters to infinite precision, which is obviously unrealistic. To take into account the uncertainties in the actual measurement of the oscillation parameters, we define the marginalized χ^2 as [12]

$$\begin{aligned}\chi^2_{\text{min}} &= \text{Min}\Bigg[\chi^2(\xi_{\text{k}})+\left(\frac{|\Delta\text{m}^2_{31}|^{\text{true}}-|\Delta\text{m}^2_{31}|}{\sigma(|\Delta\text{m}^2_{31}|)}\right)^2 \\ &+\left(\frac{\sin^2 2\theta^{\text{true}}_{23}-\sin^2 2\theta_{23}}{\sigma(\sin^2 2\theta_{23})}\right)^2+\left(\frac{\sin^2 2\theta^{\text{true}}_{13}-\sin^2 2\theta_{13}}{\sigma(\sin^2 2\theta_{13})}\right)^2\Bigg]. \end{aligned} \tag{2.21}$$

The three terms added to $\chi^2(\xi_k)$ are known as *priors*. For our combined (beam and atmospheric) analysis, we take the χ^2 contributions from both the beam and the atmospheric simulations (inside the square bracket in eqn. 2.21) and then do the minimization to obtain the total minimized χ^2. Below we mention a few more informations regarding the χ^2 analysis.

- For the marginalization procedure, we allow θ_{23}, θ_{23}, $|\Delta m^2_{31}|$ and $\delta_{\rm CP}$ to vary within the following ranges:
  $\theta_{23} \in [36^\circ, 54^\circ]$,
  $\theta_{13} \in [5.5^\circ, 11^\circ]$,
  $|\Delta m^2_{31}| \in [2.19, 2.62] \times 10^{-3}$ eV^2,
  $\delta_{\rm CP} \in [-\pi, \pi]$.

- In computing $\chi^2_{\rm min}$, we add the priors for the neutrino parameters which assigns a penalty for moving away from the true value. During marginalization, as the value of an oscillation parameters shifts further from its true value, Eq. (2.21) suggests that the corresponding prior will be larger resulting in a higher χ^2 value.

- Finally, after adding the priors, we determine $\chi^2_{\rm pull}$ (see Eq. 2.18). This is a multi-dimensional parameter space minimization of the function $\chi^2(\alpha, \beta, \dots)$, where α, $\beta, \dots$ are the parameters over which marginalization is required. For the purpose of this multi-minimization, we have used the NLopt library [207]. We do the minimization first over the entire multi-dimensional parameter space to locate the global minimum approximately, and then use the parameters corresponding to this as a guess to carry out a local minimum search to locate the minimized χ^2 within the parameter space accurately. We carry out this minimization routine using a simplex algorithm described in Ref. [208] , and implemented within the NLopt library.

2.4 Results: mass hierarchy

Since $\delta_{\rm CP}$ will likely remain undetermined by experiments preceding DUNE, we analyze the sensitivity to the mass hierarchy as a function of this parameter. The analysis is carried out by assuming one of the hierarchies to be *true* and then determining by means of a χ^2 test (using our simulation: see sections 2.2 and 2.3), how well the opposite hierarchy (in the *test* dataset) can be excluded. We marginalize over the present day uncertainties of each of the prior determined parameters.

The $\delta_{\rm CP}$ dependence of the sensitivity to the mass hierarchy arises through the oscillation probability [209],

2.4.1 Analysis with a 35 kt unmagnetized LAr FD

As is illustrated from Fig. 2.4, mass hierarchy resolution benefits significantly from having an ND. But, note that the results with or without an ND are similar for regions

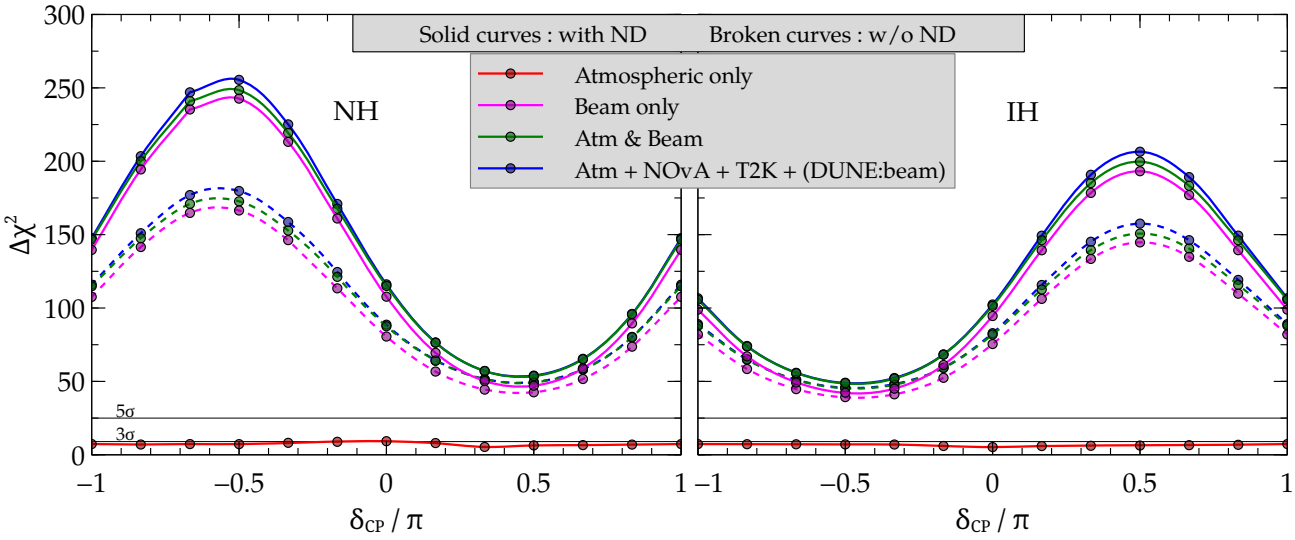

Figure 2.4: Sensitivity to the mass hierarchy as a function of true δ_{CP} for a true normal hierarchy (NH) and a true inverted hierarchy (IH) with an 350 kt-yr exposure at the unmagnetized far detector configured with and without a near detector (ND). A run-time of 5 years each (3×10^{21} protons on target) with a ν and $\bar{\nu}$ beam is assumed. The combined sensitivity with NOνA (15 kt TASD, 3 yrs. ν + 3 yrs. $\bar{\nu}$) and T2K (22.5 kt water cerenkov, 5 yrs. ν) data is also shown.

of δ_{CP} where the sensitivity is worse ($\delta_{CP} \in [45°, 135°]$ for the normal hierarchy and $\delta_{CP} \in [-135°, -45°]$ for the inverted hierarchy).

Since the wrong hierarchy can be excluded by the DUNE beam-only experiment to significantly more than 5σ with an unmagnetized LAr FD and an exposure of 350 kt-yrs. without the help of ND, the added contributions of both the atmospheric neutrinos, and the better signal and background systematics provided by an ND, are not essential for this measurement.[10]

Similar conclusions can be drawn for a 10 kt FD from Fig. 2.5. For a 100 kt-yr exposure, the combined analysis resolves the hierarchy to more than 5σ for a large δ_{CP} fraction, and to more than 3σ for all values of δ_{CP}. We have also shown the sensitivity to mass hierarchy for NOvAin fig. 2.6 just for having an idea of the magnitude of the χ^2.

2.4.2 Exposure analysis

We now evaluate the exposure needed to resolve the mass hierarchy for the entire range of δ_{CP}. In Fig. 2.7, we show the CP fraction (f($\sigma > 3$)) for which the sensitivity to mass

[10]This is consistent with the discussion in sec. 2.1 regarding DUNE's high capability of resolving mass hierarchy by itself

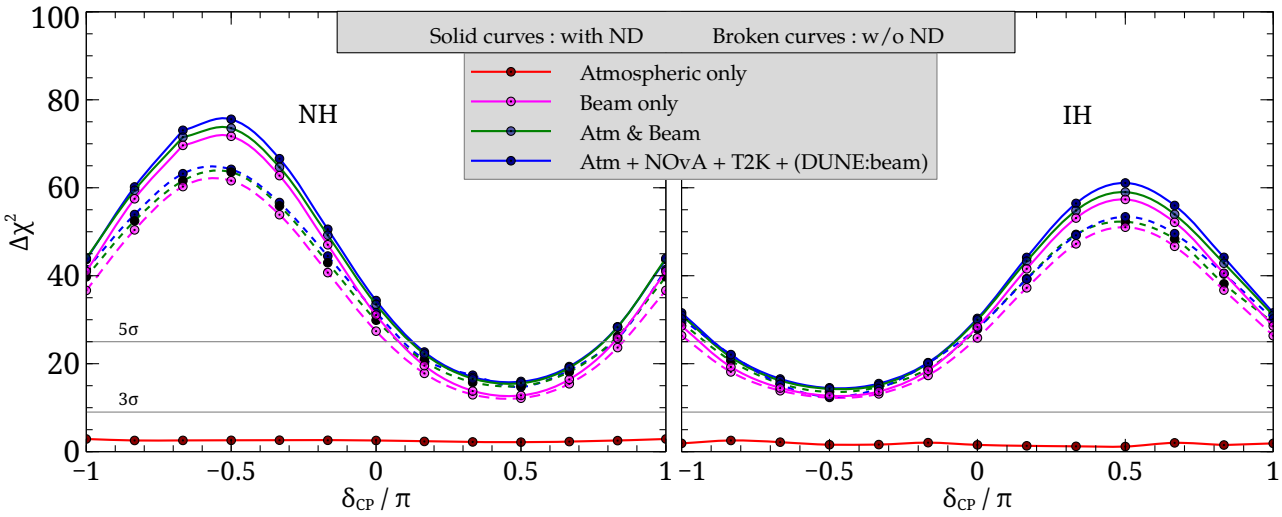

Figure 2.5: Similar to Fig. 2.4 but for a 100 kt-yr unmagnetized LAr FD.

hierarchy is greater than 3σ, as a function of exposure. Salient points evident from Fig. 2.7 are:

- For a beam only analysis, we see that a 3σ determination of the hierarchy for any $\delta_{\rm CP}$ value is possible with a roughly 50 kt-MW-yr exposure. This means the hierarchy can be resolved by a 35 kt FD and a 700 kW beam in about two years.
- A near detector does not significantly reduce the exposure needed for a 3σ measurement.
- Information from atmospheric neutrinos reduces the exposure required to only about 45 kt-MW-yr.
- A further combination with NOνA and T2K data provides minor improvement.

2.4.3 Variation of systematics

In Fig. 2.8, we show the maximum sensitivity to the mass hierarchy for the entire $\delta_{\rm CP}$ (true) space as a function of the exposure. We have allowed for variations in systematics for DUNE with an ND that are 3 times as large or small as those in Table 2.2). The width of the band produced by this procedure may be considered as a measure of the effect of systematics on the hierarchy sensitivity when an ND is used (which seems to be the likely scenario in practice) along with an FD. We observe the following features from Fig. 2.8:

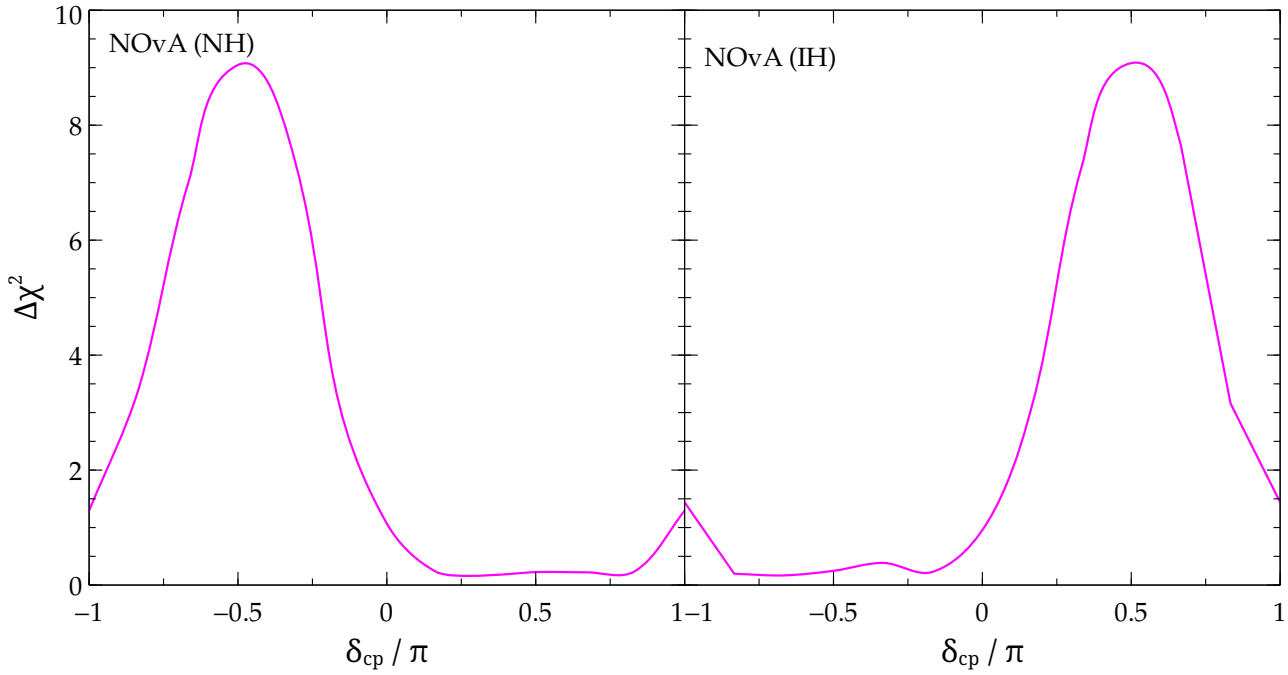

Figure 2.6: The sensitivity to mass hierarchy for NOvA alone for 3 years of ν and 3 years of $\bar{\nu}$ running.

- For the NH (left panel), both 3σ and 5σ levels of sensitivity can be reached with an exposure of about 50 and 120 kt-MW-yr, respectively. This is consistent with Fig. 2.7 wherein the solid magenta curve in the left panel reaches unity at roughly 50 kt-MW-yr.

- For exposures below $\sim$ 20 kt-MW-yr, the sensitivity is not statistically significant ($\lesssim 1.5\sigma$).

- The variation of systematics has a small effect on the sensitivities for lower exposures ($\lesssim$ 100 kt-MW-yr) and the effect gets slightly magnified for larger exposures, as evident from the widening of the bands.

- The hierarchy sensitivity for a true IH scenario (right panel of Fig. 2.8) shows qualitatively similar behaviour as that for NH.

2.4.4 Effect of magnetization

In Fig. 2.9, we compare the sensitivity to the mass hierarchy of an unmagnetized and magnetized 100 kt-yr LAr FD for a true NH. As discussed earlier, magnetizing the detector

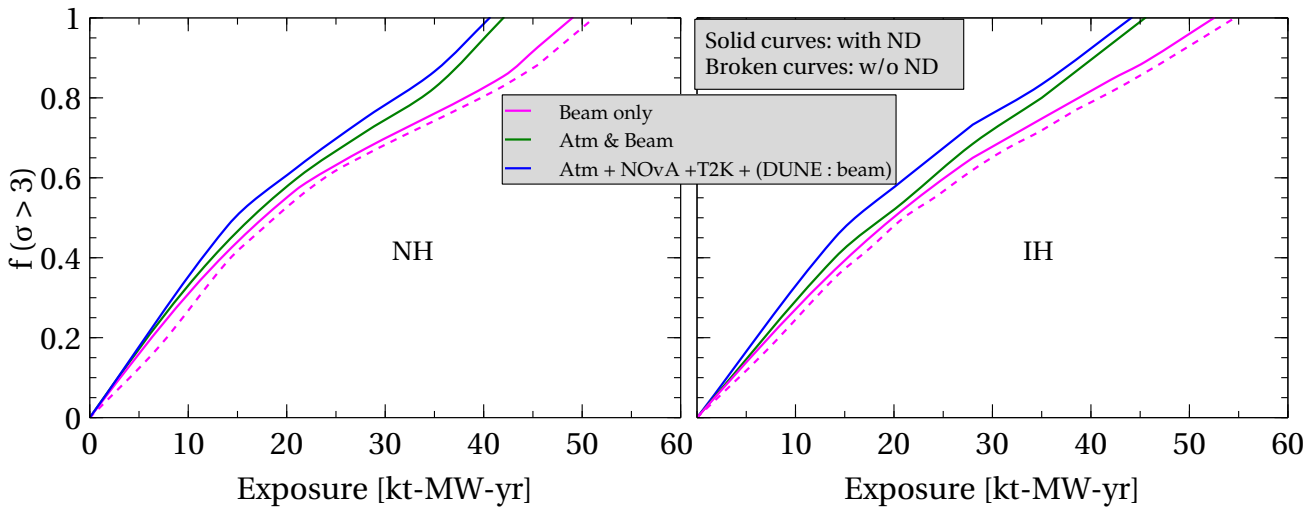

Figure 2.7: The fraction of CP phases for which the sensitivity to the mass hierarchy exceeds 3σ as a function of DUNE exposure, for different unmagnetized detector configurations. The time exposure refers to calendar years for DUNE with 1.65×10^7 seconds of uptime per year. The entire NOνA and T2K datasets are assumed to be available when DUNE starts taking data (and do not contribute to the exposure shown).

volume holds significance for the atmospheric neutrino analysis, since it allows the discrimination of neutrinos and antineutrinos in the flux. Consequently, for the magnetized detector the atmospheric neutrinos alone contribute an almost 3σ sensitivity, thus also enhancing the combined sensitivity; the beam-only results remain unaffected by magnetization.

2.4.5 Effect of increasing the beam power

So far we have analysed the sensitivity with a 700 kW proton beam. In Fig. 2.10, we illustrate the consequence of upgrading the beam power to 2.3 MW which is roughly 3 times the previous value. We observe that ramping up the beam power seems to have more effect on the ND + FD analysis (solid curves) than that on the FD analysis alone (dashed curves) and this is notably visible in the range $\delta_{\rm CP} \in [-\pi, 0]$. In the region $\delta_{\rm CP} \in [0, \pi]$, we observe that the increase in sensitivity is roughly 3 times (from magenta to green curves).

2.4.6 A qualitative understanding of the χ^2 curves

Some understanding of the qualitative nature of the results may be gleaned from considering the relevant expressions at the level of oscillation probabilities. For the sake of

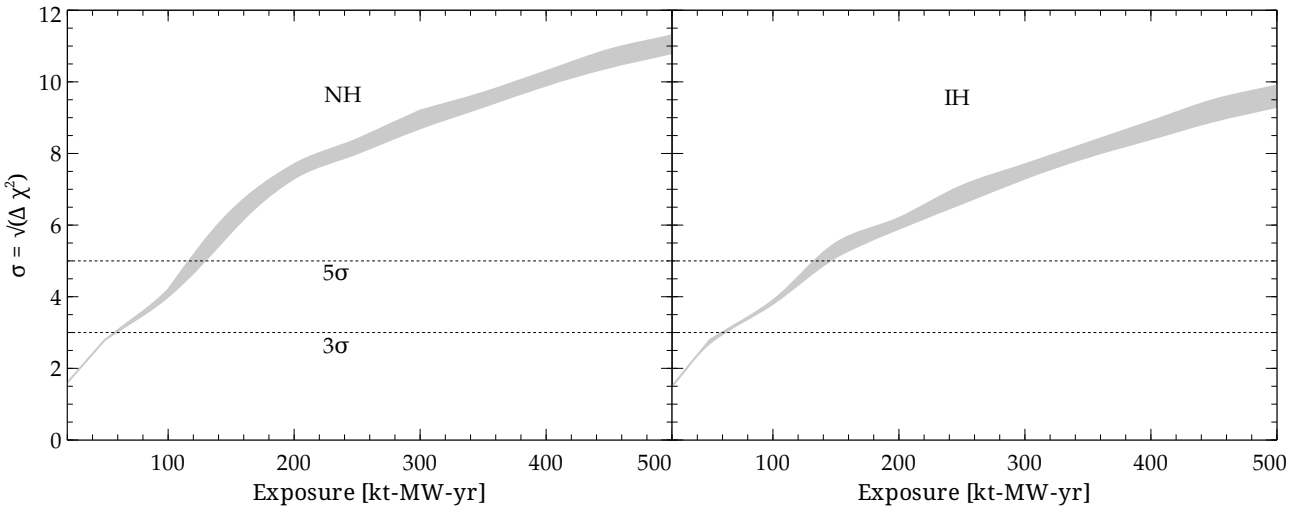

Figure 2.8: Maximum sensitivity to the mass hierarchy for all values of δ_{CP} allowing for different systematics (see Sec. 2.4.3), as a function of exposure. Only beam data (with both an FD and ND) have been considered.

completeness we give the expressions for all the relevant probabilities [50] in a compact form (valid for constant matter density):

1. Normal mass hierarchy (NH):

$$\begin{aligned} P^{NH}_{\mu e} &= x^2 + y^2 + 2xy\cos(\delta + \lambda L/2) \\ \bar{P}^{NH}_{\mu e} &= \bar{x}^2 + y^2 + 2\bar{x}y\cos(\delta - \lambda L/2) \\ P^{NH}_{\mu\mu} &= a + b + c + e - y^2 - d^2 - 2yd\cos\delta \\ \bar{P}^{NH}_{\mu\mu} &= a + b + \bar{c} + \bar{e} - y^2 - \bar{d}^2 - 2y\bar{d}\cos\delta \end{aligned} \tag{2.22}$$

2. Inverted mass hierarchy (IH):

$$\begin{aligned} P^{IH}_{\mu e} &= \bar{x}^2 + y^2 - 2\bar{x}y\cos(\delta - \lambda L/2) \\ \bar{P}^{IH}_{\mu e} &= x^2 + y^2 - 2xy\cos(\delta + \lambda L/2) \\ P^{IH}_{\mu\mu} &= a - b + \bar{c} + \bar{e} - y^2 - \bar{d}^2 + 2y\bar{d}\cos\delta \\ \bar{P}^{IH}_{\mu\mu} &= a - b + c + e - y^2 - d^2 + 2yd\cos\delta \end{aligned} \tag{2.23}$$

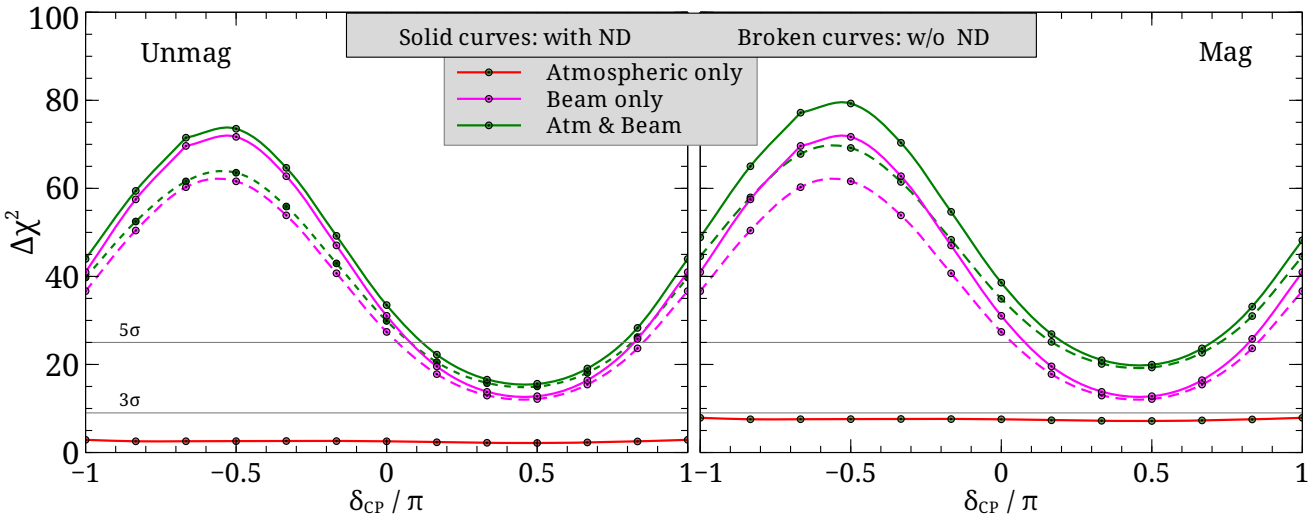

Figure 2.9: Sensitivity to the mass hierarchy with a 100 kt-yr exposure with a magnetized (mag) and unmagnetized (unmag) FD. The true hierarchy is normal.

where

$$
\begin{aligned}
x &= s_{2\times13}s_{23}\frac{\sin\{(1-r_A)\lambda L/2\}}{(1-r_A)} \\
y &= r_\lambda s_{2\times12}c_{23}\frac{\sin(r_A\lambda L/2)}{r_A} \\
a &= 1 - s^2_{2\times23}\sin^2(\lambda L/2) - r^2_\lambda c^4_{12}s^2_{2\times23}(\lambda L/2)^2\cos\lambda L \\
b &= r_\lambda c^2_{12}s^2_{2\times23}(\lambda L/2)\sin\lambda L \\
c &= \frac{1}{2r_A}r^2_\lambda s^2_{2\times12}s^2_{2\times23}\big[\sin(\lambda L/2)\frac{\sin(r_A\lambda L/2)}{r_A}\cos\{(1-r_A)\lambda L/2\} - (\lambda L/4)\sin\lambda L\big] \\
d &= 2s_{13}s_{23}\frac{\sin(1-r_A)\lambda L/2}{1-r_A} \\
e &= \frac{2}{1-r_A}s^2_{13}s^2_{2\times23}\big[\sin(\lambda L/2)\cos(r_A\lambda L/2)\frac{\sin\{(1-r_A)\lambda L/2\}}{1-r_A} - (r_A\lambda L/4)\sin\lambda L\big]
\end{aligned}
\tag{2.24}
$$

, where we have used the notation: $s_{2\times13} = \sin 2\theta_{13}$, $s_{23} = \sin\theta_{23}$ *etc.*

For the anti-neutrino channel, we need the following substitutions : $\delta \to -\delta$ and $r_A \to -r_A$. For going from NH to IH, we need to substitute : $r_A \to -r_A$, $\lambda \to -\lambda$ and $r_\lambda \to -r_\lambda$. To qualitatively understand the sinusoidal shape of the χ^2 curves that are typical of mass hierarchy (in figs. 2.4, 2.5, 2.9, 2.10), we plot $P_{\mu e}$ and $P_{\bar{\mu}\bar{e}}$ for both hierarchy as a function of the CP phase $\delta_{\rm CP}$ for the energy 2.5 GeV in fig. 2.11, the baseline being 1300 km, the

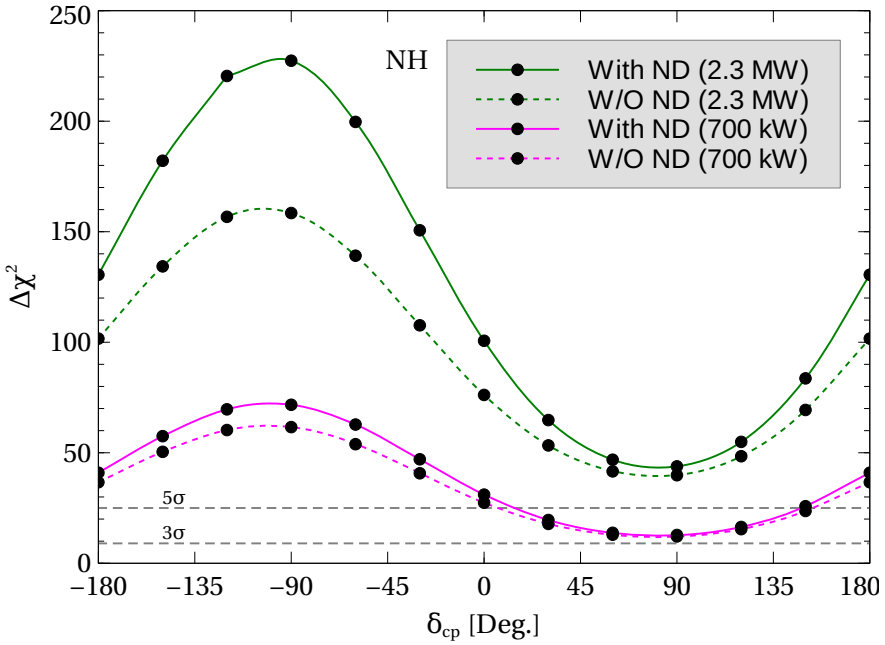

Figure 2.10: Beam-omly sensitivity to the mass hierarchy with a 100 kt-yr exposure with two different beam power. The true hierarchy is normal.

same as that of DUNE. [11]

As discussed in sec. 2.3, the test values of θ_{23}, Δm^2_{31} and $\delta_{\rm CP}$ were marginalised over the ranges $[36°, 54°]$, $[2.19, 2.62] \times 10^{-3}$ eV^2 and $[-\pi, \pi]$ respectively during the calculation of χ^2. It is the marginalization over test $\delta_{\rm CP}$ which has the biggest impact since this parameter is completely undetermined and is allowed to vary over the full range: $[-\pi, \pi]$. Ignoring systematic uncertainties, a basic definition of χ^2 when the true hierarchy is normal (and the test hierarchy is inverted), is given by (following eq. 2.17): [12]

$$\begin{aligned}\chi^2(\delta_{true}) &\approx \min_{\delta_{test},\Delta m^2_{31},\theta_{23}} \sum_E \left(\frac{\left[N^{\mu e}_{NH}(\delta_{true}) - N^{\mu e}_{IH}(\delta_{test})\right]^2}{N^{\mu e}_{NH}(\delta_{true})} + \frac{\left[\bar{N}^{\mu e}_{NH}(\delta_{true}) - \bar{N}^{\mu e}_{IH}(\delta_{test})\right]^2}{\bar{N}^{\mu e}_{NH}(\delta_{true})} \right) \\ &\approx \min_{\delta_{test}} \sum_E \frac{\left[P^{NH}_{\mu e}(\delta_{true}) - P^{IH}_{\mu e}(\delta_{test})\right]^2}{P^{\mu e}_{NH}(\delta_{true})} \Phi\sigma + \text{antineutrino term} \end{aligned} \tag{2.25}$$

, (where $N_{NH}(\bar{N}_{NH})$ and $N_{IH}(\bar{N}_{NH})$ are the no. of neutrino (antineutrino) events for the $\nu_\mu \to \nu_e$ channel in an energy bin for normal and inverted hierarchy respectively. Φ, σ

[11] As discussed in sec. 2.1, 2.5 GeV is the energy which gives the peak of the appearance probability and the contribution to resolve hierarchy and the CP issue comes from this energy. So an examination of the probabilities at this energy is most likely to give a qualitative insight into the nature of χ^2.

[12] Here we consider the $\nu_\mu \to \nu_e$ channel only, since this is the dominant contributor to the χ^2. The other relevant channel $\nu_\mu \to \nu_\mu$ gives very small χ^2 as explained later in the present subsection.

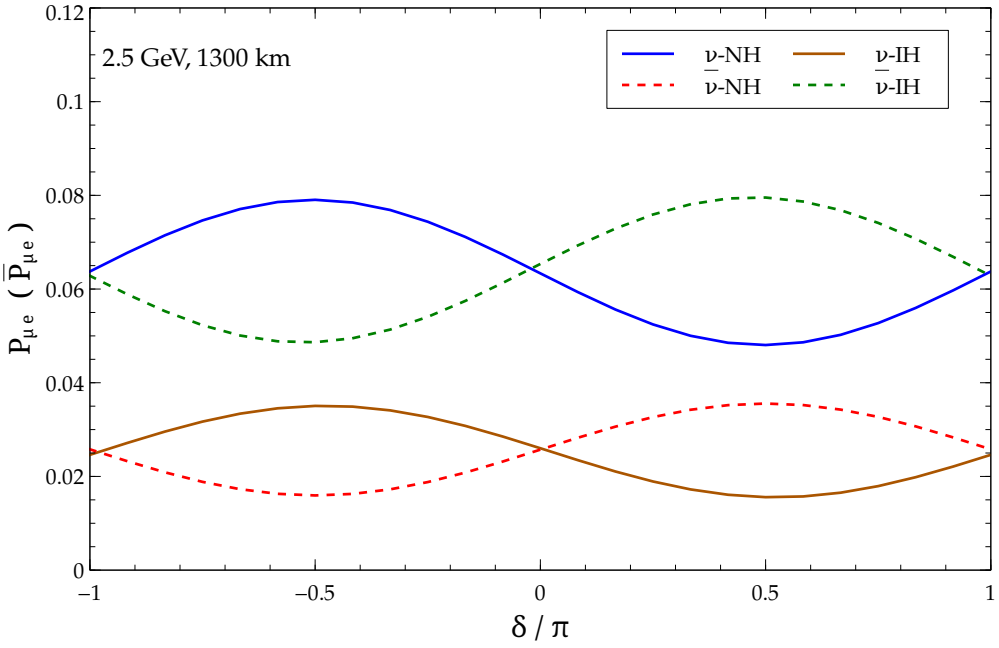

Figure 2.11: $P_{\mu e}$ and $P_{\bar{\mu}\bar{e}}$ as a function of $\delta_{\rm CP}$ for the energy 2.5 GeV and for the DUNE baseline 1300 km. The curves for both hierarchies are shown as given in the legend.

are the relevant flux and the cross sections and are independent of δ. Note that, the antineutrino events are considerably suppressed because of much less flux and crosssection. Also, as already discussed, the dominant contribution to χ^2 for DUNE will come from the energy bin containing 2.5 GeV.)

As is evident from fig. 2.11, for $E \approx 2.5$ GeV, for any δ_{true} (along the solid blue curve), the minimization over δ_{test} (such that $(P_{NH}(\delta_{true}) - P_{IH}(\delta_{test})$ is minimum) along the solid brown curve will always select $\delta_{test} \approx -\pi/2$. [13] hence from eq. 2.25, we can now conclude that χ^2 roughly follows the behaviour:

$$\begin{aligned}\chi^2(\delta_{true}) &\sim \frac{[P^{NH}_{\mu e}(\delta_{true}) - P^{IH}_{\mu e}(\delta_{test} \approx -\pi/2)]^2}{P^{\mu e}_{NH}(\delta_{true})} \quad \text{(for } E \approx 2.5 \text{ GeV)} \\ &\sim \left\{ \frac{[(x^2 - \bar{x}^2)^2 + 4y^2(x \sin\delta_{true} + \bar{x})^2 - 4y(x \sin\delta_{true} + \bar{x})(x^2 - \bar{x}^2)]}{x^2 + y^2 - 2xy \sin\delta_{true}} \right\} \quad (2.26) \\ &\quad \text{(using eqs. 2.22 and 2.23)}\end{aligned}$$

In fig. 2.12, the individual terms of the numerator of eq. 2.26 and also the numerator have been shown as a function of δ_{true}. We can clearly see that the numerator (red curve

[13] The brown solid curve always lies below blue solid curve in fig. 2.11. Hence the peak of the brown curve (*i.e.*, $\delta_{test} \approx -\pi/2$) will always give the minimum vertical distance with any point on the solid blue curve (*i.e.*, δ_{true}).

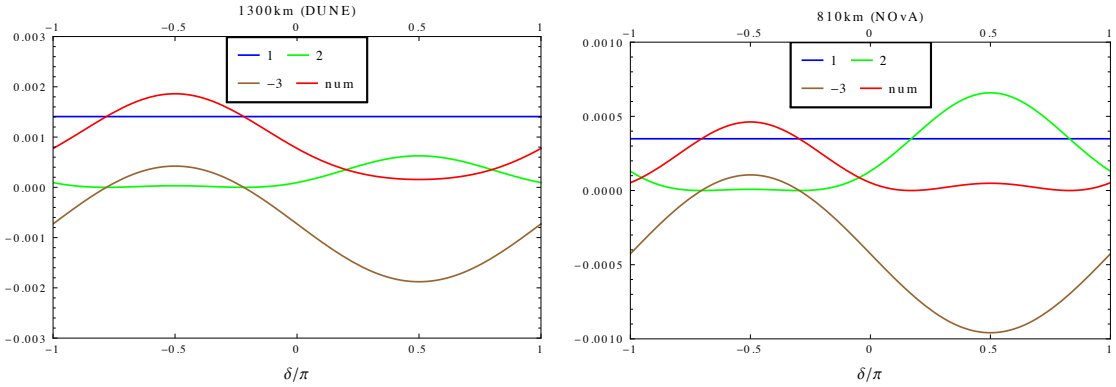

Figure 2.12: The 1st term (blue), 2nd term (green) and the 3rd term (brown) of the numerator of eq. 2.26 and also the numerator (red) are shown as a function of δ for two different experiments,- DUNE (left panel) and NOvA(right). The true hierarchy is assumed to be normal.

in the left panel of fig. 2.12) behaves very similarly as the χ^2 curve for mass hierarchy (the solid magenta curve in the left panel of fig. 2.4) when the true hierarchy is normal. The first term $(x^2 - \bar{x}^2)^2$ increases with matter effect and is independent of δ. This term basically sets the *scale* of the χ^2. It is the third term $(-4y(x \sin\delta_{true} + \bar{x})(x^2 - \bar{x}^2))$, which gives the typical shape of the χ^2 curve as a function of δ_{true}. For a shorter baseline experiment NOvA($L = 810$ km), our analysis (right panel of fig. 2.12) shows that the numerator of eq. 2.26 has a smaller peak at $\delta_{\rm CP} - \pi/2$ and is mostly flat in the region $\delta_{\rm CP} \in [0, \pi]$. This qualitative behaviour is also in good agreement with the hierarchy sensitivity analysis for NOvA in fig. 2.6.

Because of the strong parameter space degeneracies involved in the appearance channel probability [Eq. (2.2)], neither the T2K nor the NOvA experiments are capable of significantly improving the mass hierarchy sensitivities in their respective configurations. It is apparent that the mass hierarchy study benefits immensely from the longer baseline as well as improved systematics of the DUNE set-up as compared to T2K and NOvA.

Since the mass hierarchy will be determined at 3σ with relatively little exposure (see Fig. 2.7), henceforth, we assume the mass hierarchy to be known. It is well known that studies of the octant degeneracy and CP violation benefit significantly from knowledge of the mass hierarchy.

2.5 Results: CP violation

Of the six oscillation parameters, $\delta_{\rm CP}$ is the least well known. Part of the reason for this was the difficulty in experimentally determining the value of θ_{13}. With reactor experi-

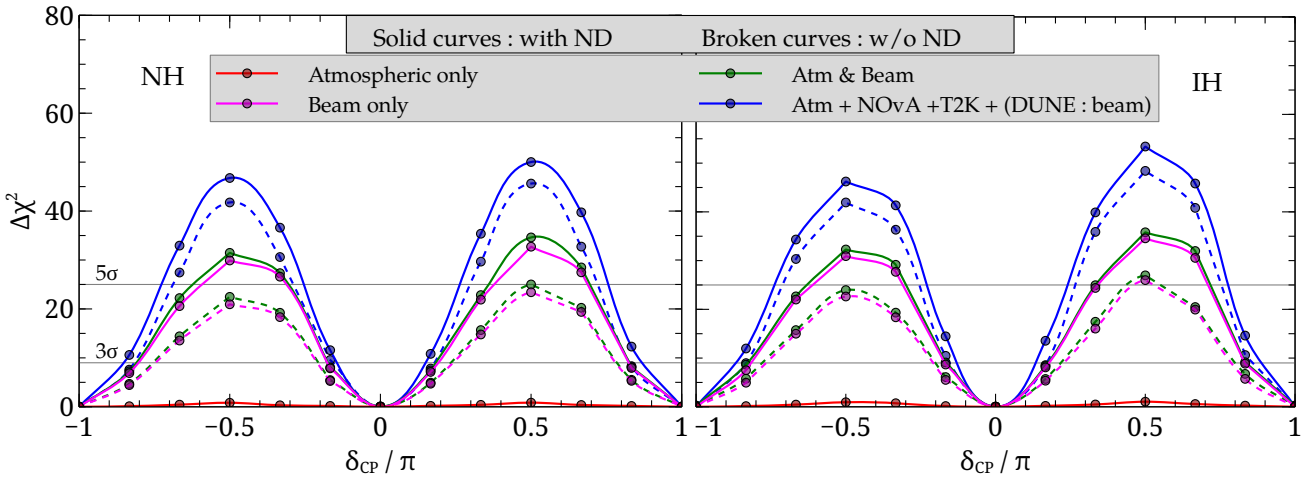

Figure 2.13: Sensitivity to CP violation for a 350 kt-yr unmagnetized FD exposure assuming $\sigma(\sin^2 2\theta_{13}) = 0.05 \times \sin^2 2\theta_{13}$.

ments over the last three years having made significant progress toward the precision determination of the latter, and it being established by now that the value of θ_{13} is non-zero by a fair amount, the precision determination of $\delta_{\rm CP}$ in a future experiment should be possible.

In the following we study the sensitivity of the DUNE to CP-violation in the neutrino sector brought about by a non-zero $\delta_{\rm CP}$ phase. To determine the $\Delta\chi^2$ that represents the experiment's sensitivity to CP violaion, we assume a test $\delta_{\rm CP}$ value of 0 (or π) and compute the $\Delta\chi^2$ for any non-zero (or $\neq \pi$) true $\delta_{\rm CP}$. Since the disappearance channel probability $P_{\mu\mu}$ is only mildly sensitive to the $\delta_{\rm CP}$, CP-violation in the neutrino sector can only be studied by experiments sensitive to the appearance channel $\nu_\mu \to \nu_e$.

Due to the non-zero value of θ_{13} being now established, other experiments sensitive to the $\nu_\mu \to \nu_e$ appearance channel, including the T2K and NOvA, are also strongly poised to look for CP violation. Consequently, this is one study where combining data from DUNE, T2K and NOvA proves to be significantly beneficial.

2.5.1 Analysis with a 35 kt unmagnetized LAr FD

To study CP violation, reduced systematics courtesy the placement of an ND proves to be beneficial (Fig. 2.13). Maximal CP violation can be ruled out at more than 5σ by a beam only analysis with a 350 kt-yr exposure in conjunction with the ND. However, 5σ resolution toward ruling out maximal CP-violation can even be achieved despite the absence of

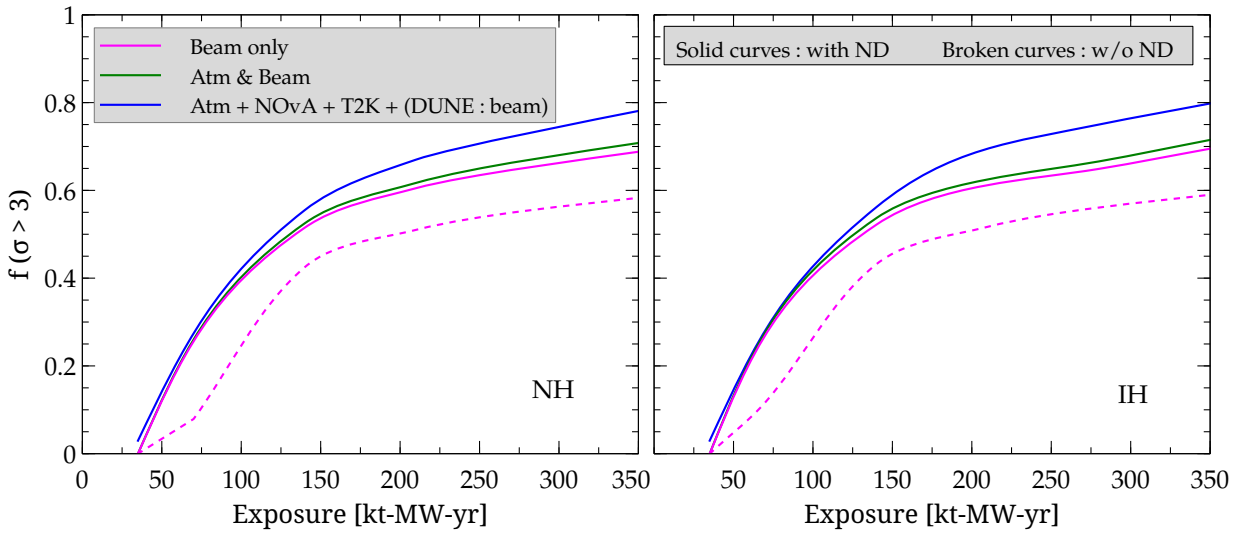

Figure 2.14: The fraction of CP phases for which the sensitivity to CPV exceeds 3σ as a function of exposure.

an ND by combining results from the T2K, NOvA and the DUNE.

2.5.2 Exposure analysis

In Fig. 2.14, we show the CP fraction for which CP violation can be established at 3σ. Needless to say, the CP fraction has to be less than unity since even an almost ideal experiment cannot exclude CP violating values of the phase that are close to the CP conserving values, 0 and π. In the context of CP violation, the CP fraction is a measure of how well an experiment can probe small CP violating effects. From Fig. 2.14, we find:

- There is no sensitivity to CP violation at the 3σ level for exposures smaller than about 35 kt-MW-yr. The sensitivity gradually increases with exposure and the CP fraction for which 3σ sensitivity is achieved approaches 0.4 (without an ND) and 0.5 (with an ND) for a 125 kt-MW-yr exposure. The CP fraction plateaus to a value below 0.8 for an exposure of 350 kt-MW-yr with all data combined.

- A near detector certainly improves the sensitivity to CP violation.

- The CPV sensitivity is ~ 0 around $\delta_{true} = 0, \pm\pi$. Hence, it is not possible for the CP fraction to reach 1 even if very high exposure used.

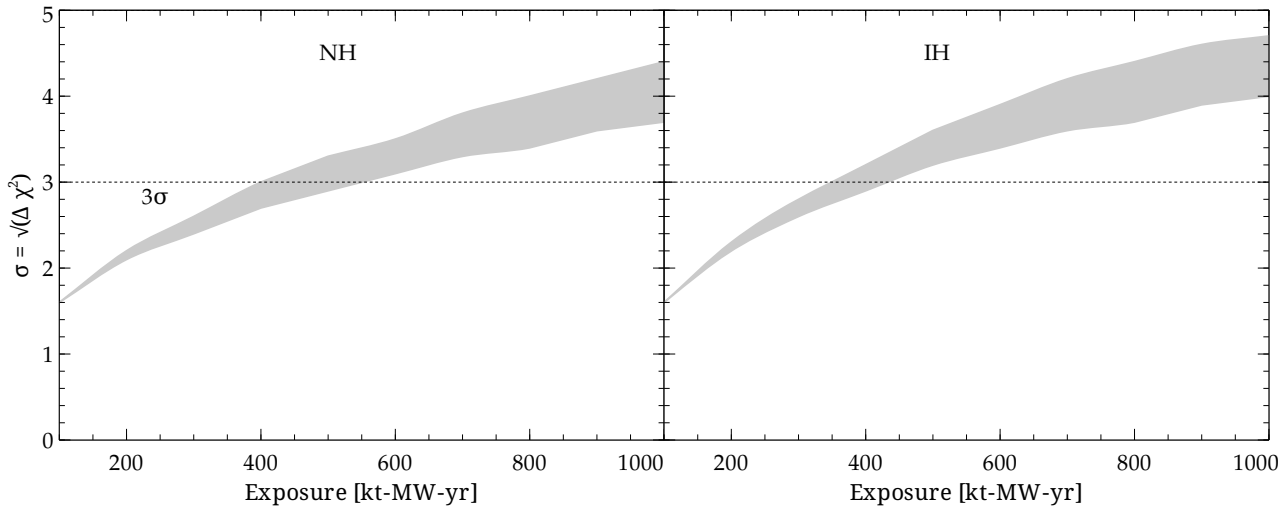

Figure 2.15: Similar to Fig. 2.8, but for the maximum sensitivity to CP violation for 70% of the $\delta_{\rm CP}$ parameter space.

2.5.3 Variation of systematics

Figure 2.15 shows the maximum sensitivity to CP violation that can be achieved for 70% of the $\delta_{\rm CP}$ parameter space. As in fig. 2.8 we show the sensitivity as a band on varying the systematics. The notable features of Fig. 2.15 are,

- To resolve CP violation at the level of 3σ for 70% region of the $\delta_{\rm CP}$ space, a fairly long exposure is needed. For NH, it is roughly $400 - 500$ kt-MW-yr. while for IH it is $350 - 450$ kt-MW-yr. depending on the systematics.)
- For such long exposures, the sensitivity band becomes appreciably wide indicating a strong dependence on the systematics. In comparison, the sensitivities to the mass hierarchy and octant were less dependent on systematics since the corresponding exposures were smaller. This reinforces the need for an ND.

2.5.4 Effect of magnetization

As can be seen from Fig. 2.13, the sensitivity of atmospheric neutrinos to CPV is negligible, hence magnetizing the detector does not help.

It is obvious that CP-violation is the study that stands to benefit most from the combination of results from the T2K, NOvA and the DUNE. Even potentially low sensitivity to

maximal CP-violation due to the absence of ND can be overcome by the combination of χ^2 data from the three experiments. However, a large volume FD (35 kt) for the DUNE is almost certainly an absolute necessity, if any sensitivity to CP-violation has to be detected within a reasonable time frame, irrespective of the benefits of combining results from other experiments such as the T2K and NOvA.

The atmospheric neutrino flux has practically no role to play in the resolution of this physical problem.

2.5.5 An understanding of the CPV sensitivity curves

We contrast the CP conserving test dataset ($\delta_{\rm CP} = 0, \pi$) with the true dataset where the true $\delta_{\rm CP}$ lies in the entire allowed range $[-\pi, \pi]$ for the calculation of the sensitivity to CP violation. Hence it is obvious that the maximum sensitivity is obtained when the true $\delta_{\rm CP}$ is farthest from both 0 and π and minimum when the true $\delta_{\rm CP}$ is 0 or π. We can see that this is indeed the case in fig. 2.13. Nevertheless following similar discussion for mass hierarchy (in subsec. 2.4.6), we express this in terms of the probabilities below. From Eqs. 2.22 and 2.23 we can write,

1. $\nu_\mu \to \nu_e$ and $\bar{\nu}_\mu \to \bar{\nu}_e$ (appearance channel) :

$$\begin{aligned} P_{\mu e} &\simeq a_{\mu e} + b_{\mu e} \sin\delta + c_{\mu e} \cos\delta \\ P_{\bar{\mu}\bar{e}} &\simeq \bar{a}_{\mu e} - \bar{b}_{\mu e} \sin\delta + \bar{c}_{\mu e} \cos\delta \end{aligned} \tag{2.27}$$

   $\delta \to -\delta$ for antineutrinos and the coefficients can be found in Ref. [210]. Thus, $P_{\mu e}$ contains linear polynomials of $\sin\delta$ and $\cos\delta$.

2. $\nu_\mu \to \nu_\mu$ and $\bar{\nu}_\mu \to \bar{\nu}_\mu$ (disappearance channel) :

$$\begin{aligned} P_{\mu\mu} &\simeq a_{\mu\mu} + c_{\mu\mu} \cos\delta \\ P_{\bar{\mu}\bar{\mu}} &\simeq \bar{a}_{\mu\mu} + \bar{c}_{\mu\mu} \cos\delta \end{aligned} \tag{2.28}$$

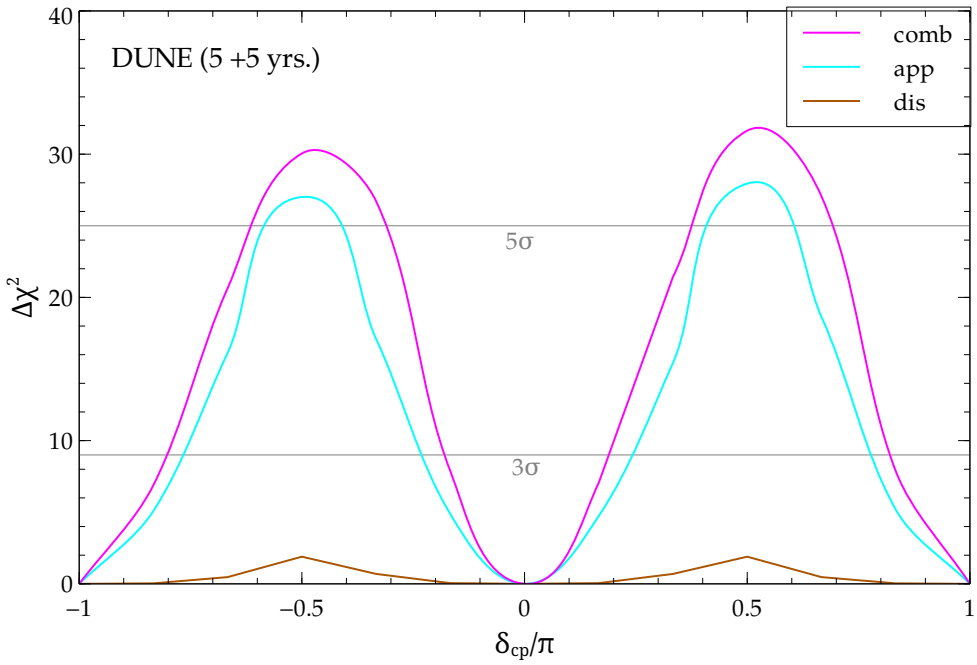

Figure 2.16: The sensitivity to CP violation at DUNE for a 350 kt-MW-yr exposure, showing the contribution from the appearance ($\nu_\mu \to \nu_e$, cyan) and the disappearance ($\nu_\mu \to \nu_\mu$, brown) channels to the total combined χ^2. Here the hierarchy is presumed to be known as normal and the presence of an ND has also been assumed. Note that, the combined χ^2 (magenta) is the same as the solid magenta curve in the left panel of fig. 2.13.

Following the χ^2 definition in eq. 2.17 the sensitivity to CP violation can be expressed as (ignoring the systematic uncertainties),

$$
\begin{aligned}
\chi^2 \;&\sim\; \min_{\delta_{test}=0,\pi} \left(\chi^2_{\nu_\mu\to\nu_e} + \chi^2_{\bar\nu_\mu\to\bar\nu_e} + \chi^2_{\nu_\mu\to\nu_\mu} + \chi^2_{\bar\nu_\mu\to\bar\nu_\mu}\right) \\
&\sim\; \min_{\delta_{test}=0,\pi} \frac{\left(P_{\mu e}(\delta_{true}) - P_{\mu e}(\delta_{test}=0,\pi)\right)^2}{P_{\mu e}(\delta_{true})} + \left[\text{similar term for the other channels}\right] \\
&\quad \big(\text{the cross-section and the flux were not included in this simplified analysis} \\
&\quad \text{since they are not dependent on the CP phase } \delta_{\rm CP}.\big) \\
&\sim\; \min_{\delta_{test}=0,\pi} \Big[\left(b_{\mu e}\sin\delta_{true} + c_{\mu e}\cos\delta_{true} - c_{\mu e}\cos\delta_{test}|_{0,\pi}\right)^2 \\
&\quad + \left(-\bar b_{\mu e}\sin\delta_{true} + \bar c_{\mu e}\cos\delta_{true} - \bar c_{\mu e}\cos\delta_{test}|_{0,\pi}\right)^2 \\
&\quad + \left(c_{\mu\mu}\cos\delta_{true} - c_{\mu\mu}\cos\delta_{test}|_{0,\pi}\right)^2 + \left(\bar c_{\mu\mu}\cos\delta_{true} - \bar c_{\mu\mu}\cos\delta_{test}|_{0,\pi}\right)^2 \Big] \qquad (2.29) \\
&\quad \text{(using eqs. 2.27 and 2.28)}
\end{aligned}
$$

In the last step above, the first two terms (containing the μe index) give the contribution from the $\nu_\mu \to \nu_e$ appearance channel while the last two terms (containing the $\mu\mu$ index)

give the contribution from the $\nu_\mu \to \nu_\mu$ disappearance channel. Fig. 2.16 shows the individual contribution of these two channels to the total combined χ^2. As expected, the appearance channel is dominant and a look at eq. 2.29 suggests that it is the presence of the CP-odd term ($\sin\delta$-term) which makes this particular channel dominant. This CP odd-term is maximum at $\delta_{true} = \pm\pi/2$ and zero at $\delta_{true} = 0, \pm\pi$.

On the other hand, even if one expects no CP sensitivity for the $\nu_\mu \to \nu_\mu$ channel (in the light of the discussion in the beginning of the sec. 2.5), it gives a small nonzero sensitivity to CP violation having peaks at $\sim \pm\pi/2$ as seen in fig. 2.16. In fact, the sensitivity we study is mathematically a sensitivity to how well the true values of δ can be separated from the CP conserving values and is a good and standard measure of the sensitivity to CP violation [14, 175]. The presence of the $\cos\delta$-term [14] gives rise to a small but non-zero sensitivity coming from this channel. It is also clear from eq. 2.29, that the χ^2 from the $\nu_\mu \to \nu_\mu$ channel has its peak when $\cos\delta_{true}$ vanishes (*i.e.*, $\delta_{true} = \pm\pi/2$) and is zero when $\cos\delta_{true}$ is maximal (*i.e.*, $\delta_{true} = 0, \pm\pi$).

[14] To be precise, the presence of an always non-zero $\cos\delta_{test}$ term ($\delta_{test} = 0, \pi$) according to the χ^2 definition is the reason why $\nu_\mu \to \nu_\mu$ channel gives nonzero CPV sensitivity unless $\delta_{true} = \delta_{test}$.

Chapter 3

Study of CP Violation and mass hierarchy at long baselines in presence of one $\sim O(1eV)$ sterile neutrino

A major goal of present and future long-baseline neutrino oscillation experiments is to establish that leptons violate CP, or else to place a stringent upper limit on any such violation. Our thinking about these experiments usually assumes the standard neutrino paradigm, in which there are just three neutrino mass eigenstates separated by just two independent mass-squared splittings, three mixing angles θ_{ij}, and just one CP-violating phase $\delta_{\rm CP}$ relevant to oscillation. However, a variety of short-baseline anomalies [76, 79, 82, 211, 212] hint at the possible existence of short-wavelength oscillations, driven by one or more $O(1\ \text{eV}^2)$ mass-squared splittings that are much larger than the two splittings of the standard paradigm. These short-wavelength oscillations are purportedly already significant when the (Travel distance L)/(Energy E) of neutrinos in a beam is only ~ 1 km/GeV. Of course, they are still present at the far detector of any long-baseline experiment, where L/E is, say, ~ 500 km/GeV. In this work [213, 214] we have explored the consequences of the short-wavelength oscillations - should they be real - for measurements at long baselines, especially measurements that probe CP violation. We find that these consequences could be considerable. For example, it is possible for long-baseline results, interpreted without taking the short-wavelength oscillations into account, to imply that CP violation is very small or totally absent, when in reality it is very large. In addition, long-baseline measurements interpreted as determining the sole oscillation-relevant CP-violating phase in the standard paradigm could in fact be measuring something else.

The large splittings hinted at by the short-baseline anomalies imply the existence of additional, largely sterile, neutrino mass eigenstates, beyond the three of the standard

scenario (referred to as 3+0 in what follows). These additional mass eigenstates introduce not only additional splittings but also additional mixing angles and phases. For simplicity, we restrict ourselves to the scenario, referred to as 3+1, with only one additional mass eigenstate. In this scenario, there are six mixing angles (the standard $3+0$ mixing angles $\theta_{12}, \theta_{13}, \theta_{23}$ and the $3+1$ mixing angles $\theta_{14}, \theta_{24}, \theta_{34}$), and three CP-violating phases [1] that can affect oscillation. The standard Dirac CP phase δ is associated with the $1-3$ mixing angle in the standard parameterization and thus $\delta \equiv \delta_{13}$. For the 3+1 scenario, we have chosen the two additional phases associated with the $2-4$ and the $3-4$ mixing angles. This is further discussed in the beginning of sec. 3.2. Denoting the mass eigenstates of 3+0, as usual, as ν_1, ν_2, ν_3, and the additional mass eigenstate as ν_4, and defining the mass-squared splittings as $\Delta m^2_{ij} = m^2_i - m^2_j$ (i, j = 1, 2, 3, 4 & $i \neq j$), we have, according to present data,

$$\Delta m^2_{41} \sim \Delta m^2_{42} \sim \Delta m^2_{43} >> |\Delta m^2_{31}| \sim |\Delta m^2_{32}| >> \Delta m^2_{21}. \tag{3.1}$$

Since the probability of an oscillation driven by a splitting Δm^2_{ij} is proportional to $\sin^2 \Delta_{ij}$, where $\Delta_{ij} = 1.27 \times \frac{\Delta m^2_{ij}[\mathrm{eV}^2] \times L[km]}{E[GeV]}$, when L/E $\sim$ 500 km/GeV, the short-wavelength oscillations driven by the large splittings involving ν_4 will be averaged to an L/E-independent value by the finite energy resolution of any realistic detector. But these rapid oscillations are still present and can have a major impact.

We perform our calculations for the 3+1 scenario mainly in the context of the proposed Deep Underground Neutrino Experiment (DUNE) [13,14,172–175] and also on the shorter baseline experiments NOvA [9,215], T2K [10,196,197] and T2HK [15,216]. While we do not explore 3+N scenarios with N>1, we expect that if the consequences of having one extra neutrino for long-baseline measurements are substantial, those of having more than one must be substantial as well, since the world with one extra neutrino is in a sense a special case of that with more than one.

Previous work examining the effects of sterile neutrinos at long baselines includes several studies of neutrino factories feeding baselines of about 3000 km - 7500 km, with muon energies in the range 20 GeV - 50 GeV, focussing on effects at both near and far detectors [217–221]. More recent work [222] includes a study of effects relevant to T2K [223] and a combined study [224] for T2K, MINOS [53] and reactor experiments. Additionally,

[1] In the general case of n flavors the leptonic mixing matrix $U_{\alpha i}$ depends on $(n-1)(n-2)/2$ Dirac-type CP-violating phases. For $n = 4$ (*i.e.*, the $3+1$ scenario) no. of CP violating phases is $(4-1)(4-2)/2 = 3$. If the neutrinos are Majorana particles, there are $(n-1)$ additional, so called Majorana-type CP-violating phases.

issues having some overlap with those addressed here for DUNE have been discussed in [225], and, very recently, in [226–228].

3.1 Simulation of sterile neutrinos

In this section, we describe the details of the simulation technique adopted in estimating the sensitivities and other the results obtained. We have used the GLoBES [189, 190] software package for performing all our analysis. For extending the simulation to the 3+1 scenario, we used [229]; which is an add-on to the default GLoBES software. Our assumptions regarding the values and ranges of the oscillation parameters for the 3+0 sector are as follows.

- θ_{12} and θ_{13} are taken to be $33.48°$ and $8.5°$ respectively [5].
- Δm^2_{21} is taken to be 7.5×10^{-5} eV^2 while Δm^2_{31} is set to be 2.457×10^{-3} eV^2 (-2.374×10^{-3} eV^2) for NH (IH) [5].
- The currently-allowed 3σ range on θ_{23} is $[38.3°, 53.3°]$ with the best fit at $42.3°(49.5)°$ for NH (IH) [5]. The θ_{23} best fit values from the global analyses [230, 231] are somewhat different from [5]. In this work, we make the simplifying assumption that 2-3 mixing is maximal i.e. $\theta_{23} = 45°$. However, the conclusions we draw also apply to non-maximal 2-3 mixing.

It is anticipated that even if the 3+0 scenario is not realised in nature, the above values and ranges will still hold to a very good approximation[2].

The additional mass square difference Δm^2_{41}, relevant for the 3+1 scenario is assumed to be $1\ ev^2$, which is consistent with [233–235][3]. Our assumed ranges for the sterile sector mixing angles corresponding to the 3+1 scenario (for $\Delta m^2_{41} = 1\ ev^2$) draw upon current constraints and are as follows:

- Measurements at the Daya Bay experiments put constraints on the effective mixing angle in the electron anti-neutrino disappearance channel. This effective mixing

[2]Some of our early calculations showed that the disappearance data *at the far detector* is less affected by the active-sterile mixing angles compared to the appearance data. Thus, the measurements which depend on $P_{\mu\mu}$ like $\sin^2 2\theta_{23}$ or $|\Delta m^2_{31}|$ are expected to change less with the change of theoretical framework from 3+0 to 3+1. Likewise, it was shown in [232] that θ_{13} measurements at the reactor neutrino experiments will be robust even if there are sterile neutrinos.

[3]The allowed values of Δm^2_{41} roughly lies in the interval $[0.1, 10]\ ev^2$ [233–235]. Even if we take Δm^2_{41} to be $0.1\ ev^2$ or $10\ ev^2$, the assumption in eq. 3.1 holds and all our analyses also go through.

angle is the same as θ_{14} under the choice of PMNS parameterisation in this work. Based on [233], we assume $\theta_{14} \leq 13^\circ$ at 99% C.L.

- Both MINOS and the IceCube experiments are sensitive to the 2-4 mixing angle. With their current data, only $\theta_{24} \leq 7^\circ$ can be allowed at 99% C.L. [234, 235]
- The MINOS experiment with its observed CC as well NC events spectra can constrain the 3-4 mixing angle. From [234], we have $\theta_{34} \leq 25^\circ$ at 90% C.L.

In addition, we also vary δ_{13}, δ_{24} and δ_{34} for 3+1 and δ_{CP} for 3+0 over the full possible range of $[-180^\circ, 180^\circ]$. Finally, the DUNE fluxes were obtained from [192]. In table 3.1, we give the various information regarding the simulations of the experiments DUNE, T2K, NOvAand T2HK[4]

[4]These simulations details are slightly different from the ones used in the discussion of chapter 2 and use more updated information.

Detector details	Normalisation error		Energy calibration error	
	Signal	Background	Signal	Background
DUNE(1300 km) Runtime (yr) = 5 ν + 5 $\bar{\nu}$ 1.0 MW proton beam 120 GeV proton energy delivers $\sim 10^{21}$ POT/yr 35 kton, LArTPC $\varepsilon_{app} = 80\%$, $\varepsilon_{dis} = 85\%$ $R_\mu = 0.20/\sqrt{E}$, $R_e = 0.15/\sqrt{E}$	$\nu_e : 5\%$ $\nu_\mu : 5\%$	$\nu_e : 10\%$ $\nu_\mu : 10\%$	$\nu_e : 2\%$ $\nu_\mu : 5\%$	$\nu_e : 10\%$ $\nu_\mu : 10\%$
NOvA(810 km) Runtime (yr) = 3 ν + 3 $\bar{\nu}$ 0.7 MW proton beam 120 GeV proton energy delivers $\sim 6 \times 10^{20}$ POT/yr 14 kton, TASD $\varepsilon_{app} = 55\%$, $\varepsilon_{dis} = 85\%$ $R_\mu = 0.06/\sqrt{E}$, $R_e = 0.085/\sqrt{E}$	$\nu_e : 5\%$ $\nu_\mu : 2.5\%$	$\nu_e : 10\%$ $\nu_\mu : 10\%$	$\nu_e : 0.01\%$ $\nu_\mu : 0.01\%$	$\nu_e : 0.01\%$ $\nu_\mu : 0.01\%$
T2K (295 km) Runtime (yr) = 3 ν + 3 $\bar{\nu}$ 770 kW proton beam 50 GeV proton energy delivers $\sim 8.3 \times 10^{20}$ POT/yr 22.5 kton, WC $\varepsilon_{app} = 50\%$, $\varepsilon_{dis} = 90\%$ $R_\mu = 0.085/\sqrt{E}$, $R_e = 0.085/\sqrt{E}$	$\nu_e : 5\%$ $\nu_\mu : 2.5\%$	$\nu_e : 5\%$ $\nu_\mu : 20\%$	$\nu_e : 0.01\%$ $\nu_\mu : 0.01\%$	$\nu_e : 0.01\%$ $\nu_\mu : 0.01\%$
T2HK(295 km) Runtime (yr) = 1 ν + 3 $\bar{\nu}$ 7.5 MW proton beam 30 GeV proton energy delivers $\sim 1.6 \times 10^{22}$ POT 560 kton, WC $\varepsilon_{app} = 50\%$, $\varepsilon_{dis} = 90\%$ $R_\mu = 0.085/\sqrt{E}$, $R_e = 0.085/\sqrt{E}$	$\nu_e : 5\%$ $\nu_\mu : 2.5\%$	$\nu_e : 5\%$ $\nu_\mu : 20\%$	$\nu_e : 0.01\%$ $\nu_\mu : 0.01\%$	$\nu_e : 0.01\%$ $\nu_\mu : 0.01\%$

Table 3.1: Detector configuration, efficiencies, resolutions and systematic uncertainties for DUNE [13,14], NOvA [9], T2K [10], T2HK [15].

3.2 Result: The $3{+}1$ electron appearance probability in vacuum and matter

For CPV discovery in long baseline super-beam experiments, the electron neutrino appearance probability $P(\nu_\mu \to \nu_e)$ is crucial. We discuss its analytic form in vacuum for the $3+1$ scenario prior to discussing the matter case. While it is the latter that is relevant for DUNE in particular, and other long baseline (LBL) experiments at baselines of $O(1000)$ km in general, the form of the vacuum expression provides a useful template for the identification of terms the importance of which will be accentuated by the presence of matter.

We adopt the following parameterisation[5] for the PMNS matrix in the presence of a sterile neutrino,

$$U^{3+1}_{\rm PMNS} = O(\theta_{34},\delta_{34})O(\theta_{24},\delta_{24})O(\theta_{14})O(\theta_{23})O(\theta_{13},\delta_{13})O(\theta_{12}). \tag{3.2}$$

Here, in general, $O(\theta_{ij},\delta_{ij})$ is a rotation matrix in the ij sector with associated phase δ_{ij}. For example,

$$O(\theta_{24},\delta_{24}) = \begin{pmatrix} 1 & 0 & 0 & 0 \\ 0 & \cos\theta_{24} & 0 & e^{-i\delta_{24}}\sin\theta_{24} \\ 0 & 0 & 1 & 0 \\ 0 & -e^{i\delta_{24}}\sin\theta_{24} & 0 & \cos\theta_{24} \end{pmatrix}; O(\theta_{14}) = \begin{pmatrix} \cos\theta_{14} & 0 & 0 & \sin\theta_{14} \\ 0 & 1 & 0 & 0 \\ 0 & 0 & 1 & 0 \\ -\sin\theta_{14} & 0 & 0 & \cos\theta_{14} \end{pmatrix} \textit{etc.}$$

Using the standard formula for a flavour transition oscillation probability, we have, for the 3+1 case:

$$\begin{aligned} P^{4\nu}_{\mu e} &= 4|U_{\mu 4}U_{e4}|^2 \times 0.5 \\ &- 4Re(U_{\mu 1}U^*_{e1}U^*_{\mu 2}U_{e2})\sin^2\Delta_{21} + 2Im(U_{\mu 1}U^*_{e1}U^*_{\mu 2}U_{e2})\sin 2\Delta_{21} \\ &- 4Re(U_{\mu 1}U^*_{e1}U^*_{\mu 3}U_{e3})\sin^2\Delta_{31} + 2Im(U_{\mu 1}U^*_{e1}U^*_{\mu 3}U_{e3})\sin 2\Delta_{31} \\ &- 4Re(U_{\mu 2}U^*_{e2}U^*_{\mu 3}U_{e3})\sin^2\Delta_{32} + 2Im(U_{\mu 2}U^*_{e2}U^*_{\mu 3}U_{e3})\sin 2\Delta_{32}. \end{aligned} \tag{3.3}$$

In arriving at the above expression, we have only assumed (based on Eq. 3.1 above)

[5]The choice of parameterisation is motivated by the fact that in any parameterisation, the electron neutrino 3+1 appearance probability in vacuum turns out to be dependent on only two specific linear combinations of the three independent phases. In this parameterisation, these two linear combinations become δ_{13} and δ_{24} themselves (see eq. 3.4), making the analysis simpler. This happens because, the the first and second row elements (U_{ei} and $U_{\mu i}$) in $\mathrm{U}^{3+1}_{\rm PMNS}$ will not have θ_{34} or δ_{34} in them in this choice and this is intuitively easier to grasp.

that $\sin^2\Delta_{4i}$ averages out to be 0.5 at long baselines, and similarly $\sin 2\Delta_{4i}$ averages out to be 0, when $i = 1, 2, 3$.

After substituting the values of the $U_{\alpha i}$ in terms of the mixing angles, we obtain :

$$\begin{aligned}
P^{4\nu}_{\mu e} &= \frac{1}{2}\sin^2 2\theta^{4\nu}_{\mu e} \\
&+ (a^2\sin^2 2\theta^{3\nu}_{\mu e} - \frac{1}{4}\sin^2 2\theta_{13}\sin^2 2\theta^{4\nu}_{\mu e})\big[\cos^2\theta_{12}\sin^2\Delta_{31} + \sin^2\theta_{12}\sin^2\Delta_{32}\big] \\
&+ \cos(\delta_{13})ba^2\sin 2\theta^{3\nu}_{\mu e}\big[\cos 2\theta_{12}\sin^2\Delta_{21} + \sin^2\Delta_{31} - \sin^2\Delta_{32}\big] \\
&+ \cos(\delta_{24})ba\sin 2\theta^{4\nu}_{\mu e}\big[\cos 2\theta_{12}\cos^2\theta_{13}\sin^2\Delta_{21} - \sin^2\theta_{13}(\sin^2\Delta_{31} - \sin^2\Delta_{32})\big] \\
&+ \cos(\delta_{13}+\delta_{24})a\sin 2\theta^{3\nu}_{\mu e}\sin 2\theta^{4\nu}_{\mu e}\big[-\frac{1}{2}\sin^2 2\theta_{12}\cos^2\theta_{13}\sin^2\Delta_{21} \\
&+ \cos 2\theta_{13}(\cos^2\theta_{12}\sin^2\Delta_{31} + \sin^2\theta_{12}\sin^2\Delta_{32})\big] \\
&- \frac{1}{2}\sin(\delta_{13})ba^2\sin 2\theta^{3\nu}_{\mu e}\big[\sin 2\Delta_{21} - \sin 2\Delta_{31} + \sin 2\Delta_{32}\big] \\
&+ \frac{1}{2}\sin(\delta_{24})ba\sin 2\theta^{4\nu}_{\mu e}\big[\cos^2\theta_{13}\sin 2\Delta_{21} + \sin^2\theta_{13}(\sin 2\Delta_{31} - \sin 2\Delta_{32})\big] \\
&+ \frac{1}{2}\sin(\delta_{13}+\delta_{24})a\sin 2\theta^{3\nu}_{\mu e}\sin 2\theta^{4\nu}_{\mu e}\big[\cos^2\theta_{12}\sin 2\Delta_{31} + \sin^2\theta_{12}\sin 2\Delta_{32}\big] \\
&+ (b^2a^2 - \frac{1}{4}a^2\sin^2 2\theta_{12}\sin^2 2\theta^{3\nu}_{\mu e} - \frac{1}{4}\cos^4\theta_{13}\sin^2 2\theta_{12}\sin^2 2\theta^{4\nu}_{\mu e})\sin^2\Delta_{21},
\end{aligned} \tag{3.4}$$

where,

$$\sin 2\theta^{3\nu}_{\mu e} = \sin 2\theta_{13}\sin\theta_{23} \tag{3.5}$$

$$b = \cos\theta_{13}\cos\theta_{23}\sin 2\theta_{12} \tag{3.6}$$

$$\sin 2\theta^{4\nu}_{\mu e} = \sin 2\theta_{14}\sin\theta_{24} \tag{3.7}$$

$$a = \cos\theta_{14}\cos\theta_{24}. \tag{3.8}$$

Apropos Eq. 3.4, we make the following important points,

1. the vacuum appearance probability is independent of the 3-4 mixing angle and the associated CP phase. This important simplification, however, does not strictly carry over to the matter case. Fig. 3.1 (generated using GLoBES simulation [189, 190]) shows that, though there is very slight dependence on the angle θ_{34} (left panel) in presence of matter, the associated phase δ_{34} has quite a significant effect (right panel).

2. The mixing angles θ_{14} and θ_{24} appear together in the vacuum expression in the form of an effective mixing angle: $\sin 2\theta^{4\nu}_{\mu e} = \sin 2\theta_{14}\sin\theta_{24}$. Fig. 3.2 illustrates (left and the

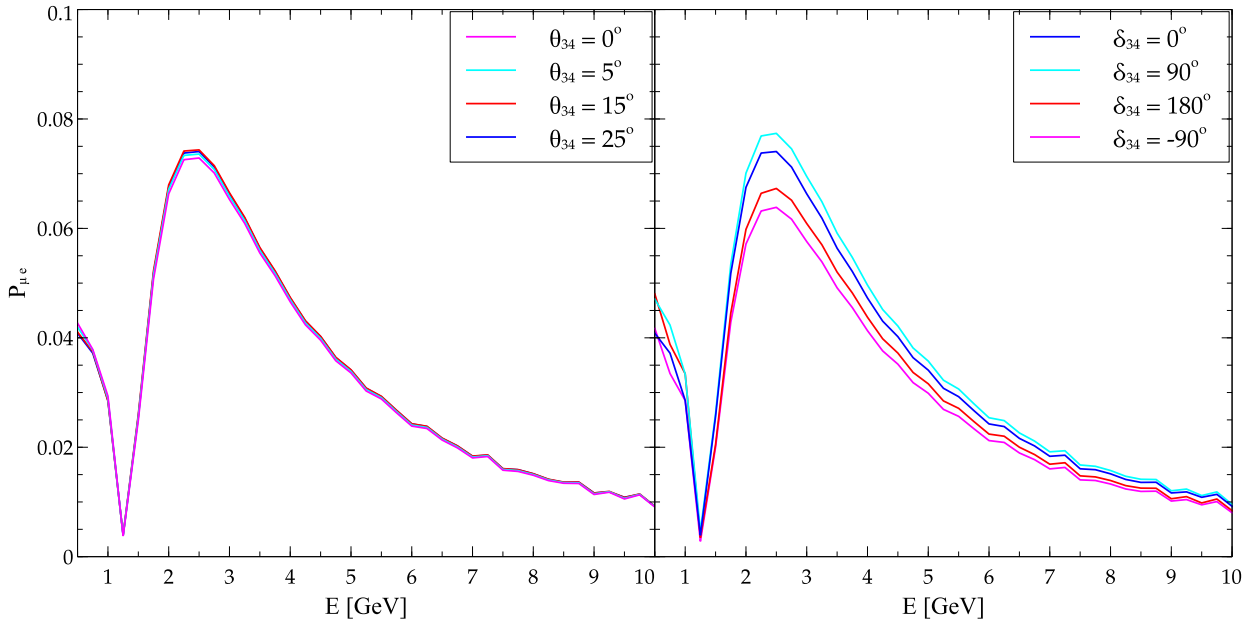

Figure 3.1: $P_{\mu e}$ vs E_ν in earth matter for 1300 km (generated using GLoBES simulation). Averaging has been done for Δm^2_{4i} induced oscillations. In the left panel, the effect of varying θ_{34} within its allowed range is shown with all the CP phases kept equal to 0. In the right panel, we show the effect of varying CP violating phase δ_{34} when $\theta_{34} = 25°$, and the other phases are 0. For both panels, we set $\theta_{14} = 12°$ and $\theta_{24} = 7°$, and the parameters related to the 3+0 sector at the best-fit values specified in Sec. 3.1.

middle panel) the significant role of the the individual mixing angles θ_{14} and θ_{24} on the the $3+1$ appearance probability. The right panel of fig. 3.2 shows the concept of the effective mixing angle $\sin 2\theta^{4\nu}_{\mu e}$. Since the value of the effective mixing angle is the same for all three choices of θ_{14}, θ_{24} as shown, the three corresponding probabilities coincide over one another. This also illustrates that the concept of effective mixing angle holds even in presence of matter.

3. It contains terms proportional to the sines and cosines of a) the $3+1$ CP phase δ_{24}, and b) the sum $(\delta_{13} + \delta_{24})$. These are interference terms, involving mixing angles from both the 3+0 and the 3+1 sector. In particular, as can be determined by inspection, the terms involving the sine and cosine of the sum of δ_{13} and δ_{24} can be significantly large (depending on the values of the phases) and lead to appreciable changes in both the amplitude of the overall probability and the extent of CP violation. These contributions become all the more significant once matter effects are large.

Fig. 3.3 emphasizes the dependencies discussed above from a slightly more general

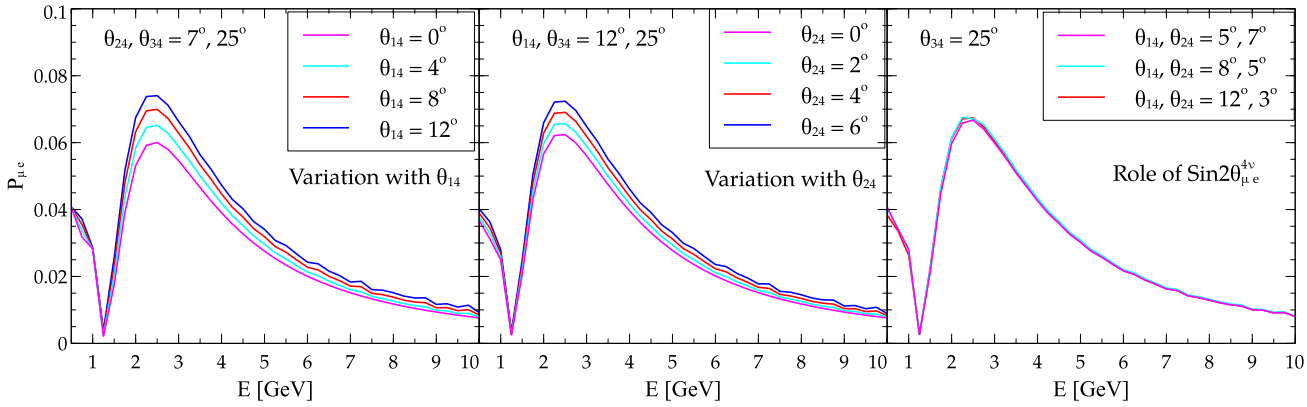

Figure 3.2: $P_{\mu e}$ vs E_ν in earth matter for 1300 km (generated using GLoBES simulation), showing the role of θ_{14} (left panel) and θ_{24} (middle) and the concept of the effective mixing angle $\sin 2\theta^{4\nu}_{\mu e} = \sin 2\theta_{14} \sin \theta_{24}$. In each panel, the values of the other fixed sterile mixing angles have been mentioned in the labels. In the third panel, the values of the doublet $\{\theta_{14}, \theta_{24}\}$ have been chosen such that the effective mixing angle is the same (≈ 0.0213).

perspective. In the right (3+1) panel, the significant differences between the solid and dashed lines of a given colour emphasize the role played by matter, while the equally significant differences between the blue and red dashed (solid) lines demonstrate the important role played by CP violating phases at long baselines in matter (vacuum) if they are non-zero. Turning to the left (3+0) panel, we note the relatively large differences between these curves and their counterparts in the right panel, underlining the significant effects of sterile neutrinos at the operational baseline for DUNE.

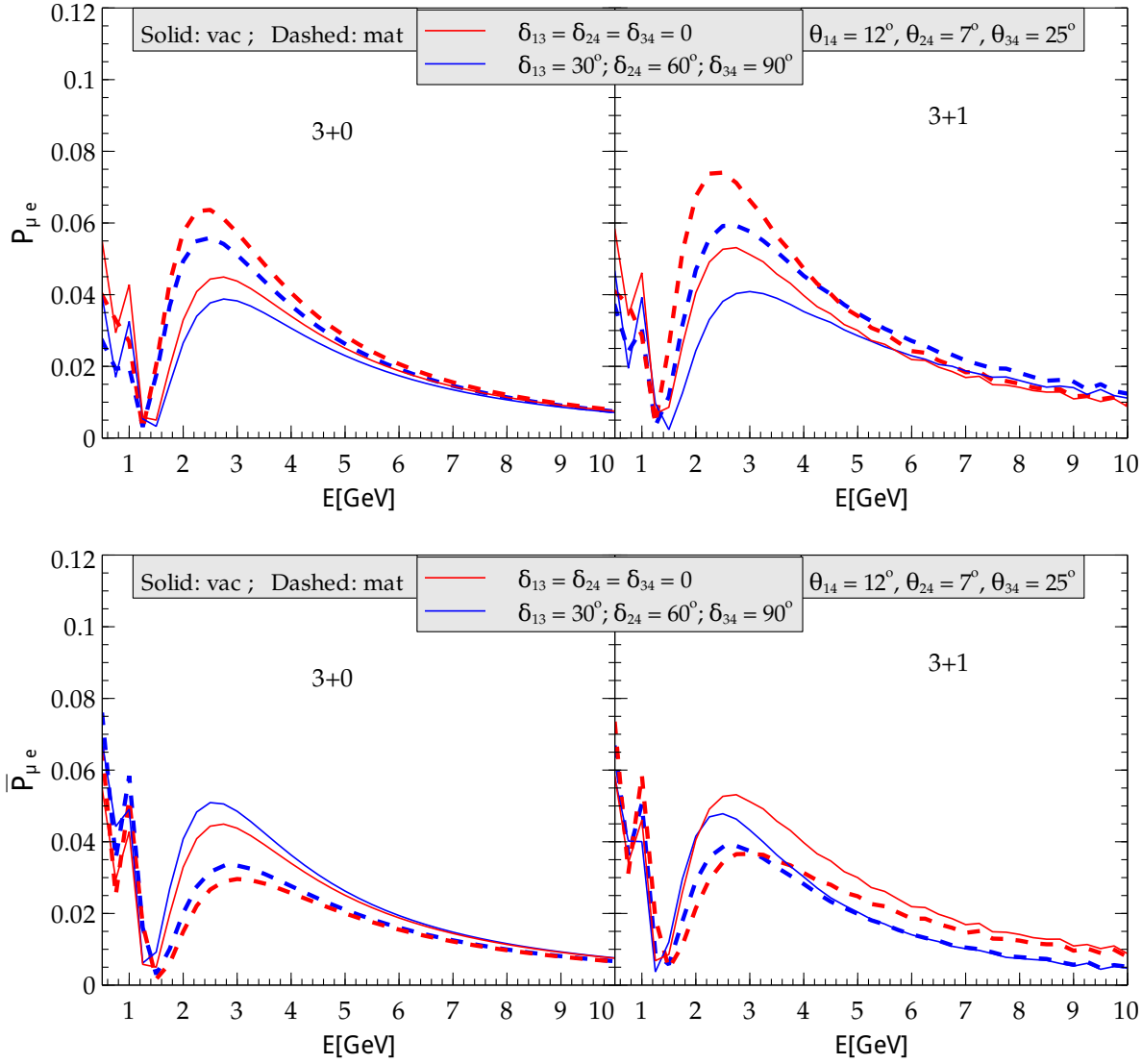

Figure 3.3: $P(\nu_\mu \to \nu_e)$ (both for vacuum and matter) for 3+0 (left panel) and 3+1 (right panel) vs. energy. The top (bottom) row is for neutrino (antineutrino). The red curves represent the CP conserving case, while the blue ones depict the case with phases set to non-zero fixed values (see the plot label). For the blue curve in the left panel, the sole 3+0 phase $\delta_{\rm CP}$ was taken as 30^o. Normal hierarchy is taken to be the true hierarchy here, and parameters related to the 3+0 sector have been set at the best-fit values specified in Sec. 3.1.

3.3 Result: A discussion of Neutrino-Antineutrino asymmetries in matter in the context of sterile neutrino

The consideration of CP violation in terms of an asymmetry defined at the probability level provides additional insight into the conclusions which can be reliably drawn from data if we do not know whether 3+0 or 3+1 is the choice nature has made. Consider the asymmetry defined as,

$$A^{\alpha\beta}_{\nu\bar{\nu}} = \frac{P_{\nu_\alpha\to\nu_\beta} - P_{\bar{\nu}_\alpha\to\bar{\nu}_\beta}}{P_{\nu_\alpha\to\nu_\beta} + P_{\bar{\nu}_\alpha\to\bar{\nu}_\beta}} \equiv \frac{\Delta P_{\alpha\beta}}{P_{\nu_\alpha\to\nu_\beta} + P_{\bar{\nu}_\alpha\to\bar{\nu}_\beta}}. \tag{3.9}$$

We begin by noting an important difference between the 3+0 and 3+1 scenarios with respect to the numerator $\Delta P_{\alpha\beta}$ of $A^{\alpha\beta}_{\nu\bar{\nu}}$. In vacuum, CPT invariance implies that $P(\nu_\beta \to \nu_\alpha) = P(\bar{\nu}_\alpha \to \bar{\nu}_\beta)$, which in turn implies that $\Delta P_{\beta\alpha} = -\Delta P_{\alpha\beta}$, and in particular that $\Delta P_{\alpha\beta} = 0$ when $\beta = \alpha$. Thus, when there are only three neutrino flavors, there are only three independent potentially non-zero CP-violating differences $\Delta P_{\alpha\beta}$ to be measured: $\Delta P_{e\mu}$, $\Delta P_{\mu\tau}$ and $\Delta P_{\tau e}$. Now, conservation of probability implies that for any number of flavors,

$$\sum_\beta P_{\nu_\alpha\to\nu_\beta} = 1 \quad \text{and} \quad \sum_\beta P_{\bar{\nu}_\alpha\to\bar{\nu}_\beta} = 1,$$

where the sums are over all β, including $\beta = \alpha$. It follows that $\sum_\beta \Delta P_{\alpha\beta} = 0$. Then, since $\Delta P_{\alpha\beta} = 0$ when $\beta = \alpha$, we conclude that in vacuum,

$$\sum_{\beta\neq\alpha} \Delta P_{\alpha\beta} = 0. \tag{3.10}$$

When there are only three flavors, this constraint implies that $\Delta P_{e\mu} + \Delta P_{e\tau} = 0$ and that $\Delta P_{\mu e} + \Delta P_{\mu\tau} = 0$. Since $\Delta P_{\beta\alpha} = -\Delta P_{\alpha\beta}$, it follows that,

$$\Delta P_{e\mu} = \Delta P_{\mu\tau} = \Delta P_{\tau e}. \tag{3.11}$$

That is, the three "independent" CP-violating differences are equal. In particular, if there are only three flavors, it is not possible for CP invariance to hold in one oscillation channel, such as $\overset{(-)}{\nu}_\mu \to \overset{(-)}{\nu}_e$, and yet be violated in another channel, such as $\overset{(-)}{\nu}_\mu \to \overset{(-)}{\nu}_\tau$.

This situation changes when there are more than three flavors. For *e.g.*, when there are four flavors, as in the 3+1 scenario, there are six independent potentially non-zero differences $\Delta P_{\alpha\beta}$: $\Delta P_{e\mu}$, $\Delta P_{\mu\tau}$, $\Delta P_{\tau e}$, ΔP_{es}, $\Delta P_{\mu s}$ and $\Delta P_{\tau s}$, where s refers to the sterile flavor. Now the constraint of Eq. 3.10 gives rise only to relations like

$$\Delta P_{e\mu} = \Delta P_{\mu\tau} + \Delta P_{\mu s}. \tag{3.12}$$

It is now perfectly possible for $\Delta P_{\mu e} (= -\Delta P_{e\mu})$, the CP-violating difference that will be the first to be probed experimentally, to be zero, while the differences $\Delta P_{\mu\tau}$ and $\Delta P_{\mu s}$ in other oscillation channels that are challenging to study, are large[6].

In Fig. 3.4, we show the spread of $A_{\nu\bar{\nu}}$[7] at $L = 1300$ km for cases chosen to illustrate some of the important features that arise due to the presence of a fourth, sterile state. The left-hand panels were created with all CP-violating phases set to zero, so the asymmetries shown in these panels are from matter effects only. The right-hand panels were created allowing the sole 3+0 CP phase $\delta_{\rm CP}$ to vary over its entire physical range in the case of 3+0, and the three CP phases δ_{13}, δ_{24} and δ_{34} to vary over their entire ranges in the case of 3+1. Thus, these panels show the impact of intrinsic CP violation. In all panels, the red curve(s) are for the 3+0 case, and the blue ones for the 3+1 case. The top two panels assume a normal hierarchy, and the bottom two an inverted hierarchy. In creating all panels, the mass splittings and mixing angles of the 3+0 sector were set to the best-fit values specified in Sec. 3.1, the splitting Δm^2_{41} of the 3+1 sector was set to 1 eV^2, and the 3+1 mixing angles θ_{14}, θ_{24} and θ_{34} were varied over their allowed ranges.

With one exception (see below), to create the curves in each panel of Fig. 3.4 for each of the two scenarios, 3+0 and 3+1, we varied the corresponding parameters until we found the parameter set that maximizes (minimizes) the energy-integrated asymmetry $A_{\nu\bar{\nu}}$ for that scenario. The energy-dependent asymmetry was then plotted vs. energy for this parameter set as a solid (dashed) curve. (Note that since it is the energy-integrated asymmetry that is being extremized, it is possible for the 3+0 energy-dependent asymmetry to be more extreme than that for 3+1 for a limited range of energy, despite the fact that the 3+0 scenario is in a sense, a special case of 3+1.) The one exception to our procedure is that, since the 3+0 sector parameters other than $\delta_{\rm CP}$ were held fixed throughout, in creating the left-hand panels, no 3+0 parameters were varied, so there is only a single curve, shown as solid, for 3+0.

From the left-hand panels of Fig. 3.4, we see that when CP is conserved, the neutrino-antineutrino asymmetry vs. energy is quite similar in the 3+0 and 3+1 scenarios. In the 3+1 scenario, this asymmetry is confined to a rather narrow band as the 3+1 mixing angles

[6]We note that any long baseline experiment involves earth-matter effects, which break CPT (in addition to CP). Such breaking is extrinsic, and due to the asymmetry of the earth matter through which the neutrinos propagate. While this may appear to destroy the conclusions reached above, which depend on CPT invariance, this is not the case as long as an experiment seeks to measure intrinsic (*i.e.*driven by phases in the mixing matrix) CP violation and devises appropriate means to do so.

[7]Henceforth we drop the superscripts α and β and take $A_{\nu\bar{\nu}}$ to denote the asymmetry for $\alpha = \mu$ and $\beta = e$.

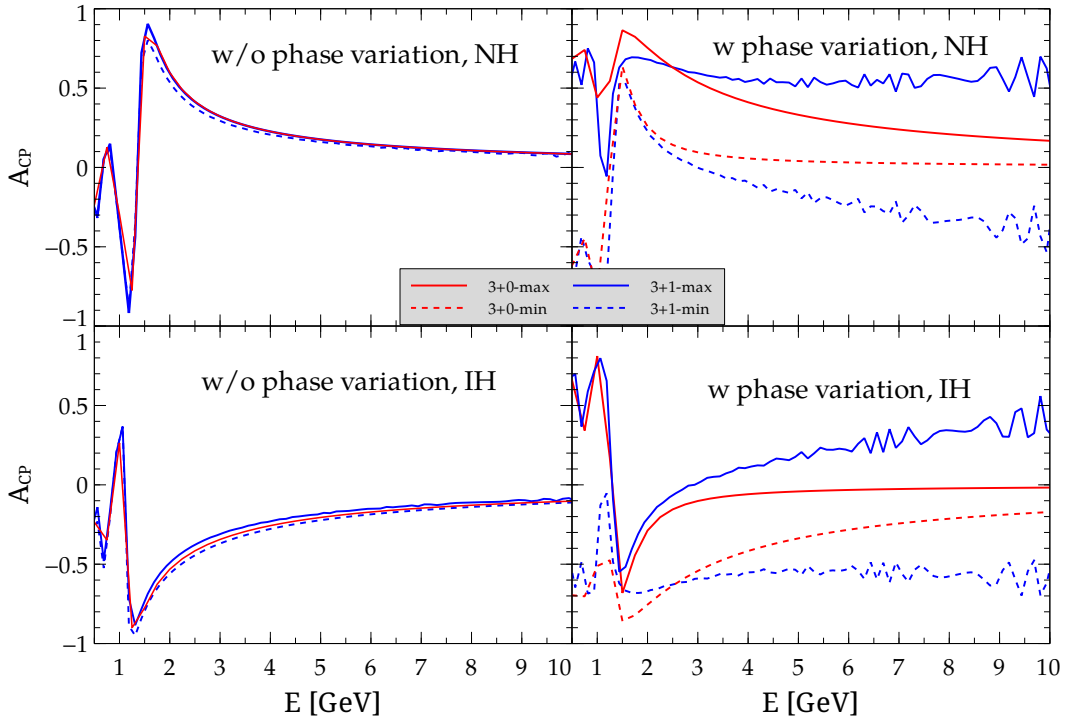

Figure 3.4: The neutrino-antineutrino asymmetry $A_{\nu\bar{\nu}}$ vs. energy E. See text for explanation and discussion.

are varied. Although it is not shown, we have found that it is confined to a similar narrow band in the 3+0 scenario if the 3+0 parameters θ_{23} and Δm^2_{31} are varied within their experimental uncertainties. Clearly, if an experiment were to measure an asymmetry vs. energy that consistently lies outside the similar, narrow 3+0 and 3+1 bands that correspond to CP conservation, we would have evidence that CP is violated so long as nature has chosen either the 3+0 or 3+1 scenario. However, a measured asymmetry between $\nu_\mu \to \nu_e$ and $\bar{\nu}_\mu \to \bar{\nu}_e$ that lies within these similar narrow bands would not unambiguously signal that there is no CP violation in neutrino oscillation. As explained above, when there are more than three flavors, as in the 3+1 scenario, it is possible for there to be little or no CP violation in one oscillation channel, and yet a large CP violation in some other channel. In addition, for either the 3+0 or 3+1 case, it might happen that for some non-zero values of the CP-violating phases and mixing angles slightly different from those corresponding to the CP-conserving bands, the asymmetry still lies within those bands within uncertainties.

The right-hand panels in Fig. 3.4 show that when intrinsic CP is violated, $A_{\nu\bar{\nu}}$ can be anywhere in a large range. Moreover, for 3+1, this range is much larger than for 3+0,

and includes almost all of the 3+0 range. Thus, we see that sterile neutrinos with $O(1)$ eV^2 masses can very substantially impact CP-violation measurements at long baselines. While a measured asymmetry outside the band allowed for 3+0 would be evidence for new physics beyond 3+0, one inside that band would leave uncertain the precise origin of the observed CP violation.

3.4 Result: Event Rates at DUNE in the 3+1 and 3+0 scenarios

In this section we illustrate how the probability level discussions in the previous sections 3.2 and 3.3 translate to the level of observable events in the detector. Fig. 3.5 shows the spread of binned events at DUNE as a function of the reconstructed neutrino energy for the 3+0 case and the 3+1 case. For the 3+0 case, we varied only $\delta_{\rm CP}$ in the range $[-180°, 180°]$ to first find the $\delta_{\rm CP}$ which maximises (minimises) total no. of events and then plotted the maximum / minimum event spectrum corresponding to this value of $\delta_{\rm CP}$ as function of energy to obtain the events band shown in red. For 3+1, we chose three sets of $(\theta_{14}, \theta_{24}, \theta_{34})$ values - $(12°, 7°, 25°)$, $(8°, 5°, 15°)$ and $(4°, 3°, 5°)$. For all these three cases, we varied the phases δ_{13}, δ_{24} and δ_{34} in the range $[-180°, 180°]$ each to find those sets of $\{\delta_{13}, \delta_{24}, \delta_{34}\}$ which gives the maximum and the minimum total no. of events (*i.e.*, summed over the energy bins). The upper and the lower boundary of the event spectrum were then plotted for these choices of $\{\delta_{13}, \delta_{24}, \delta_{34}\}$ as a functions of energy[8]. The resulting event-bands are shown in blue, green and magenta, respectively. The left (right) panels show the neutrino (anti-neutrino) rates, while the top (bottom) panels are for the NH (IH) scenario.

It can be seen that for all three sets of θ_{14}, θ_{24}, the 3+1 band can potentially encompass the 3+0 band, leading to substantial degeneracy. When the number of events falls in the overlapping region between these two bands (which is the red region in Fig. 3.5), there is considerable ambiguity as to whether the events are produced by a certain value of $\delta_{\rm CP}$ in the 3+0 sector or by some combination of θ_{34}, δ_{13}, δ_{24} and δ_{34} in the 3+1 sector.

Fig. 3.5 also shows that the 3+1 band gets wider as the values of θ_{14}, θ_{24} and hence the effective mixing angle $\sin 2\theta^{4\nu}_{\mu e}$ increase. Indeed, for sufficiently large 3+1 mixing angles,

[8]Thus, for one particular upper (or lower) boundary the choice of $\{\delta_{13}, \delta_{24}, \delta_{34}\}$ is the same throughout the energy range. We have also observed (although not shown here) that, if $\{\delta_{13}, \delta_{24}, \delta_{34}\}$ were instead varied for each energy bin individually to find the maximum/ minimum event for that energy bin, the resulting event band spectra looked very similar to fig. 3.5. Obviously, the values of $\{\delta_{13}, \delta_{24}, \delta_{34}\}$ would be different for each energy bin.

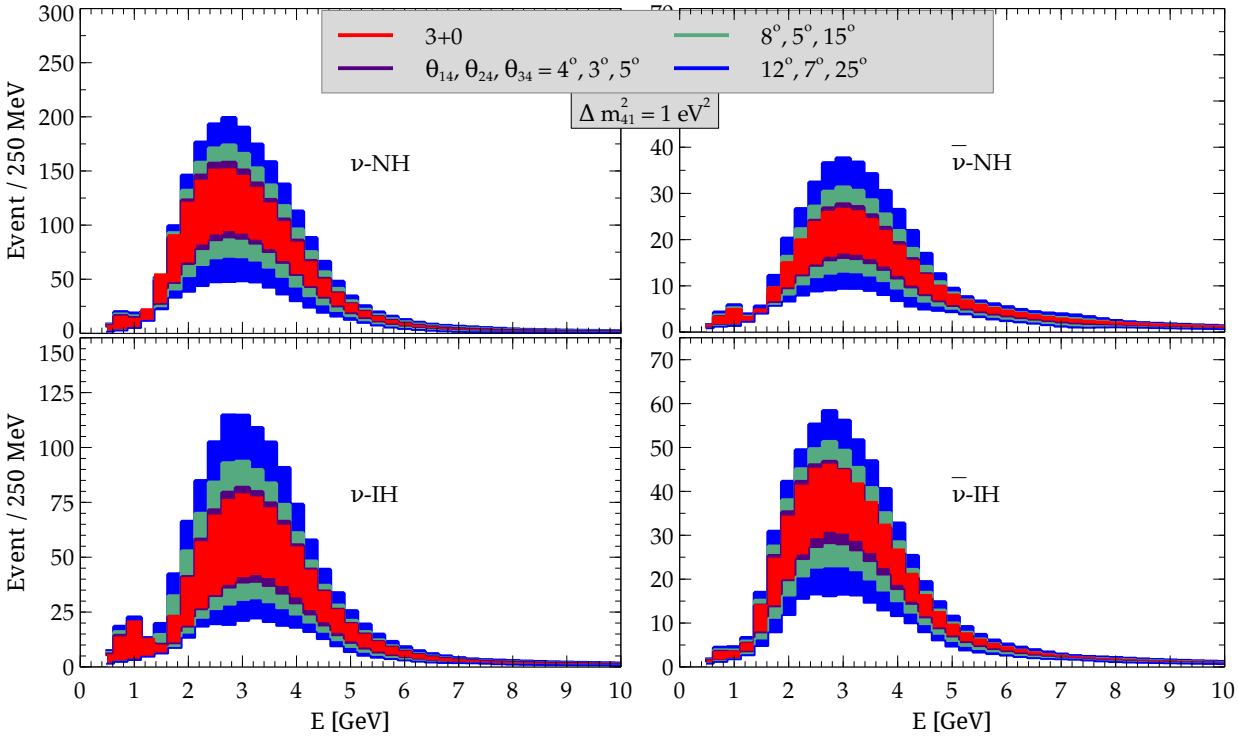

Figure 3.5: Neutrino and anti-neutrino event rates in DUNE plotted as a function of the reconstructed neutrino energy. The vertical spread for a given color for an energy bin shows the maximum and the minimum events rates possible.

the 3+1 band is substantially larger than its 3+0 counterpart. An observed surfeit or a dearth of events compared to those expected in the 3+0 case, especially near the event maxima (around the region 2-4 GeV), could be a pointer to the presence of sterile states.

3.5 Result: Sensitivity to CP Violation

So far, in sections 3.2, 3.3 and 3.4 we have discussed the significant effect of one $O \sim 1\ eV$ sterile neutrino in the probability and the event levels. We now see how significant the effect of sterile neutrino is when translated to the χ^2 level, in particular in the measurement of CP violation and mass hierarchy at long baselines. Similar methodology for χ^2 calculation as in sec. 2.3 was also implemented here using the GLoBES package [189,190].

For CP violation sensitivity, we ask the question (see also the beginning of sec. 2.5) how well the true dataset containing all the values of the CP phase ($\in [-\pi, \pi]$) can be distinguished from the test dataset containing only the CP conserving values of the phase (0 or π). In the true dataset we choose three sets

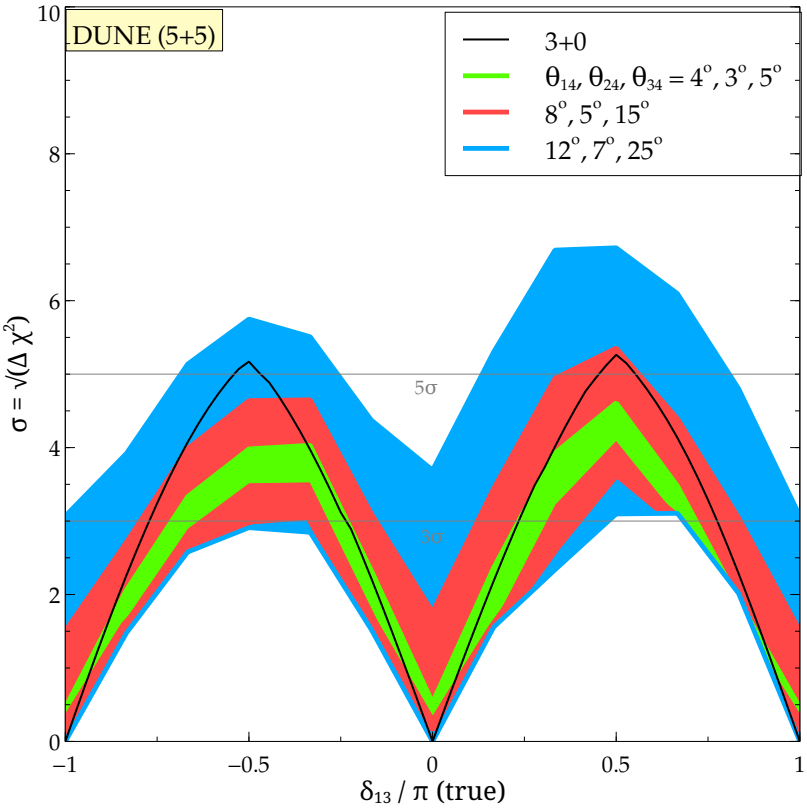

Figure 3.6: Sensitivity to CP violation as a function of the true CP violating phase δ_{13} for DUNE for 5 yrs. of neutrino and 5 yrs. of antineutrino running. Different colors correspond to different choice of true $\theta_{14}, \theta_{24}, \theta_{34}$ as shown in the key. Variation of true δ_{24} and δ_{34} results in the colored bands which show the minimum and maximum of the marginalised sensitivity that can be obtained for a particular δ_{13}. The black curve corresponds to sensitivity to CP violation in 3+0.

of the true active-sterile mixing angles $(\theta_{14}, \theta_{24}, \theta_{34}) = (4^o, 3^o, 5^o)$, $(8^o, 5^o, 15^o)$ and $(12^o, 7^o, 25^o)$ and vary the values of true CP phases in the full interval $\{-\pi, \pi\}$. On the other hand, since for the $3 + 1$ scenario, there are two more additional CP phases, the test dataset contains 8 possible CP conserving cases: $\{\delta_{13}^{test}, \delta_{24}^{test}, \delta_{34}^{test}\} = \{0, 0, 0\}, \{\pi, 0, 0\}, \{0, \pi, 0\}, \{0, 0, \pi\}, \{\pi, \pi, 0\}, \{\pi, 0, \pi\}, \{0, \pi, \pi\}, \{\pi, \pi, \pi\}$[9] and also contains the variation of the test $\theta_{14}, \theta_{24}, \theta_{34}$ in the allowed ranges: $[0°, 12°], [0°, 7°], [0°, 25°]$ respectively. We thus calculate the χ^2 between the true and test dataset using GLoBES and minimise it over these 8 test CP conserving cases to quote the most conservative estimate. The χ^2 so obtained, is also minimised over the test $\theta_{14}, \theta_{24}, \theta_{34}$ samples in the allowed range in

[9]Note that, this assumes that the experiment cannot pinpoint the source of CP violation (*i.e.*, whether it is coming from δ_{13} or δ_{24} or δ_{34}) in presence of 1 sterile neutrino. In the standard $3 + 0$ case (discussed in chapter 2), since there is only one relevant CP phase (the Dirac CP phase δ_{CP} or δ_{13}), the source of CP violation is obvious. But the scenario becomes much more complicated in presence of 2 more additional CP phases in $3 + 1$ scenario.

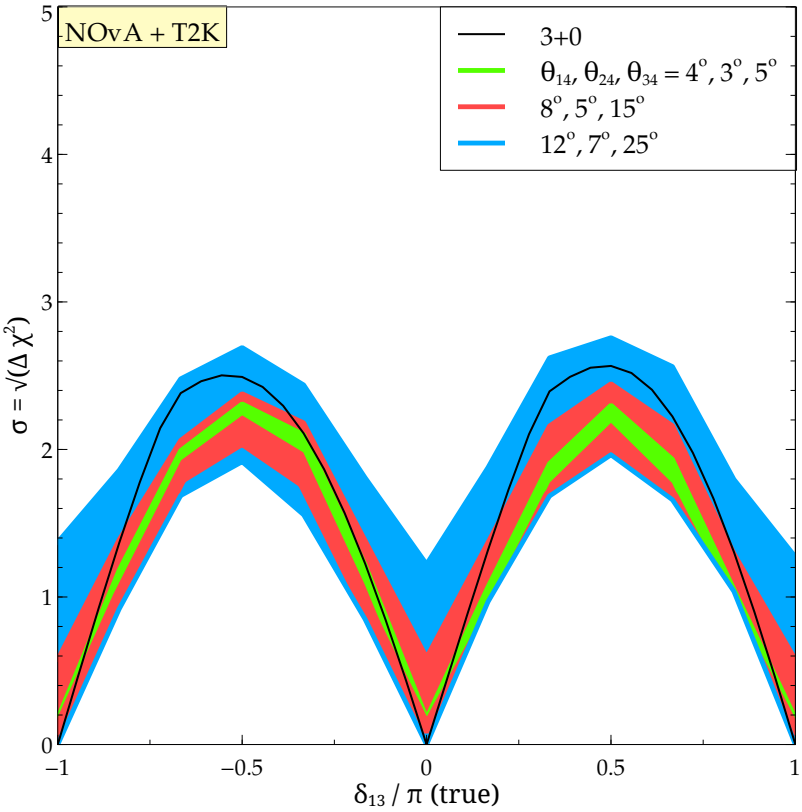

Figure 3.7: Similar to fig. 3.6 but for the combined NOvA and T2K with 3 yrs. of neutrino and 3 yrs. of antineutrino running for both the experiments.

the fit, so as to account for the lack of information regarding active-sterile mixings. This gives us a marginalised χ^2 as a function of the true parameters. We did not marginalise over the 3+0 parameters, or the hierarchy[10]. For a particular true δ_{13}, we show the maximum and the minimum of the marginalised χ^2 that can be obtained corresponding to a variation of the other two true CP phases δ_{24} and δ_{34}- giving rise to the *bands* in fig. 3.6. For 3+0, the situation is simpler (same method as that of the standard 3ν scenario discussed in sec. 2.5), where we contrast a true $\delta_{\rm CP}$ against $\delta_{\rm CP} = 0$ and $\delta_{\rm CP} = \pi$ in the test. In figs. 3.7 and 3.8 we show the similar CPV sensitivity study for the context of other long baseline experiments NOvA+ T2K (combined) and also for T2HK.

It can be seen from figs. 3.6, 3.7, 3.8 that the existence of sterile neutrinos can significantly affect the CPV discovery potential of long-baseline experiments. This violation

[10]Our results show that a close to 5σ determination of hierarchy is very likely with the DUNE experiment, even in the 3+1 paradigm. Among other 3+0 oscillation parameters, marginalisation over θ_{23} may be important when the non-maximal true values like the ones in lower octant or higher octant are considered. Disappearance ($P_{\mu\mu}$) data fixes $\sin^2 2\theta_{23}$ very accurately and hence, marginalisation over test θ_{23} is not necessary for true $\theta_{23} = 45°$.

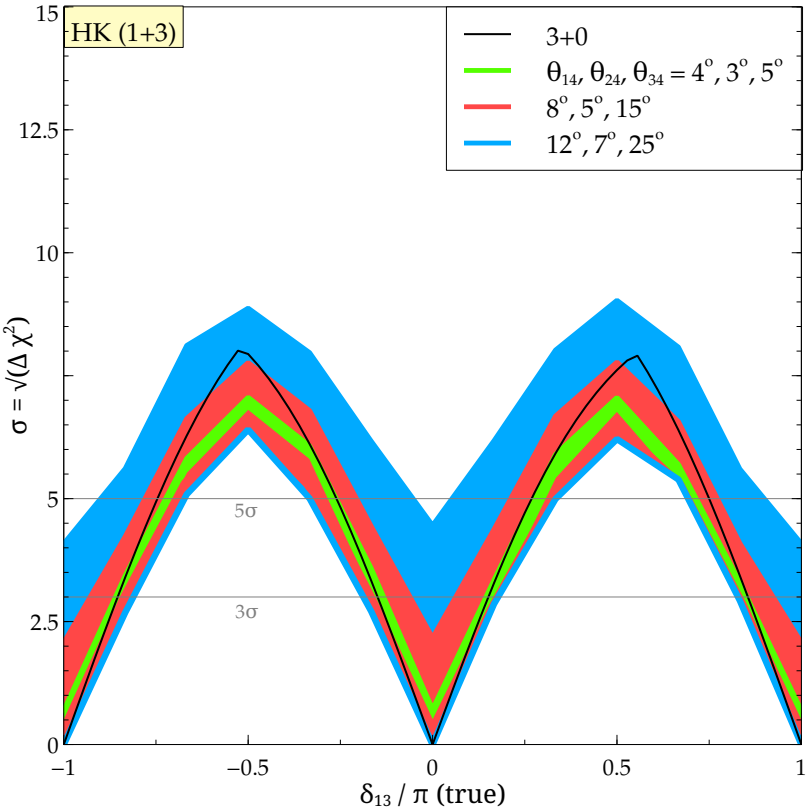

Figure 3.8: Similar to fig. 3.6 but for T2HK with 1 yr. of neutrino and 3 yrs. of antineutrino runtime.

can originate in any of the three phases and not just δ_{13}. When the active-sterile mixings are small, the general trend visible in the figures is that the sensitivity to CP violation of the experiment will be decreased compared to what we would expect in the 3+0 scenario. However, for sufficiently large mixings, the sensitivity spans both sides of the 3+0 curve; and hence, depending on the true value of the other phases - δ_{24} and δ_{34}, the sensitivity to CP violation can be greatly amplified. We also note that there can be significant amplification of CPV sensitivity for regions of δ_{13} where one expects little or none in the 3+0 scenario. For *e.g.*, in the case of DUNE (fig. 3.6), if the active-sterile mixing angles $(\theta_{14}, \theta_{24}, \theta_{34})$ are sufficiently large (closer to $12°, 7°, 25°$ respectively) the resulting CPV sensitivity can be as large as $\gtrsim 3\sigma$ even when δ_{13}^{true} is CP conserving (0 or $\pm\pi$). Hence, if sterile mixing angles are not tiny, the 3+1 (or 3+n) scenario, if realized in nature, makes the observation of generic CPV sensitivity *per se* significantly more likely than the 3+0 case, although it makes the determination of the phase (or phases) in which such violation originates much harder.

Further, we note the role of the following competing effects in the calculation of χ^2:

(a) Decrease in χ^2 due to additional test values - 3+1 scenario introduces more number of parameters in the sensitivity analysis. If marginalization is carried out over more number of test parameters, it results in a decreased value of χ^2. This is purely a statistical effect. Since the marginalisation is carried out over the same allowed ranges (${\theta_{14}}^{test} \in [0°, 12°], {\theta_{24}}^{test} \in [0°, 7°], {\theta_{34}}^{test} \in [0°, 25°]$ and the three test phases take the 8 possible CP conserving values), the magnitude of the statistical effect remains the same irrespective of the true values.

(b) Increase in χ^2 due to additional true values - In presence of 3+1 scenario there are more sources of CP violation. We now have the additional active-sterile angles $(\theta_{14}, \theta_{24}, \theta_{34})$ and a total of 3 CP phases $(\delta_{13}, \delta_{24}, \delta_{34})$. As the true values of the angles increase, the associated CP phases have more impact on χ^2. This is manifested by the widening of the sensitivity bands in figs. 3.6, 3.7, 3.8 as the strength of the mixing angles increases.

In figs. 3.6, 3.7, 3.8, when the true $(\theta_{14}, \theta_{24}, \theta_{34})$ are small (see the green bands), effect (b) is smaller than the statistical effect (effect (a)). Hence the dominant statistical effect brings the χ^2 down, as compared to the standard 3+0 result (black curves). Again, when the true values of the angles $(\theta_{14}, \theta_{24}, \theta_{34})$ increase, effect (b), overtakes effect (a) and this basically spans the χ^2 band (see the blue band) to roughly both above and below the 3+0 curve. We also note that the effect of sterile neutrinos is more pronounced at longer baseline experiments DUNE (fig. 3.6) due to higher matter effect [11].

3.6 Result: Sensitivity to mass hierarchy

In this section we follow the similar methodology as in sec. 2.4, and examine the impact of a sterile neutrino on the sensitivity to the mass hierarchy. Here, we take the same true dataset with a particular true hierarchy (assumed normal here) as in sec. 3.5. In the test dataset we take the opposite hierarchy (inverted), vary the angles in their allowed values (see sec. 3.5) and all the 3 phases over the full range $[-\pi, \pi]$. The resulting χ^2 between true and the test dataset thus gives the sensitivity to the true hierarchy being normal. This sensitivity was shown in figs. 3.9 (for DUNE) and 3.10 (for combined NOvA and T2K) [12].

[11] See fig. 3.3 to see the role of matter effect in the context of 3+1 scenario.

[12] Note that because of the larger range of marginalisation due to the variation of the test phases in the full allowed range, the statistical effect (effect (a), discussed in the previous section has a larger role in the context of mass hierarchy. This is manifested by the fact that all the 3+1 sensitivity bands lies mostly below the 3+0 sensitivity curve

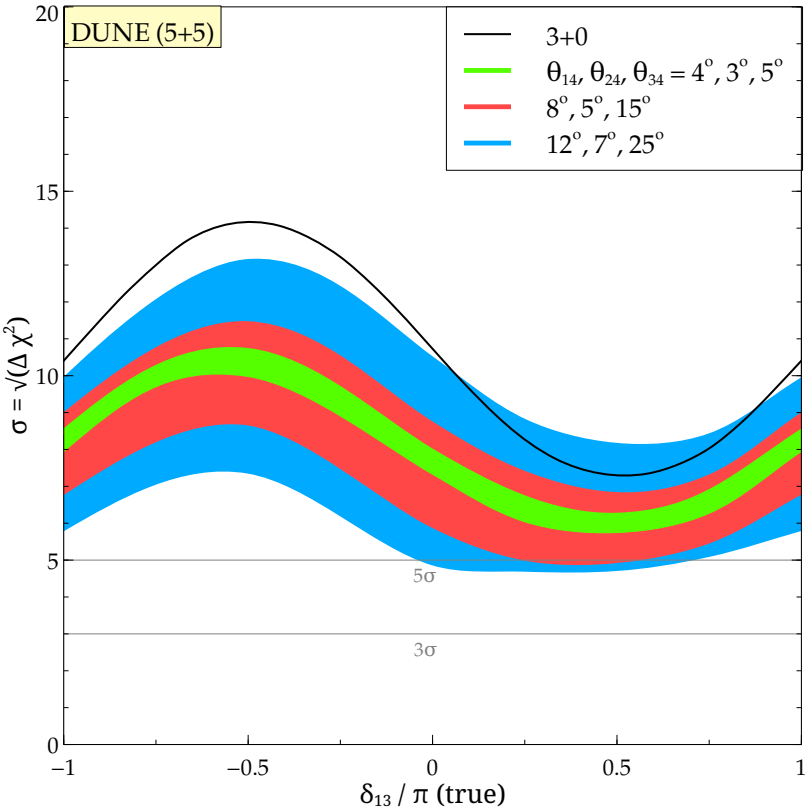

Figure 3.9: Sensitivity to mass hierarchy as a function of the true CP violating phase δ_{13} for DUNE for 5 yrs. of neutrino and 5 yrs. of antineutrino running. Different colors correspond to different choice of true $\theta_{14}, \theta_{24}, \theta_{34}$ as shown in the key. Variation of true δ_{24} and δ_{34} results in the colored bands which show the minimum and maximum of the marginalised sensitivity that can be obtained for a particular δ_{13}. The black curve corresponds to sensitivity to mass hierarchy in 3+0. Normal hierarchy was assumed to be the true hierarchy here.

Note that, as in the previous section, we did not vary the test 3+0 parameters in the fit. In the case of DUNE, we find that the 3+1 sensitivities are usually below 3+0 sensitivities except for a small region of parameter space around true $\delta_{13} = 90°$, as can be observed in Fig. 3.9. It should be noted that except for a small fraction of parameter space around true $\delta_{13} = 90°$, the sensitivity stays above 5σ C.L.

For the combined results from T2K and NOνA, it can be seen in Fig. 3.10 that there emerges the possibility of significant improvement in the hierarchy sensitivity compared to 3+0 (shown by black line) in the unfavourable regions of true δ_{13}. The extent of this enhancement is, of course, dependent on the true values of the active-sterile oscillation parameters.

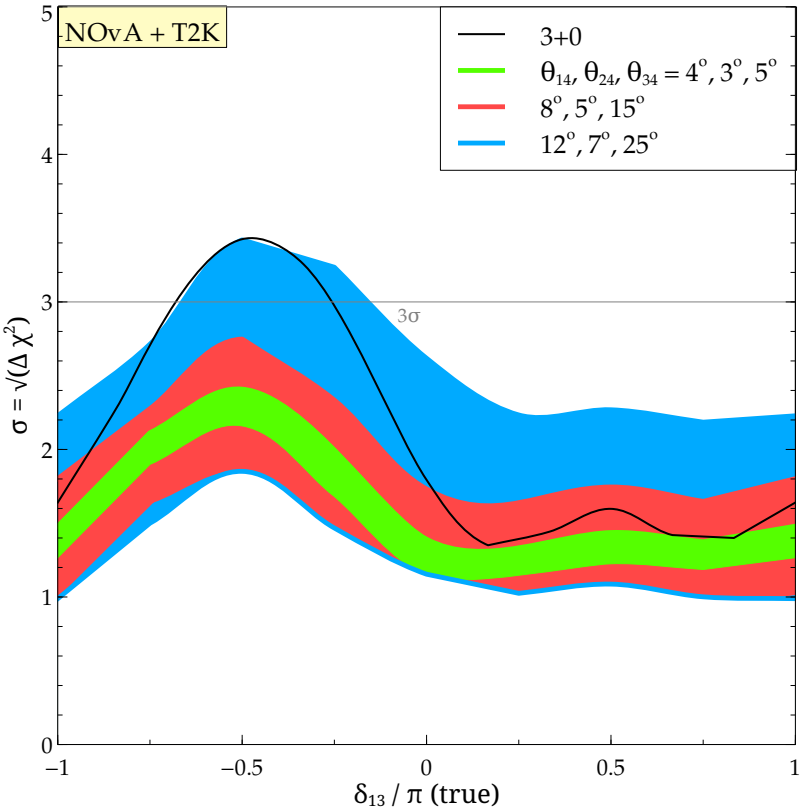

Figure 3.10: Similar to fig. 3.9 but for the combined NOvA+ T2K.

3.7 Result: DUNE's sensitivity to small active-sterile mixing angle

The Short Baseline Neutrino (SBN) program at Fermilab aims to conclusively establish the existence or else to place stringent constraints on the possible existence of the sterile neutrinos. At short baselines, the $P_{\mu e}$ oscillation probability is sensitive only to the mass-squared difference δm^2_{41} and an effective mixing angle given by $\sin^2 2\theta_{\mu e} = \sin^2 2\theta_{14} \sin^2 \theta_{24}$. For $\delta m^2_{41} \sim 1$ eV^2 induced oscillations, the SBN program can exclude at 3σ only $\sin^2 2\theta_{\mu e} \geq 0.001$ [236]. It is natural to ask how tightly active-sterile mixings need to be excluded to ensure that DUNE measurements can be safely interpreted without taking the possible existence of sterile neutrinos into account. Phrasing this question another way, we ask whether active-sterile mixings corresponding to $\sin^2 2\theta_{\mu e} < 0.001$ can be detected by the DUNE far detector. Fig. 3.11 (left panel) throws some light on this question. Here, we have compared the CP bands in event rates assuming 3+1 and 3+0 for very small mixing angles - $\theta_{14}, \theta_{24}, \theta_{34} = 3°, 2°, 10°$ ($\sin^2 2\theta_{\mu e} \approx 0.00001$). We see that the 3+1

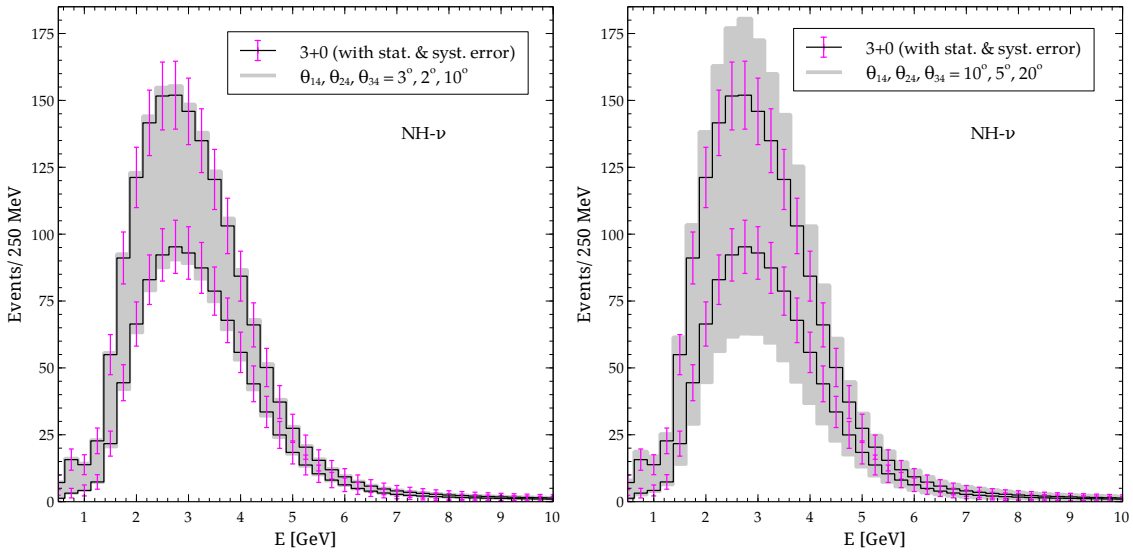

Figure 3.11: Neutrino event rates for the DUNE experiment as a function of the reconstructed neutrino energy. The black lines show the maximum and the minimum event rates corresponding to a variation of δ_{CP} in 3+0. Also shown are the corresponding statistical ($\sqrt{\text{Event no.}}$) and systematic error (2%) [4] added in quadrature for each energy bin. The grey band corresponds to the maximum and minimum event rates assuming 3+1 with $\theta_{14}, \theta_{24}, \theta_{34} = 3°, 2°, 10°$ (left panel), $\theta_{14}, \theta_{24}, \theta_{34} = 10°, 5°, 20°$ (right panel) and $\delta_{13}, \delta_{24}, \delta_{34}$ varied in $[-180°, 180°]$. Only the channel $\nu_\mu \to \nu_e$ has been considered with 5 years of ν-running assuming normal hierarchy.

band is completely degenerate with the 3+0 band (incorporating the errorbars[13]). Thus, for such small mixing angles, it seems that neither the Short Baseline experiments nor the DUNE experiment may see evidence of new physics attributable to sterile neutrinos. In the right panel of the same figure, however, we have chosen $\theta_{14}, \theta_{24}, \theta_{34} = 10°, 5°, 20°$ ($\sin^2 2\theta_{\mu e} \approx 0.0009$). These larger values, which correspond to an effective mixing angle at the 3σ sensitivity of the short-baseline experiments, lead to enhanced effects. The grey band now extends significantly beyond the expected event rates for 3+0, even after accounting for errors. This provides a suggestive estimate of how large the mixing angles need to be before sterile neutrino effects at DUNE start to be discernable.

We stress that short-baseline experiments are significantly more sensitive, by design, to CP conserving oscillatory effects in 3+1 compared to long-baseline experiments, and hence remain the definitive test by which presence or absence of sterile neutrinos can be established. Long-baseline experiments, however, can become sensitive to the presence of this sector if CPV is present. Moreover, matter enhances the effects of CP, further enabling

[13]The error for each energy bin is the quadrature sum of the statistical ($\sqrt{\text{Event no.}}$) and the systematic error (2%) [4]. The value is an estimated expected value assuming the presence of a highly capable near-detector [4].

these experiments to become, in a sense, complementary detectors of sterile neutrinos [213].

Chapter 4

CP and hierarchy measurement in the light of non standard neutrino interaction (NSI) in propagation

As discussed in chapter 2, the main focus of the ongoing and future neutrino experiments is to address the question of neutrino mass hierarchy *i.e.*, sign (Δm^2_{31}) [1], measurement of the CP phase (δ) and establishing the correct octant of the mixing angle θ_{23}. The question of whether CP is violated in the leptonic sector is of prime importance in astrophysics, cosmology and particle physics today. For the three flavour case in vacuum, the only source of CP violation in mixing phenomena is the Dirac-type CP phase, δ [237]. This is usually referred to as the intrinsic CP phase.

It is well-known that for baselines $\sim \mathcal{O}(1000)$ km, the standard Earth matter effects [33, 34] are non-negligible. This poses a problem in the determination of intrinsic CP phase as matter induces additional CP violating effects in the oscillation formalism, commonly referred to as extrinsic (fake) CP violation effects [238]. Any new physics in neutrino interactions can, in principle, allow for flavour changing interactions thereby allowing for additional CP violating phases which can complicate the extraction of the intrinsic CP phase further. The high precision offered by DUNE facilitates probing new physics phenomenon such as additional sterile neutrino states which has been recently studied [213, 226], probing Lorentz and CPT violation (e.g. in [239, 240]) as well as NSI during propagation (e.g. in [241–253] NSI in propagation has recently been studied in the context of long baselines.) with high sensitivity. In the present article, we explore the impact of NSI in propagation on CP violation signal at upcoming long baseline neutrino experiments DUNE [14, 175], T2HK [15] and also at the presently running long baseline

[1] $\Delta m^2_{31} = m^2_3 - m^2_1$.

experiments T2K [10,196,197] and NOvA [9].

4.1 Brief discussion on NSI framework

The non standard interaction (NSI) in neutrino oscillation sector has been studied in detail in literature and can be expressed as [33,85,86]

$$\mathcal{L}_{NSI} = -2\sqrt{2}G_F\varepsilon_{\alpha\beta}^{f\,f^{'}\,C}\,[\bar{\nu}_\alpha\gamma^\mu P_L\nu_\beta]\,[\bar{f}\gamma_\mu P_C f'] \,, \tag{4.1}$$

where G_F is the Fermi constant, ν_α, ν_β are neutrinos of different flavours ($\alpha, \beta = e, \mu, \tau$), and $\varepsilon_{\alpha\beta}^{f\,f^{'}\,C}$ are the NSI parameters ($f, f^{'} = e, u, d$ and $C = L, R$). If $f \neq f^{'}$, the NSI is charged current like whereas if $f = f^{'}$, the NSI is neutral current like and the parameters are defined as $\varepsilon_{\alpha\beta}^{f\,f^{'}\,C} = \varepsilon_{\alpha\beta}^{f\,C}$. The NSI operators in eq. 4.1 are non-renormalizable and also not gauge invariant. If the NSI arises at scale $M_{NP} \gg M_{EW}$ from some higher dimensional operators (of order six or higher), it would imply a suppression of at least $\varepsilon_{\alpha\beta}^{fC} \simeq (M_{EW}/M_{NP})^2$ (since $M_{EW} \sim 0.1$ TeV, for $M_{NP} \sim 1\ TeV$, we have $\varepsilon_{\alpha\beta}^{fC} \simeq 10^{-2}$ (see also [254–257])). In principle, NSI can have effects both a) on the production and detection level [85,254,258,259] [2] and also b) during the propagation of neutrinos though the matter [33,262–264]. In the present work, we discuss about the effect of NSI in propagation in the context of long baseline experiments (DUNE, T2K, NOvA and T2HK.). At the level of the underlying Lagrangian, NSI coupling of the neutrino can be to e, u, d. Phenomenologically, only the incoherent sum of contributions from different scatterers contributes to the coherent forward scattering of neutrinos on matter. If we normalize to n_e, the effective NSI parameter relevant for neutral Earth matter is,

$$\varepsilon_{\alpha\beta} \;=\; \sum_{f=e,u,d} \frac{n_f}{n_e}\varepsilon_{\alpha\beta}^{f} = \varepsilon_{\alpha\beta}^{e} + 2\varepsilon_{\alpha\beta}^{u} + \varepsilon_{\alpha\beta}^{d} + \frac{n_n}{n_e}(2\varepsilon_{\alpha\beta}^{d} + \varepsilon_{\alpha\beta}^{u}) = \varepsilon_{\alpha\beta}^{e} + 3\varepsilon_{\alpha\beta}^{u} + 3\varepsilon_{\alpha\beta}^{d} \,, \tag{4.2}$$

where n_f is the density of fermion f in medium crossed by the neutrino. Note that, only the vector sum of NSI terms, $\varepsilon_{\alpha\beta}^{f} = \varepsilon_{\alpha\beta}^{fL} + \varepsilon_{\alpha\beta}^{fR}$ appears in the oscillation formalism.

In presence of NSI, the propagation of neutrinos is governed by a Schrödinger-type equation with the effective Hamiltoninan:

$$\mathcal{H} \;=\; \mathcal{H}_{\text{vac}} + \mathcal{H}_{\text{SI}} + \mathcal{H}_{\text{NSI}} \,, \tag{4.3}$$

[2] Production and detection NSI's induce non-unitary effect, known as the so called *zero distance effect*, which means a neutrino flavor transition effect would already happen at the source even before the normal neutrino oscillation process starts. [260,261].

where $\mathcal{H}_{\rm vac}$ is the vacuum Hamiltonian and $\mathcal{H}_{\rm SI}, \mathcal{H}_{\rm NSI}$ are the effective Hamiltonians in presence of SI alone and NSI respectively. Thus,

$$\mathcal{H} = \frac{1}{2E}\left\{\mathcal{U}\begin{pmatrix} 0 & & \\ & \Delta m^2_{21} & \\ & & \Delta m^2_{31}\end{pmatrix}\mathcal{U}^\dagger + A(x)\begin{pmatrix} 1+\varepsilon_{ee} & \varepsilon_{e\mu} & \varepsilon_{e\tau} \\ \varepsilon_{e\mu}{}^\star & \varepsilon_{\mu\mu} & \varepsilon_{\mu\tau} \\ \varepsilon_{e\tau}{}^\star & \varepsilon_{\mu\tau}{}^\star & \varepsilon_{\tau\tau}\end{pmatrix}\right\}, \quad (4.4)$$

where $A(x) = 2\sqrt{2}EG_F n_e(x)$ is the standard CC potential due to the coherent forward scattering of neutrinos and n_e is the electron number density and $\varepsilon_{\alpha\beta}\,(\equiv |\varepsilon_{\alpha\beta}|\, e^{i\phi_{\alpha\beta}})$ are complex NSI parameters.

Let us now briefly mention the constraints imposed on the NC NSI parameters (for more details, see [261, 265]). With the assumption that the errors on individual NSI terms are uncorrelated, model-independent bounds on effective NC NSI terms

$$\varepsilon_{\alpha\beta} \lesssim \left\{\sum_{C=L,R}[(\varepsilon^{eC}_{\alpha\beta})^2 + (3\varepsilon^{uC}_{\alpha\beta})^2 + (3\varepsilon^{dC}_{\alpha\beta})^2]\right\}^{1/2},$$

were obtained [265] which leads to

$$|\varepsilon_{\alpha\beta}| < \begin{pmatrix} 4.2 & 0.33 & 3.0 \\ 0.33 & 0.068 & 0.33 \\ 3.0 & 0.33 & 21\end{pmatrix}, \quad (4.5)$$

for neutral Earth matter. There are also experiments which have used the neutrino data to constrain NSI parameters. The SK NSI search in atmospheric neutrinos crossing the Earth found no evidence in favour of NSI and the study led to upper bounds on NSI parameters [87] given by $|\varepsilon_{\mu\tau}| < 0.033, |\varepsilon_{\tau\tau} - \varepsilon_{\mu\mu}| < 0.147$ (at 90% CL) in a two flavour hybrid model [261][3]. The off-diagonal NSI parameter $\varepsilon_{\mu\tau}$ is constrained $-0.20 < \varepsilon_{\mu\tau} < 0.07$ (at 90% CL) from MINOS data in the framework of two flavour neutrino oscillations [88,266].

We will be interested in the most relevant channel for DUNE,- $\nu_\mu \to \nu_e$ (and the CP transformed channel, $\bar{\nu}_\mu \to \bar{\nu}_e$) where only two of the NSI parameters $(\varepsilon_{e\mu}, \varepsilon_{e\tau})$ appear in the second order expression. Taking into account the constraints from neutrino experiments, we can write (see also [267]) the more stringent bounds as,

$$|\varepsilon_{\alpha\beta}| < \begin{pmatrix} 4.2 & 0.3 & 0.5 \\ 0.3 & 0.068 & 0.04 \\ 0.5 & 0.04 & 0.15\end{pmatrix}. \quad (4.6)$$

[3]The SK collaboration uses a different normalization (n_d) while writing the effective NSI parameter (see Eq. (4.2)) and hence we need to multiply the bounds mentioned in Ref. [87] by a factor of 3.

In this work, we will explore the relatively large effect of the NSI parameters even when the tighter bounds (eq. 4.6) are taken into account. We consider $|\varepsilon_{e\mu}|, |\varepsilon_{e\tau}| < 0.1$ which are consistent with Eq. 4.6 and also the NSI phases in the allowed range, $\phi_{e\mu}, \phi_{e\tau} \in (-\pi, \pi)$. In addition, we explore the collective effect of the dominant NSI parameters $(\varepsilon_{e\mu}, \varepsilon_{e\tau})$ affecting the particular channels $\nu_\mu \to \nu_e$ (and $\bar{\nu}_\mu \to \bar{\nu}_e$) so that the impact can be understood in totality.

All the plots presented in this paper are obtained by using GLoBES [189, 190] and for the implementation of NSI into GLoBES, we have used an add-on [229] to the GLoBES software. All the experimental details are same as that considered in chapter 3.

4.2 Modification of $P_{\mu e}$ in presence of NSI in propagation

The approximate expression for oscillation probability for $\nu_\mu \to \nu_e$ for NSI case can be obtained by retaining terms of $\mathcal{O}(\varepsilon_{\alpha\beta} s_{13})$, $\mathcal{O}(\varepsilon_{\alpha\beta} r_\lambda)$, $\mathcal{O}(s_{13} r_\lambda)$, $\mathcal{O}(r_\lambda^2)$ and neglecting the

higher order terms,

$$
\begin{aligned}
P(\nu_\mu \to \nu_e) \;\simeq\;& 4s_{13}^2 s_{23}^2 \left[\frac{\sin^2(1-r_A)\lambda L/2}{(1-r_A)^2}\right] \\
&+ 8s_{13}s_{23}c_{23}(|\varepsilon_{e\mu}|c_{23}c_\chi - |\varepsilon_{e\tau}|s_{23}c_\omega) r_A \left[\cos\frac{\lambda L}{2}\frac{\sin r_A\lambda L/2}{r_A}\frac{\sin(1-r_A)\lambda L/2}{(1-r_A)}\right] \\
&+ 8s_{13}s_{23}c_{23}(|\varepsilon_{e\mu}|c_{23}s_\chi - |\varepsilon_{e\tau}|s_{23}s_\omega) r_A \left[\sin\frac{\lambda L}{2}\frac{\sin r_A\lambda L/2}{r_A}\frac{\sin(1-r_A)\lambda L/2}{(1-r_A)}\right] \\
&+ 8s_{13}s_{23}^2(|\varepsilon_{e\mu}|s_{23}c_\chi + |\varepsilon_{e\tau}|c_{23}c_\omega) r_A \left[\frac{\sin^2(1-r_A)\lambda L/2}{(1-r_A)^2}\right] \\
&+ 4|\varepsilon_{e\mu}| r_\lambda s_{2\times 12} c_{23}^3 \cos\phi_{e\mu} r_A \frac{\sin^2 r_A\lambda L/2}{r_A^2} \\
&+ 2|\varepsilon_{e\mu}| r_\lambda s_{2\times 12} s_{23}^2 c_{23} \cos\phi_{e\mu} r_A \left[\cos\frac{\lambda L}{2}\frac{\sin r_A\lambda L/2}{r_A}\frac{\sin(1-r_A)\lambda L/2}{(1-r_A)}\right] \\
&+ |\varepsilon_{e\mu}| r_\lambda s_{2\times 12} s_{23}^2 c_{23} \sin\phi_{e\mu} r_A \left[\sin\frac{\lambda L}{2}\frac{\sin r_A\lambda L/2}{r_A}\frac{\sin(1-r_A)\lambda L/2}{(1-r_A)}\right] \\
&- 4|\varepsilon_{e\tau}| r_\lambda s_{2\times 12} c_{23}^2 s_{23} \cos\phi_{e\tau} r_A \frac{\sin^2 r_A\lambda L/2}{r_A^2} \\
&+ 2|\varepsilon_{e\tau}| r_\lambda s_{2\times 12} s_{23}^2 c_{23} \cos\phi_{e\tau} r_A \left[\cos\frac{\lambda L}{2}\frac{\sin r_A\lambda L/2}{r_A}\frac{\sin(1-r_A)\lambda L/2}{(1-r_A)}\right] \\
&+ |\varepsilon_{e\tau}| r_\lambda s_{2\times 12} s_{23}^2 c_{23} \sin\phi_{e\tau} r_A \left[\sin\frac{\lambda L}{2}\frac{\sin r_A\lambda L/2}{r_A}\frac{\sin(1-r_A)\lambda L/2}{(1-r_A)}\right] \\
&+ 8r_\lambda \mathcal{J}_r \cos\delta \left[\cos\frac{\lambda L}{2}\frac{\sin r_A\lambda L/2}{r_A}\frac{\sin(1-r_A)\lambda L/2}{(1-r_A)}\right] \\
&- 8r_\lambda \mathcal{J}_r \sin\delta \left[\sin\frac{\lambda L}{2}\sin\frac{r_A\lambda L/2}{r_A}\frac{\sin(1-r_A)\lambda L/2}{(1-r_A)}\right] \\
&+ r_\lambda^2 c_{23}^2 s_{2\times 12}^2 \frac{\sin^2(r_A\lambda L/2)}{r_A^2}\,,
\end{aligned}
\tag{4.7}
$$

where $\lambda = \frac{\Delta m^2_{31}}{2E}, r_\lambda = \frac{\delta m^2_{21}}{\delta m^2_{31}}, r_A = \frac{A(x)}{\delta m^2_{31}}, A(x) = 2\sqrt{2}EG_F n_e(x)$ and
$\mathcal{J} = \frac{1}{8}\sin 2\theta_{12}\sin 2\theta_{13}\sin 2\theta_{23}\cos\theta_{13}\sin\delta_{cp}$.
$\mathcal{J}_r = \mathcal{J}/\sin\delta$ and $\chi = \phi_{e\mu} + \delta$, $\omega = \phi_{e\tau} + \delta$. Note that the two parameters, $\varepsilon_{e\mu}$ and $\varepsilon_{e\tau}$ enter in this leading order expression which implies that the rest of the NSI parameters are expected to play a sub-dominant role. The approximate expression (Eq. 4.7) allows us to illustrate the qualitative impact of the moduli and phases of NSI terms which can in principle override effects due to the vacuum oscillation phase δ for certain choice of energies. Also, the above expression is strictly valid when $r_\lambda \lambda L/2 \ll 1$ i.e. L and E are far away from the region where lower frequency oscillations dominate which is satisfied

for long baseline experiments. For the case of DUNE, we have

$$r_\lambda \lambda L/2 \approx 0.05 \left[1.267 \times \frac{\delta m^2_{21}}{7.6 \times 10^{-5}\ eV^2} \frac{L}{1300\ km} \frac{2.5\ GeV}{E}\right] < 1 \tag{4.8}$$

Note that in addition to the vacuum oscillation frequency $\lambda L/2$

$$\lambda L/2 = 1.57 \left[1.267 \times \frac{\delta m^2_{31}}{2.4 \times 10^{-3}\ eV^2} \frac{L}{1300\ km} \frac{2.5\ GeV}{E}\right] \tag{4.9}$$

which has E^{-1}-dependence on energy, matter (SI and NSI) introduces phase shifts such as $r_A \lambda L/2$ (using $A = 0.756 \times 10^{-4}\ eV^2\ \rho\ (g/cc)\ E\ (GeV)$):

$$r_A \lambda L/2 = 0.4 \left[1.267 \times 0.756 \times 10^{-4} \frac{\rho}{3.0\ g/cc} \frac{L}{1300\ km}\right], \tag{4.10}$$

which is E-independent. The probability remains finite due to the $(1 - r_A)$ and $(1 - r_A)^2$ terms in the denominator of Eq. (4.7). Substituting $\delta \to -\delta$ and $r_A \to -r_A$ in Eq. 4.7, we obtain $P(\bar{\nu}_\mu \to \bar{\nu}_e)$. Now let us discuss different limiting cases of Eq. 4.7:

- *Vacuum ($r_A \to 0$, $\varepsilon_{\alpha\beta} \to 0$) :*
  When $r_A \to 0$, we recover the vacuum limit as expected [50]. This vacuum expression is identical to eqn. 2.2 (in the limit $r_A \to 0$). Note that this expression is upto 2nd order in $\sin\theta_{13}$ and r_λ.

- *SI ($\varepsilon_{\alpha\beta} \to 0$, $r_A \neq 0$) :*
  Only the first and last three lines of Eq. 4.7 are non-zero in this case when only SI are operating [210, 268]. The CP violation sensitivity is due to the terms proportional to $r_\lambda s_{13} \sim 0.03$ in this case as expected from standard matter case. When $r_A \to 1$, we are close to the resonance condition ($r_A = \cos 2\theta_{13}$ since θ_{13} is small). Note that, this limiting case is also consistent with eqn. 2.2.

- *NSI-dominated regime ($r_A \neq 0$ and $\varepsilon_{e\mu}, \varepsilon_{e\tau} \neq 0$) :*
  If we neglect terms of $\mathcal{O}(r_\lambda s_{13})$, $\mathcal{O}(r^2_\lambda)$, we get the first four lines with non-zero terms in Eq. 4.7. The sole sensitivity to CP violating phase comes from the NSI terms. In this case, the CP violating effects appearing in second and third line are proportional to $s_{13}|\varepsilon_{e\mu}|$ or $s_{13}|\varepsilon_{e\tau}|$. We can note that NSI effects with $|\varepsilon_{\alpha\beta}| \simeq 0.1$ can in principle override the standard CP violating effects in matter by one order of magnitude as $r_\lambda \simeq 0.03$.

  Another interesting aspect of this limit is that it would correspond to setting $\delta m^2_{21} = 0$, which means we are effectively describing a two flavour case. In such a situation,

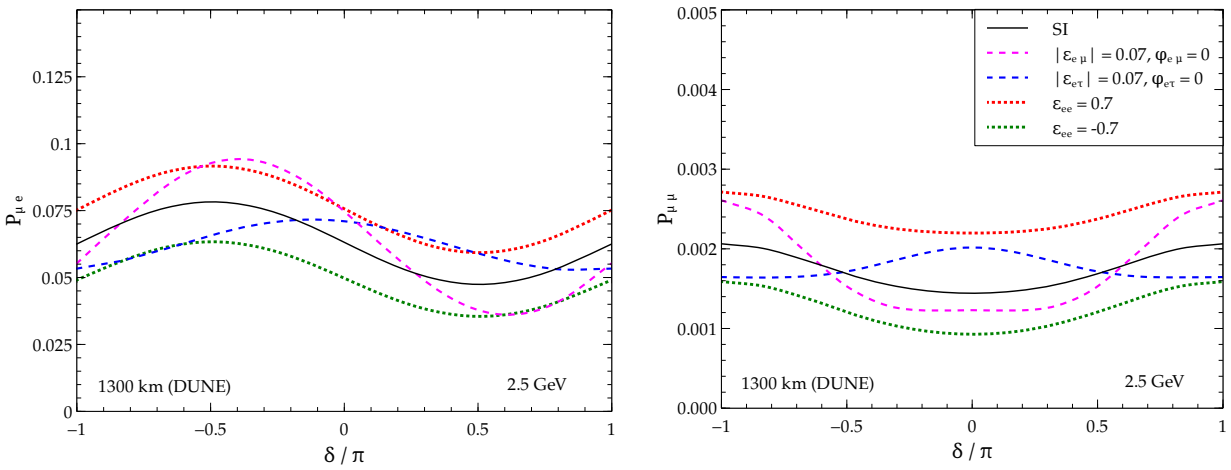

Figure 4.1: Effect of individual NSI terms in the $P_{\mu e}$ and $P_{\mu\mu}$ as a function of δ for $E = 2.5$ GeV and $L = 1300$ km. The solid black curve represents SI case while the dashed (dotted) curves represent the case of off-diagonal (diagonal) NSI parameters. The NSI phases $\phi_{e\mu}$ and $\phi_{e\tau}$ are set to zero.

as argued in Kikuchi et al. [269], phase reduction is possible as one ends up with effectively one combination of phases such as $\chi = \delta + \phi_{e\mu}$ (or, $\omega = \delta + \phi_{e\tau}$) rather than individual phases δ and $\phi_{e\mu}$. This implies that if we are in the NSI dominated regime, it appears from the probability expression (Eq. 4.7) that there are degeneracies arising due to interplay of vacuum and NSI phases. We will refer to this as the *vacuum-NSI CP phase degeneracy*. However, it turns out that once we take subdominant terms due to $r_\lambda \neq 0$ into consideration, the individual vacuum CP phase and NSI CP phase dependencies start showing up (through terms in lines 5-12 on RHS of Eq. 4.7) and such terms clearly aid in breaking of these vacuum-NSI CP phase degeneracies.

4.3 Result: Manifestations of NSI effects on probability and events

We consider appearance ($\nu_\mu \to \nu_e$) and disappearance ($\nu_\mu \to \nu_\mu$) channels that are relevant in the context of accelerator-based neutrino oscillation experiments considered in the present work. For the case of NSI, we discuss the differences arising due to the two leading non-zero NSI parameters, viz., $\varepsilon_{e\mu}, \varepsilon_{e\tau}$ affecting the probability, asymmetry and events by a visual comparison of the plots for NSI case with those for the SI case. In order to understand all the subtle effects arising due to non-zero NSI terms, we first discuss the

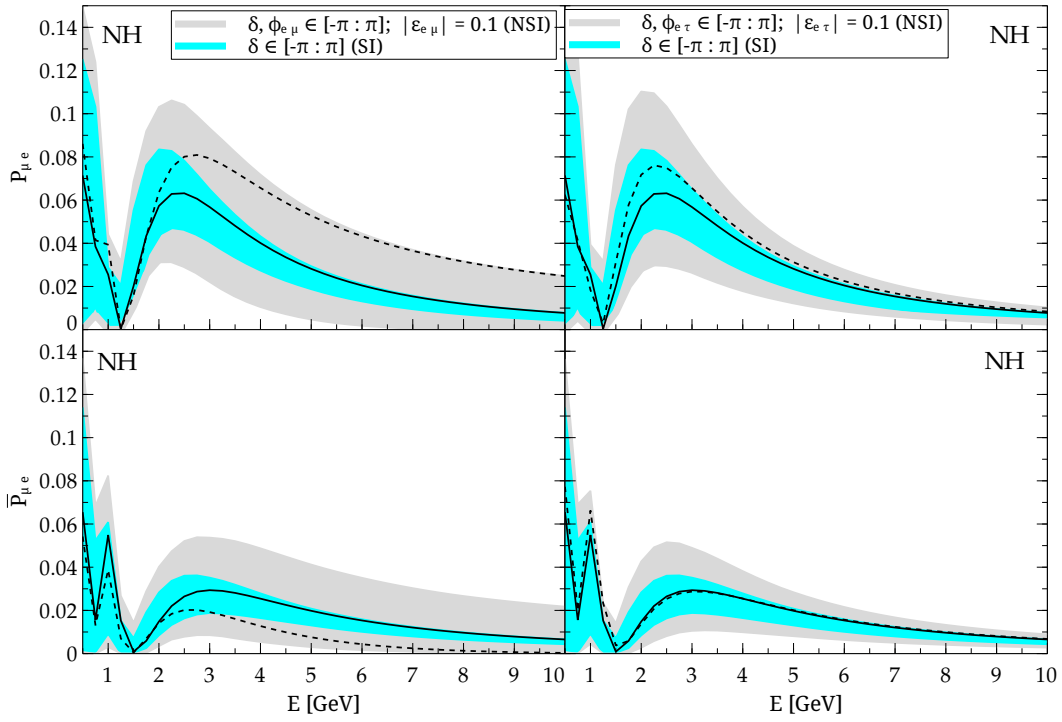

Figure 4.2: $P(\nu_\mu \to \nu_e)$ and $P(\bar{\nu}_\mu \to \bar{\nu}_e)$ are plotted plotted as a function of energy for $L = 1300$ km and the role of individual NSI parameters is depicted by varying the phases of NSI parameters keeping the moduli fixed and assuming NH. The relevant phases ($\delta, \phi_{e\mu}$ on the left side or $\delta, \phi_{e\tau}$ on the right side) are varied in the allowed range as specified in the figure. The cyan band corresponds to SI with $\delta \in (-\pi, \pi)$. The solid black line depicts the case of SI with $\delta = 0$ and dashed black line depicts the case of NSI with $|\varepsilon_{e\mu}| = 0.1$ in the left panel and $|\varepsilon_{e\tau}| = 0.1$ in the right panel.

isolated case (one NSI parameter non-zero at a time) and then collective case (the relevant NSI parameters are taken non-zero simultaneously).

1. *Impact of individual NSI terms:*
   In Fig. 4.1, the impact of individual NSI terms on $P_{\mu e}$ and $P_{\mu\mu}$ is shown for the baseline corresponding to DUNE ($L = 1300$ km) at a fixed value of energy $E = 2.5$ GeV. We note from this figure that in presence of the off-diagonal NSI parameters, there is a considerable shift in the position of the peak/ trough of the probability curves. For the diagonal parameter ε_{ee}, for both $P_{\mu e}$ and $P_{\mu\mu}$, the effect is like a uniform enhancement (reduction) of the probability values from the SI case depending upon the sign of ε_{ee}. Fig. 4.2 depicts the effect due to the variation of the individual SI/ NSI phases. The cyan band represents the SI case ($\delta \in (-\pi : \pi)$) while the grey band is for NSI($\delta \in (-\pi : \pi)$, $\phi_{e\mu} \in (-\pi : \pi)$ or $\phi_{e\tau} \in (-\pi : \pi)$). For the case of NSI, we have used $|\varepsilon_{e\mu}| = 0.1$ and $|\varepsilon_{e\tau}| = 0.1$ in the left and right panel respectively.

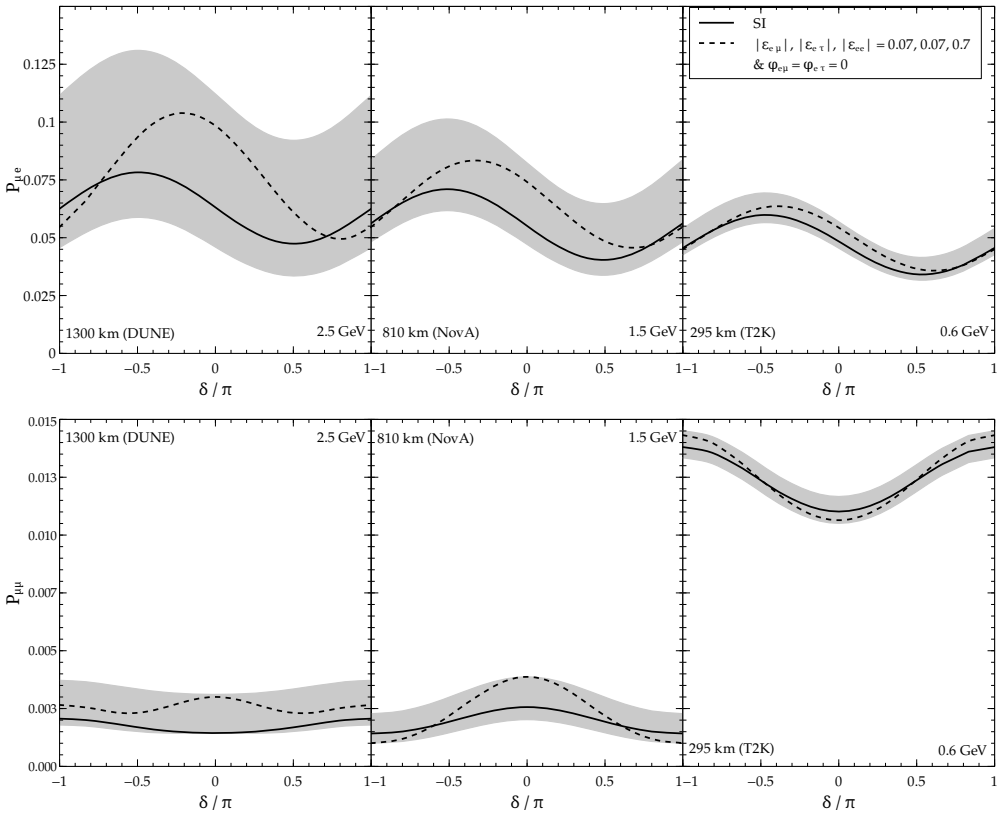

Figure 4.3: Combined effect of three NSI terms ($\varepsilon_{e\mu}, \varepsilon_{e\tau}, \varepsilon_{ee}$) in the electron appearance and muon disappearance probability as a function of δ (for fixed E and L for DUNE, NOvA and T2K). The solid black curve represents SI while the dashed black curve represents NSI for the particular choice of absolute value of NSI parameters as mentioned in the legend. The grey band shows the spread when in addition the NSI phases are varied in the allowed range *i.e.*, $\phi_{e\mu}, \phi_{e\tau} \in [-\pi, \pi]$.

The solid line (black) shows the SI case ($\delta = 0$) while the dashed line (black) depicts the case of NSI with all phases set to zero for either $|\varepsilon_{e\mu}| = 0.1$ or $|\varepsilon_{e\tau}| = 0.1$. The general effect of varying the phases is that it leads to a band (cyan) around the solid black line in case of SI. For NSI case, there is further broadening of bands (shown in grey) on both sides of the SI (cyan) band. From Eq. 4.7, the terms in lines 2-10 are responsible for the grey band.

2. *Impact of collective NSI terms:* In Fig. 4.3, the collective impact of NSI terms is shown for three different experiments at different fixed energies relevant to those experiments. The largest effect of NSI terms can be seen for $P_{\mu e}$ and for DUNE and it diminishes as we go to T2K. For $P_{\mu\mu}$, the effect is similar for all the three experiments so the baseline does not seem to play much role here.

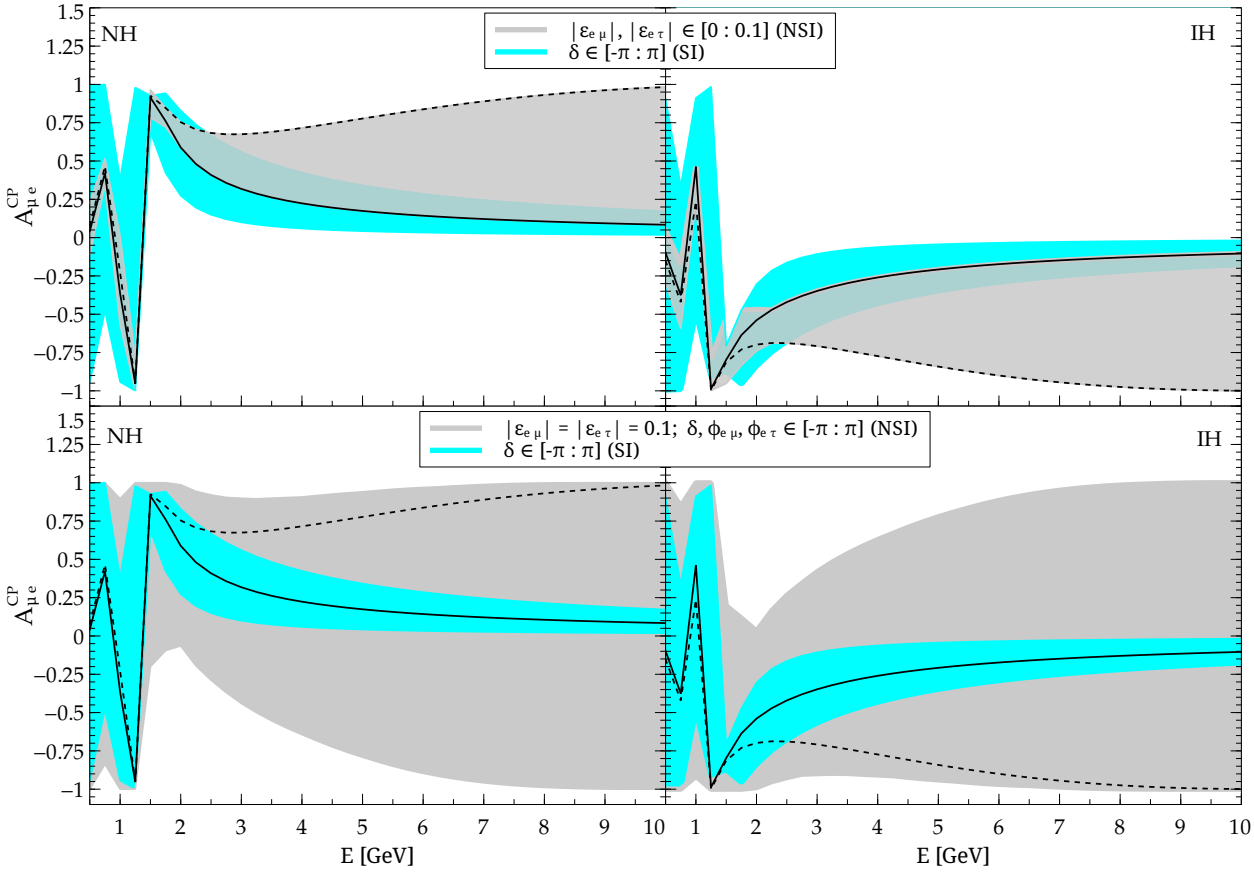

Figure 4.4: Impact of collective NSI terms on the CP asymmetry bands as a function of energy for $L = 1300$ km for NH and IH. Only the moduli of NSI parameters ($|\varepsilon_{e\mu}|, |\varepsilon_{e\tau}|$) are varied in the top row and only the phases (δ,$\phi_{e\mu}, \phi_{e\tau}$) for $|\varepsilon_{e\mu}| = |\varepsilon_{e\tau}| = 0.1$ are varied in the allowed range as specified in the figure in the bottom row. The cyan band corresponds to SI with $\delta \in (-\pi, \pi)$. The solid black line depicts the case of SI with $\delta = 0$ and dashed black line depicts the case of NSI with $|\varepsilon_{e\mu}| = |\varepsilon_{e\tau}| = 0.1$.

Having discussed the imprint of individual and collective NSI terms on the $P(\nu_\mu \to \nu_e)$ and $P(\bar{\nu}_\mu \to \bar{\nu}_e)$, let us now turn to the CP asymmetry $A^{CP}_{\mu e}(\delta)\,\delta$. In Fig. 4.4, the maximum and minimum $A^{CP}_{\mu e}(\delta)\,\delta$ is plotted and the SI (NSI) cases are shown as cyan (grey) bands as a function of E for the two hierarchies. The maximum and minimum values are obtained by varying the relevant vacuum (the Dirac phase) and NSI parameters (moduli and/ or phases) in the allowed range mentioned in the figure caption. Once again the cyan band corresponds to the case of SI and the grey band corresponds to NSI. The solid black line depicts the SI curve for $\delta = 0$ and dashed black line depicts the collective NSI curve ($|\varepsilon_{e\mu}| = 0.1$ and $|\varepsilon_{e\tau}| = 0.1$) (see caption of Fig. 4.4). The discussion of $P(\nu_\mu \to \nu_e)$ and $P(\bar{\nu}_\mu \to \bar{\nu}_e)$ above is reflected in the $A^{CP}_{\mu e}(\delta)\,\delta\delta$ curves. The top row in Fig. 4.4 shows the impact of varying the moduli of collective NSI terms while the bottom row shows the

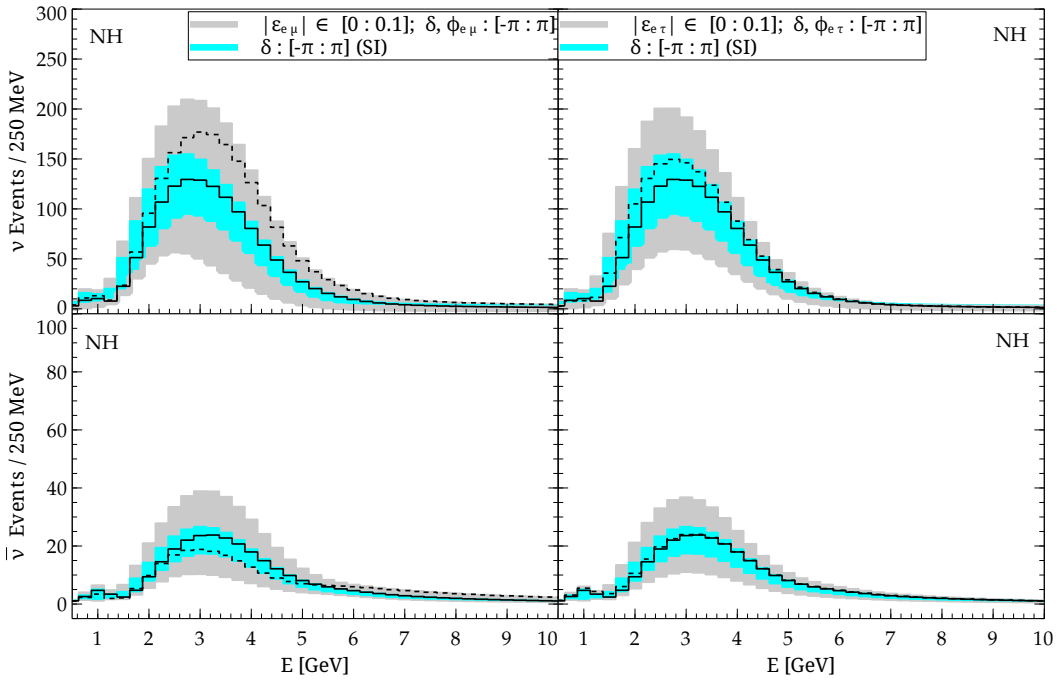

Figure 4.5: Impact of individual NSI terms on the ν and $\bar{\nu}$ events plotted as a function of energy at DUNE far detector for NH. The cyan band depicts the case of SI with $\delta \in [-\pi : \pi]$ while the grey band depicts the case of NSI with variation in the moduli and phase of the relevant NSI parameter as specified in the figure. The black solid (dashed) line depicts the case of SI with $\delta = 0$ (NSI with all phases set to zero).

impact of varying the phases keeping the moduli fixed ($|\varepsilon_{e\mu}| = 0.1$ and $|\varepsilon_{e\tau}| = 0.1$). The grey band in the top row depicts the fake CP effect in the same spirit as matter effects arising due to SI while the grey band in the bottom row contain fake CP effect *a la* SI along with the contributions to the intrinsic CP phase ($\delta_{\rm CP}$) arising due to non-zero NSI CP phases. For $E < 1.5\ GeV$, the two curves corresponding to SI and NSI almost coincide. The difference in cyan and grey bands increases with increasing the energy beyond $1.5\ GeV$. The most dramatic aspect of NSI is that the naive argument of needing large L/E (and hence small E for fixed value of L) in order to obtain large asymmetries due to matter effects, does not work any more and we can obtain large asymmetries even at large energies, as is reflected from the asymmetry plots in Fig. 4.4. This implies that detection of large asymmetry (≈ 1), especially at high energies ($E \approx 8 - 10$ GeV) will indicate to the possible presence of nonstandard interactions. The case of NH and IH show opposite sign of asymmetry in the grey band (top row). However, when phases are taken into account, the change of sign due to change of hierarchy is buried because the $A^{CP}_{\mu e}\,(\delta_{\rm CP})$ band spans almost throughout the entire range $[-1 : 1]$

In Fig. 4.5, we show electron neutrino and antineutrino event histograms for SI and

NSI (when one single off-diagonal NSI parameter $|\varepsilon_{e\mu}|$ or $|\varepsilon_{e\tau}|$ are varied along with the relevant CP phases.). These histograms show the maximum spread in the events when the relevant parameters (in case of SI, δ and in case of NSI, moduli and phases of the single NSI parameter $\varepsilon_{e\mu}$ or $\varepsilon_{e\tau}$) are varied over the allowed range specified in the figure. The region between maximum and the minimum event rates is shown as shaded cyan (grey) band in case of SI (NSI). It should be noted that the set of varied oscillation parameters (SI phase or NSI phases) that give the spread in the event rates in each bin in Fig. 4.5 are in general different. We make the following observations from Fig. 4.5.

- The event spectrum follows the probability plots and there is large difference near the first oscillation maximum of $\nu_\mu \to \nu_e$ probability even in the standard matter case which gets enhanced in presence of NSI.
- Though the asymmetries are fairly large in the higher energy regime, the number of events are not so large in high energy bins due to the small flux at those energies. This holds for NH as well as IH.
- There are overlapping regions where SI and NSI results are consistent with one another due to a certain favourable choice of parameters. We refer to these as the NSI-SI degeneracies. Due to presence of these new degeneracies, it becomes hard to ascribe the signal to SI alone or to NSI. The two bands corresponding to SI and NSI phase variations respectively are overlapping for a wide range of energies including those where the flux peaks.

Parameter	True value	Marginalisation range
SI		
θ_{12} [deg]	33.5	-
θ_{13} [deg]	8.5	-
θ_{23} [deg]	45	-
δm^2_{21} [eV^2]	7.5×10^{-5}	-
δm^2_{31} (NH) [eV^2]	$+2.45 \times 10^{-3}$	-
δm^2_{31} (IH) [eV^2]	-2.46×10^{-3}	-
δ	-	$[-\pi : \pi]$
NSI		
$\lvert\varepsilon_{ee}\rvert$	$0.1, 0.4, 0.7$	$[0 : 1.00]$
$\lvert\varepsilon_{\mu\mu}\rvert$	0.05	$[0 : 0.06]$
$\lvert\varepsilon_{\tau\tau}\rvert$	$0.04, 0.08, 0.12$	$[0 : 0.15]$
$\lvert\varepsilon_{e\mu}\rvert$	$0.01, 0.04, 0.07$	$[0 : 0.10]$
$\lvert\varepsilon_{e\tau}\rvert$	$0.01, 0.04, 0.07$	$[0 : 0.10]$
$\lvert\varepsilon_{\mu\tau}\rvert$	$0.01, 0.04$	$[0 : 0.04]$
$\phi_{e\mu}$	-	$[-\pi : \pi]$
$\phi_{e\tau}$	-	$[-\pi : \pi]$
$\phi_{\mu\tau}$	-	$[-\pi : \pi]$

Table 4.1: SI and NSI parameters used in our study. For latest global fit to neutrino data see [16].

4.4 Results: Sensitivity to CP Violation

In this section, we will illustrate how the CPV sensitivity, obtained by assuming the standard 3ν scenario gets severely affected when nonstandard interactions are present. The χ^2 methodology implemented in GLoBES for this study follows similar procedures as in chapter 3. In order to obtain the sensitivity to CP violation we need to ask the following question[4] - what is the sensitivity with which a particular experiment can discriminate between CP conserving $(0, \pi)$ and CP violating values $(\neq 0, \pi)$ of the CP phase. In the standard scenario, there is only one CP phase in the neutrino oscillation formalism. However when we consider NSI, naturally more parameters in the form of moduli and phases of NSI parameters enter the oscillation formalism which lead to genuine and fake CP violating effects. In the standard $3+0$ case (discussed in chapter 2), since there is only one relevant CP phase (the Dirac CP phase $\delta_{\rm CP}$ or δ_{13}), the source of CP violation is obvious. But the scenario becomes much more complicated in presence of additional NSI CP phases. Like in chapter 3 we do not marginalise over the standard oscillation parameters except δ whose true value is unknown. As we are investigating the role of NSI in the present study, we marginalize over the allowed range of moduli and phases of the relevant NSI parameters (see table 4.1 for the true values and the range of marginalization of the parameters considered.). Our choice of range of NSI parameters is consistent with the existing constraints (Eq. 4.6).

4.4.1 Impact of individual and collective NSI terms on CPV sensitivity

Before we describe the impact of a particular NSI parameter (*i.e.* $\varepsilon_{e\mu}$ or $\varepsilon_{e\tau}$) we would like to point out that there are two effects responsible for altering the value of the χ^2 which compete with each other[5]. In general, we first note that NSI introduces more number of parameters (in the form of moduli of NSI terms and the associated CP phases) in the sensitivity analysis and also introduces more sources of CP violation. One can have the following possibilities :

(a) Decrease in χ^2 due to additional test values - If marginalization is carried out over more number of test parameters, it naturally results in a decreased value of χ^2. This is purely a statistical effect.

[4]This question is similar to the one discussed in the context of CPV sensitivity studies as discussed in section 3.5

[5]These two competing effects are similar to the ones guiding the value of χ^2 in presence of a sterile neutrino,- see section 3.5.

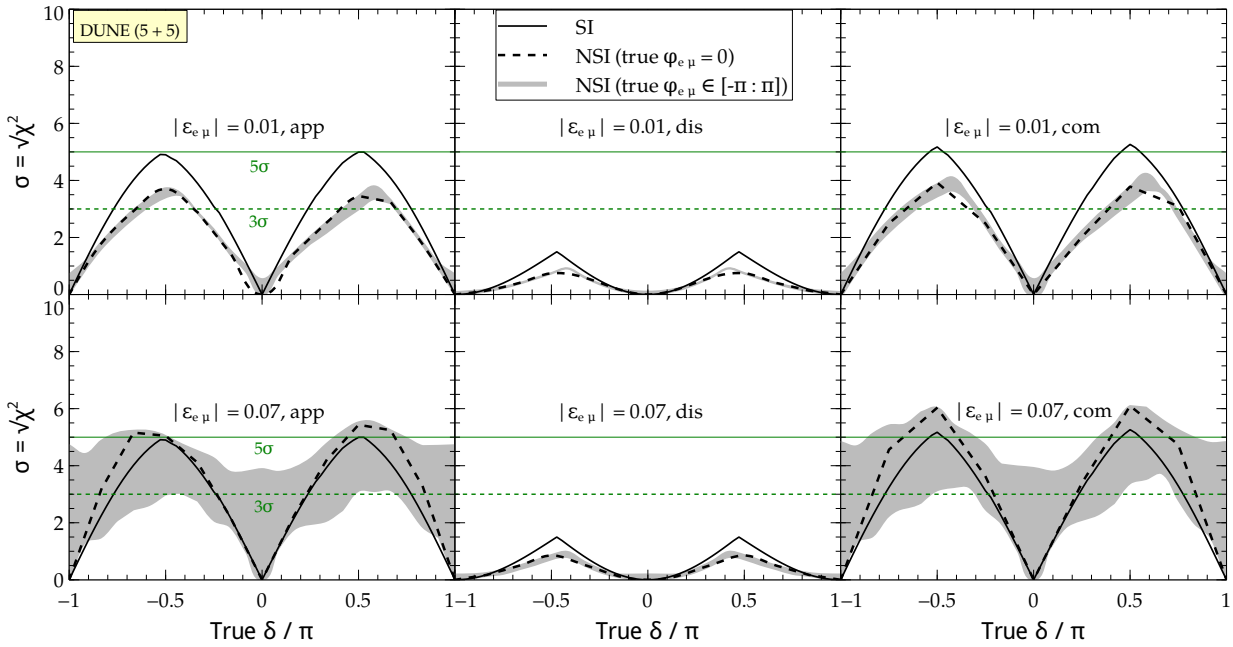

Figure 4.6: The impact of $\varepsilon_{e\mu}$ on the significance with which the CP violation can be determined as a function of the value of δ at DUNE for an exposure of 350 kt.MW.yr assuming NH. The solid black curve represents the sensitivity for our reference design. Both the moduli and phases are varied as mentioned in the legend. The appearance and disappearance channels are shown separately and the sensitivity obtained by combining both the channels is also shown in the last column.

(b) Increase in χ^2 due to larger strength of true values - In addition to more parameters in the test dataset (as mentioned in effect (a) above), one has to deal with a larger set of parameters in the true dataset as well. The variation over the values of the true NSI phases ($\varphi_{e\mu}$ or $\varphi_{e\tau}$) tends to broaden the grey band provided the true value of the moduli ($|\varepsilon_{e\mu}|$ or $|\varepsilon_{e\tau}|$) of the relevant NSI term is large.

In Fig. 4.6, we show the sensitivity to CP violation by exploiting appearance and disappearance channels (in isolation and combined) for the off-diagonal NSI parameter, $\varepsilon_{e\mu}$ and compare it with the sensitivity obtained in case of SI as a benchmark. The 3σ (5σ) value is shown as horizontal green dashed (solid) line to serve as a reference. Let us first describe the SI case (shown as solid black curves). The $P_{\mu e}$ channel naturally dominates the sensitivity of CP violation The mild CP sensitivity of the $P_{\mu\mu}$ is increases the value χ^2 by a small amount. The maximum (minimum) sensitivity in case of SI is attained when $\delta \simeq \pm\pi/2$ ($\delta = 0, \pm\pi$). In presence of NSI, in general the maximum χ^2 is very slightly shifted from the SI maximum, $\delta = \pm\pi/2$. This is due to the shift in the position of peaks and dips from the SI curve at the level of probability.

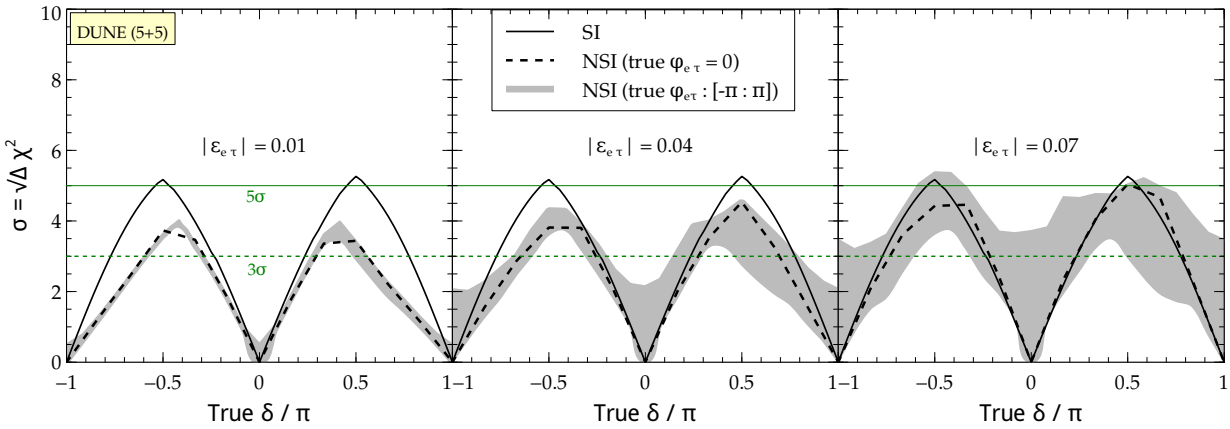

Figure 4.7: The impact of $\varepsilon_{e\tau}$ on the significance with which the CP violation can be determined as a function of the value of δ at DUNE for an exposure of 350 kt.MW.yr assuming NH. The solid black curve represents the sensitivity for reference design. Both the moduli and phases are varied as mentioned in the legend. The combined sensitivity of appearance and disappearance channels is shown in the plot.

In $P_{\mu e}$, the presence of additional CP phases in presence of NSI makes it possible for the effect (b) to overtake (a) if the value of the associated NSI amplitude/ modulus is large enough. If we see the top row of Fig. 4.6, the value of NSI parameter is small (true $|\varepsilon_{e\mu}| = 0.01$) and the black dashed curve (true $|\varepsilon_{e\mu}| \neq 0$) and the grey band (true $|\varepsilon_{e\mu}| \neq 0$, $\varphi_{e\mu} \in [\pi : \pi]$) are always below the SI case due to dominant effect (a) above. But for true $|\varepsilon_{e\mu}| = 0.07$, effect (b) becomes larger than effect (a) and we note that the NSI (with $|\varepsilon_{e\mu}| \neq 0$) overtakes SI. Consequently, the grey band spreads around the SI curve. The

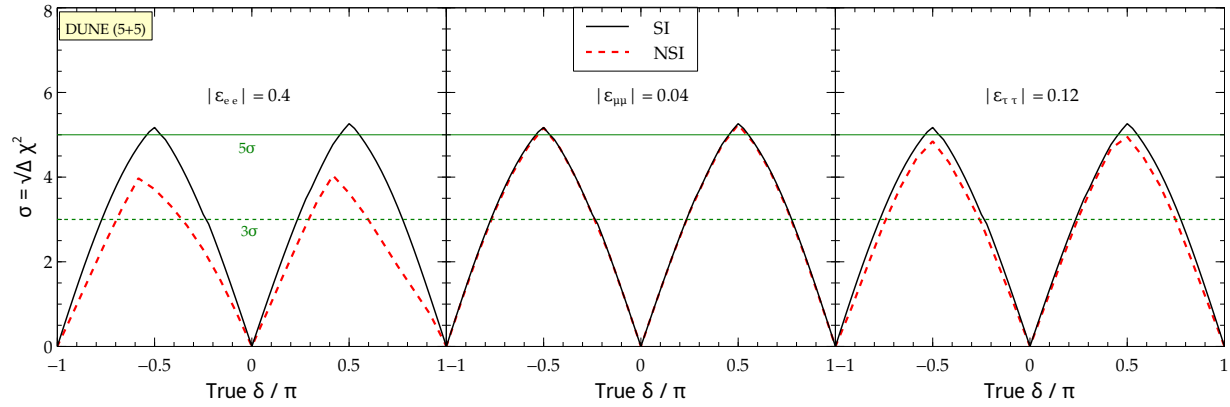

Figure 4.8: The impact of $|\varepsilon_{ee}|$, $|\varepsilon_{\mu\mu}|$ and $|\varepsilon_{\tau\tau}|$ on the significance with which the CP violation can be determined as a function of true value of δ at DUNE for an exposure of 350 kt.MW.yr assuming NH. The solid black curve represents the SI sensitivity for our reference design. The sensitivity obtained by combining the appearance and disappearance channels is shown.

most surprising outcome is that there can be $\geq 3\sigma$ sensitivity to CP violation even when $\delta = 0, \pm\pi$ (SI, CP conservation) for some (un)favourable choice of NSI moduli and phases. We can see this in the bottom panel of left and right plot of Fig. 4.6. As can be seen from the middle plots in the top and bottom rows of Fig. 4.6 corresponding to $P_{\mu\mu}$, such an overtaking is not possible due to the mild CP sensitivity of the $\nu_\mu \to \nu_\mu$ channel even if the NSI parameter is large.

In Fig. 4.7, the combined (appearance + disappearance) sensitivity to CP violation is shown both for SI and when the NSI parameter $\varepsilon_{e\tau}$ is incorporated. The effects are comparable in strength and similar in nature to that of $\varepsilon_{e\mu}$ described above. The impact of the off-diagonal NSI parameter $\varepsilon_{\mu\tau}$ on the CP sensitivity is found to be negligible even if we choose values close to the upper limit of the allowed range (~ 0.33) and hence is not shown here.

Having described the effect of off-diagonal NSI terms, we now address the impact of the diagonal ones - $\varepsilon_{ee}, \varepsilon_{\mu\mu}, \varepsilon_{\tau\tau}$. We show the impact of the three diagonal NSI parameters (ε_{ee}, $\varepsilon_{\mu\mu}$ and $\varepsilon_{\tau\tau}$) in Fig. 4.8. The effect of $\varepsilon_{\mu\mu}$ is very small as it is the most constrained parameter (Eq. 4.6). For the choice of values of the NSI parameters, the CP sensitivity sees a drop most likely due to the statistical effect (a) dominating in these cases.

After understanding the impact of individual diagonal as well as off-diagonal NSI terms, we now address the collective effect of the most influential NSI terms as far as CP sensitivity is concerned. In Fig. 4.9, we show the collective impact of the three terms ($|\varepsilon_{ee}|$, $|\varepsilon_{e\mu}|$, $|\varepsilon_{e\tau}|$) which show the largest impact when considered in isolation. We note that when the NSI terms are small (1st panel of Fig. 4.9), the associated phases of the NSI terms (even if taken collectively) do not contribute in an observable manner to (b) and (a) dominates. However when we take somewhat larger values, we see the interplay of the two effects (a) and (b) with the possibility of second effect (b) overtaking the first (a) as we go from small to large values keeping the marginalisation range intact.

We summarize the impact of NSI on the CP violation sensitivity at long baselines as shown in Fig. 4.9 for DUNE. If we compare the solid and dashed black curves, we note that for small values of parameters $(0.01, 0.01, 0.1)$ NSI brings down the χ^2 from $\sim 5\sigma$ to $\sim 3\sigma$ at $\delta \sim \pm\pi/2$ for the case of zero NSI phases. The impact of true non-zero NSI phases can be seen in the form of grey bands for the choice of moduli of the NSI terms. For larger values of parameters $(0.07, 0.07, 0.7)$ NSI can drastically alter the χ^2 not only at $\delta \simeq \pm\pi/2$ (SI, maximum) but at almost all values of δ including at $\delta = 0, \pm\pi$ if we allow for phase variation. For some particular choice of the NSI moduli and phases, we note that in this case, the χ^2 may decrease from $\sim 5\sigma$ to $\sim 2.5\sigma$ or may also increase to $\gtrsim 5.5\sigma$ not only

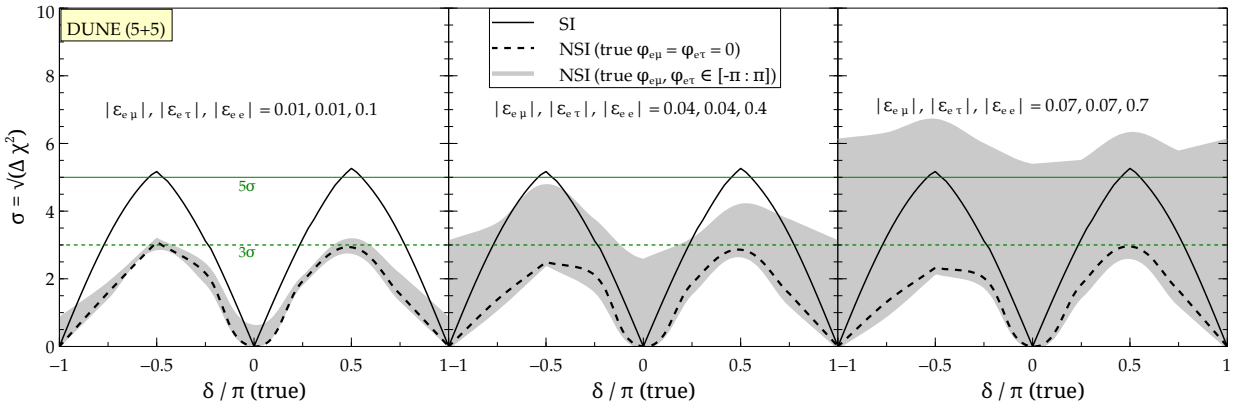

Figure 4.9: CP sensitivity for collective NSI terms at DUNE.

at $\delta \simeq \pm\pi/2$ but for most values of δ. This can lead to a misleading inference that CP is violated even when we have CP conservation in the SI case ($\delta = 0, \pm\pi$). Here the phases have a bigger impact which can be seen as widening of the grey bands as we go from smaller to larger moduli of NSI terms.

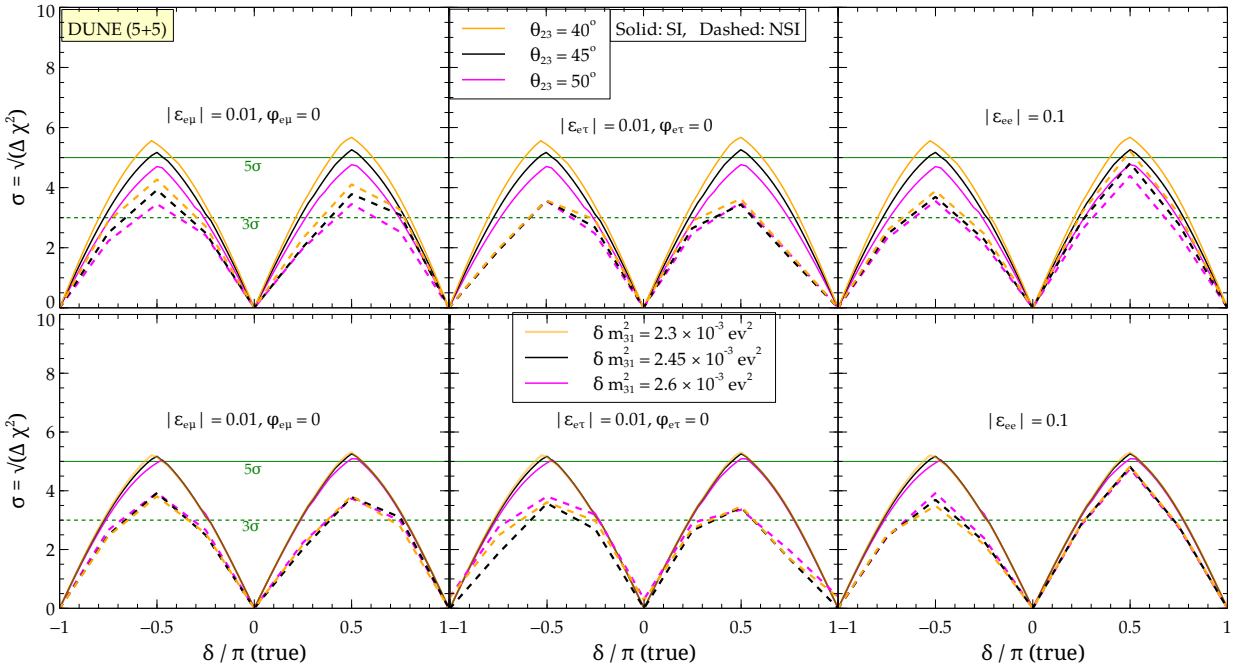

Figure 4.10: The dependence of CP sensitivity on the value of θ_{23} and δm^2_{31} varied in the allowed range.

4.4.2 Dependence on θ_{23} and δm^2_{31}

The variation in CP sensitivity due to different values of θ_{23} and δm^2_{31} in the allowed range is shown in Fig. 4.10 for SI and NSI cases (zero NSI phases). For θ_{23}, as can be seen from the solid curves for SI, the significance (in presence of diagonal and off-diagonal NSI) decreases almost uniformly for all values of δ as θ_{23} becomes larger. The $P_{\mu e}$ increases with θ_{23} and therefore the χ^2 decreases.

For δm^2_{31}, the solid curves for SI show that the sensitivity does not change significantly for all values of δ_{CP} as δm^2_{31} is varied. The true value of δm^2_{31} does not impact $P_{\mu e}$ and therefore the χ^2 remains almost the same.

4.4.3 Comparison with T2K, NOvA, T2HK experiments

We have shown the CP violation sensitivity at DUNE in Fig. 4.9 and discussed the features in subection 4.4.1. In Fig. 4.11, we show the CP sensitivity for T2K(top row), NOvA(middle row) as well as a combination of T2K , NOvA, and DUNE(bottom row)[6]. As in Fig. 4.9, the characteristic double peak is seen for all the three cases in Fig. 4.11. If we now look at T2K and NOvA individually, we note that the CP violation sensitivity almost never reaches 3σ (it barely touches $\sim 1.6\sigma$ (for T2K) and $\sim 1.8\sigma$ (for NOvA)). This means that these two current experiments considered in isolation are not so much interesting as far as CP violation sensitivity is concerned. This does not come as a surprise as these are not optimized for CP sensitivity. However, if we combine data from these two experiments with DUNE, we note that CP violation sensitivity improves slightly (from $\sim 5.1\sigma$ to $\sim 5.6\sigma$ in the SI case near the peak. For NSI (zero NSI phases, dashed black curve) it improves marginally from $\sim 3\sigma$ to $\gtrsim 3\sigma$. In general, we note that the if phases are taken into account, the grey bands expand and even out as we go from small to large NSI, the peaks at $\delta \sim \pm\pi/2$ smoothen out which means that there is no clear demarkation of CP conserving ($\delta = 0, \pm\pi$) and CP violating values of δ.

In Fig. 4.12, we show the CP violation sensitivity for T2HK. We note that T2HK offers CP sensitivity that is competitive with DUNE individually as well as T2K, NOvA and DUNE combined (SI and NSI both). This can be ascribed to the high statistics offered by the T2HK. Near the peak, we note that it can go upto $\sim 8\sigma$ for SI and $\gtrsim 5\sigma$ for NSI (zero phases). Another intriguing feature from T2HK panel is that the NSI phases do not have as dramatic effect as seen for DUNE when the NSI terms are large - this can

[6]For T2K, NOvAand T2HK similar experimental specifications and simulation details as was used in the context of sterile neutrinos (see chapter 3) has also been used here

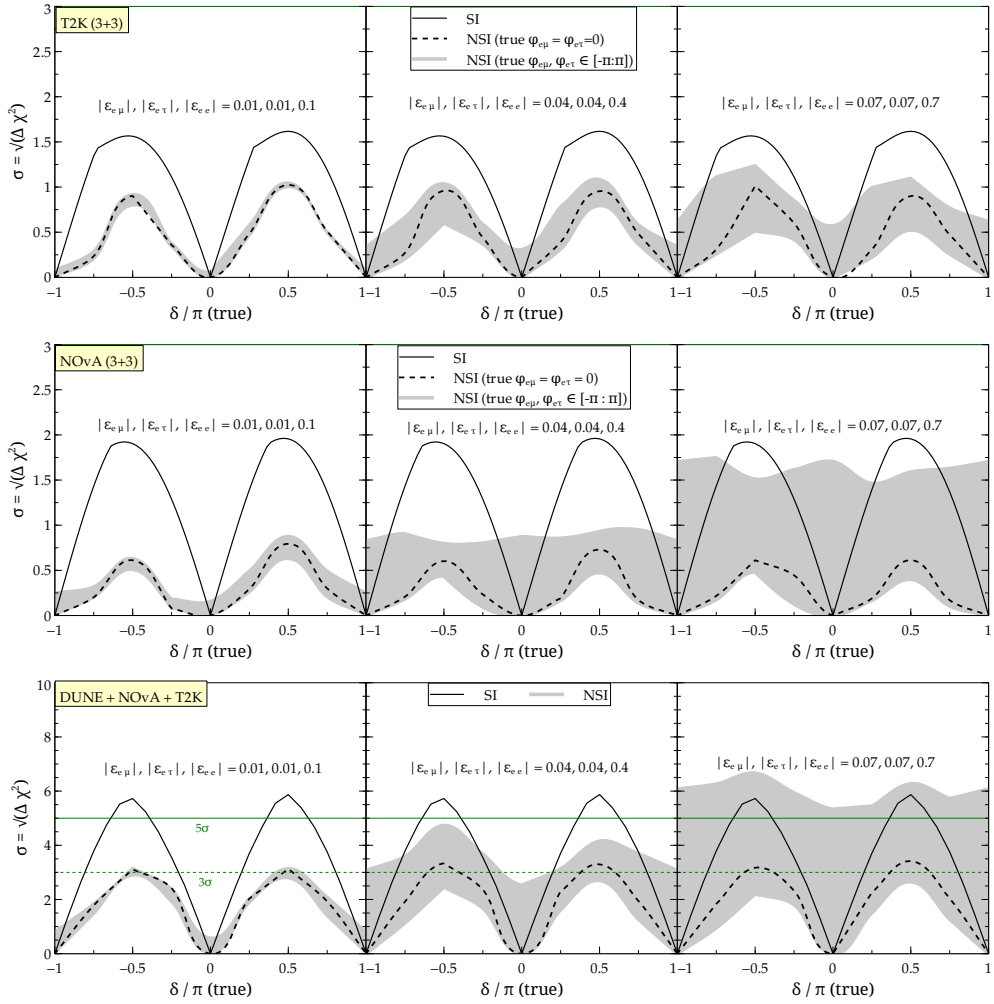

Figure 4.11: CP violation sensitivity at T2K, NOvA and T2K+NOvA+DUNE for collective NSI case and SI as a function of true δ.

be seen as shrinking of the grey regions in Fig. 4.12 (top panel, right most plot). This is due to the fact that the baseline of 295 km is way too short for matter effects (SI and NSI both) to develop and play a significant role[7]. This demonstrates the complementarity of bigger detectors (T2HK) vis-a-vis the long baselines involved (DUNE) where no clear demarkation of CP conserving ($\delta = 0, \pm\pi$) and CP violating values of δ is noticed.

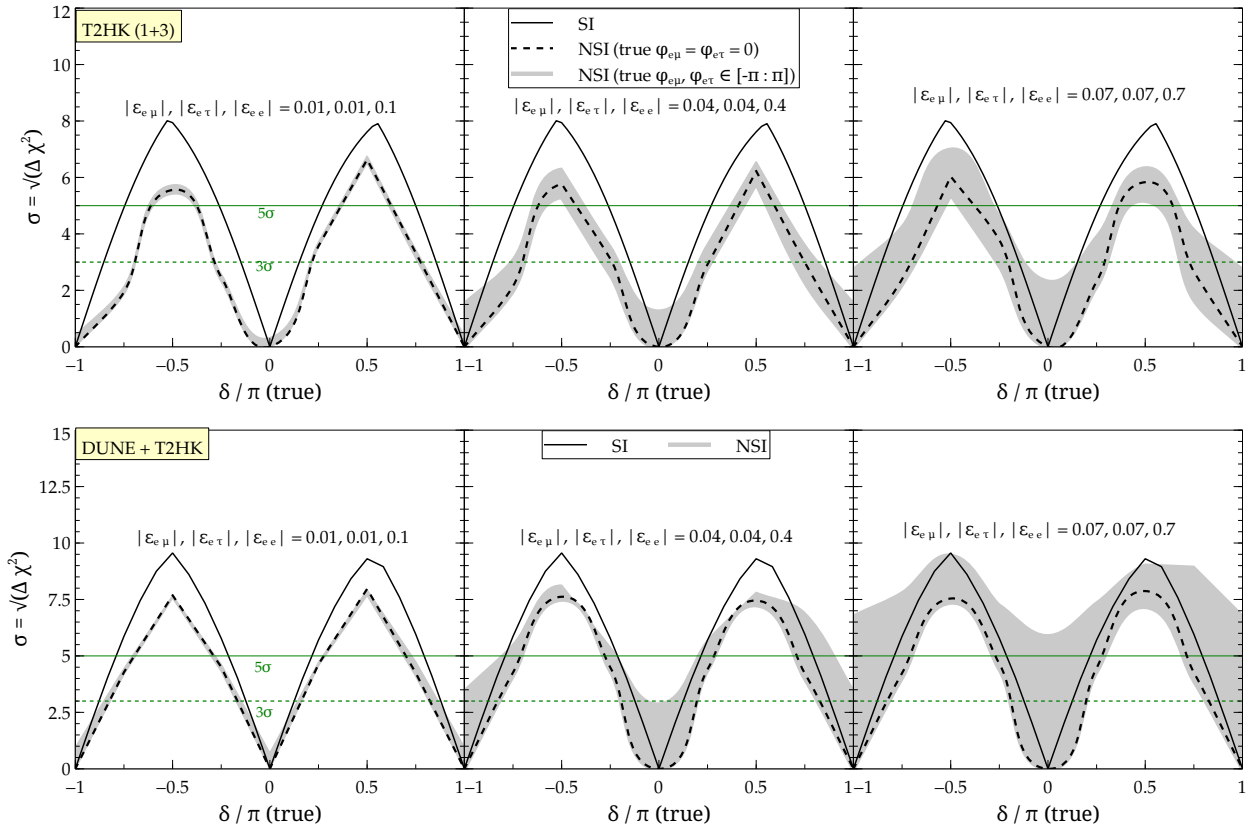

Figure 4.12: CP violation sensitivity at T2HK and T2HK+DUNE for collective NSI case and SI as a function of true δ.

4.4.4 Optimal exposure for CP violation discovery

In this subsection, we discuss the CP fraction ($f(\sigma > 3)$),- the fraction of the true $\delta_{\rm CP}$ space for which the CPV sensitivity is above 3σ[8] In Fig. 4.13, we show the CP fraction as a function of exposure. For SI, we note that $f(\sigma > 3)$ rises from 0 to ~ 0.4 as a function of exposure initially as we go from $50 - 150$ kt.MW.yr but saturates to a value $f(\sigma > 3) \simeq 0.5 - 0.55$ as we go to exposures beyond ~ 350 kt.MW.yr. Increasing the exposure further does not change this value drastically beyond $f(\sigma > 3) \simeq 0.5$. This is not unexpected as we have already noticed that it is challenging to exclude those values of CP phase which lie close to the CP conserving values (*i.e.*, 0 and π). So, in case of SI, the choice of optimal exposure is expected to be $\simeq 350$ kt.MW.yr.

Let us now discuss the impact of NSI on the choice of the optimal exposure. For the

[7]Similar feature can also be seen from the T2K panel in Fig. 4.11.

[8]See subsection **??** for the discussion of the CP fraction at DUNE in the context of SI only. Note that, a slightly different configuration of DUNE was used there and the flux used was also different.

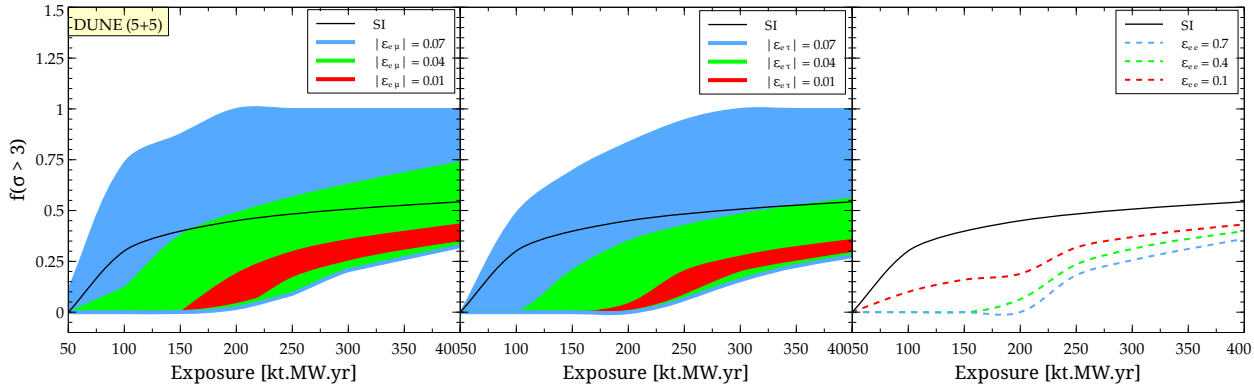

Figure 4.13: The CP fraction $f(\sigma > 3)$ for which the sensitivity to CP violation is greater than 3σ as a function of exposure for SI and NSI case assuming NH. The three plots correspond to three different NSI parameters taken one at a time with full phase variation. The red, green and blue shaded regions correspond to different values of $\varepsilon_{e\mu}$ and $\varepsilon_{e\tau}$.

NSI case, the three panels in Fig. 4.13 correspond to the three different NSI terms (taken in isolation). There are three coloured regions (blue, green, red) for the off-diagonal NSI terms which correspond to the three values of moduli of NSI parameters along with their respective phase variation (analogous to the grey bands seen in Fig. 4.6 and 4.7). For the diagonal NSI terms, there are three dashed lines (blue, green, red) corresponding to three different values of diagonal NSI parameter ε_{ee} (see Fig. 4.8). The plot on the left shows the impact of $\varepsilon_{e\mu}$. Even with the phase variation, $f(\sigma > 3)$ (shown as red band) remains below the SI curve for small value of $\varepsilon_{e\mu}$ ($|\varepsilon_{e\mu}| = 0.01$). This is due to the dominating statistical effect (a) mentioned in the subsection 4.4.1. For intermediate and large values of $\varepsilon_{e\mu}$ ($|\varepsilon_{e\mu}| = 0.04, 0.07$) on the other hand, $f(\sigma > 3)$ gets distributed over a larger range of values for some favourable choice of parameters (due to the interplay of the two competing effects (a) and (b) mentioned in subsection 4.4.1), as can be seen from the green and blue bands.

Incorporating the phase variation of the NSI parameter leads to an increase in the value of $f(\sigma > 3)$ and it can reach ~ 1 when the exposure is barely 200 kt.MW.yr (for some choice of phases, some part of the grey band is above the 3σ line in Fig. 4.6 and 4.7 for all true values of δ). Similar effects are seen for the other off-diagonal parameter, $\varepsilon_{e\tau}$ which is shown in the middle panel. However for the diagonal NSI parameter ε_{ee} (which is real), we note that the $f(\sigma > 3)$ (blue, green and red dashed lines) is always smaller than in the SI case for a given choice of systematics (see also Fig. 4.8). This is again due to the statistical effect.

We have checked that if we take the true hierarchy as inverted hierarchy (IH) instead

NSI term	NH		IH	
	$f(\sigma > 3)$ (NSI)	$f(\sigma > 3)$ (SI)	$f(\sigma > 3)$ (NSI)	$f(\sigma > 3)$ (SI)
$\lvert\varepsilon_{e\mu}\rvert = 0.01$	$0.32 - 0.40$	0.52	$0.35 - 0.42$	0.58
$\lvert\varepsilon_{e\mu}\rvert = 0.04$	$0.30 - 0.69$	0.52	$0.33 - 0.78$	0.58
$\lvert\varepsilon_{e\mu}\rvert = 0.07$	$0.27 - 1.00$	0.52	$0.32 - 1.00$	0.58
$\lvert\varepsilon_{e\tau}\rvert = 0.01$	$0.26 - 0.32$	0.52	$0.23 - 0.32$	0.58
$\lvert\varepsilon_{e\tau}\rvert = 0.04$	$0.24 - 0.53$	0.52	$0.22 - 0.84$	0.58
$\lvert\varepsilon_{e\tau}\rvert = 0.07$	$0.23 - 1.00$	0.52	$0.21 - 1.00$	0.58
$\varepsilon_{ee} = 0.01$	0.40	0.52	0.36	0.58
$\varepsilon_{ee} = 0.04$	0.36	0.52	0.30	0.58
$\varepsilon_{ee} = 0.07$	0.31	0.52	0.27	0.58

Table 4.2: $f(\sigma > 3)$ at an exposure of 350 kt.MW.yr for DUNE (see Fig. 4.13).

of NH, the impact of NSI shown in Fig. 4.13 is grossly the same (see Table 4.2). The impact of individual NSI terms on the value of $f(\sigma > 3)$ at an exposure of 350 kt.MW.yr (which is the optimal choice for SI) at DUNE is listed in Table 4.2 for NH and IH.

4.4.5 Role of systematics

The impact of different assumptions on systematics can be seen in Fig. 4.14. The nominal and optimal set of systematics is mentioned in Table 4.3. The black solid curve represents our nominal choice of systematics given in Table 4.3 while the blue solid curve is for an optimal choice mentioned in [14]. The green (magenta) band corresponds to NSI case for off-diagonal parameters $\varepsilon_{e\mu}, \varepsilon_{e\tau}$ with full phase variation for nominal (optimal) choice of systematics. The green (magenta) dashed curve is for ε_{ee} for nominal (optimal) choice of systematics.

It can be seen that $f(\sigma > 3)$ nearly reaches its maximum (~ 0.55) possible value at around 1300 km for SI (see Fig. 4.14). This implies that for the given configuration of the far detector planned for DUNE (see Table 4.3), the optimal distance to be able to infer the highest fraction of the values of the CP phase is ~ 1300 km. Clearly, even in case of SI, better systematics is expected to lead to a larger $f(\sigma > 3)$ for a given baseline, say at 1300 km - it changes from ~ 0.55 to ~ 0.71. For the SI case, better systematics ensures better detectability of CP violation quantified in terms of fraction $f(\sigma > 3)$ and at the same time, does not alter the optimal baseline choice for CP violation sensitivity. In case of NSI, the green (magenta) band shows the effect of two choices of systematics and there

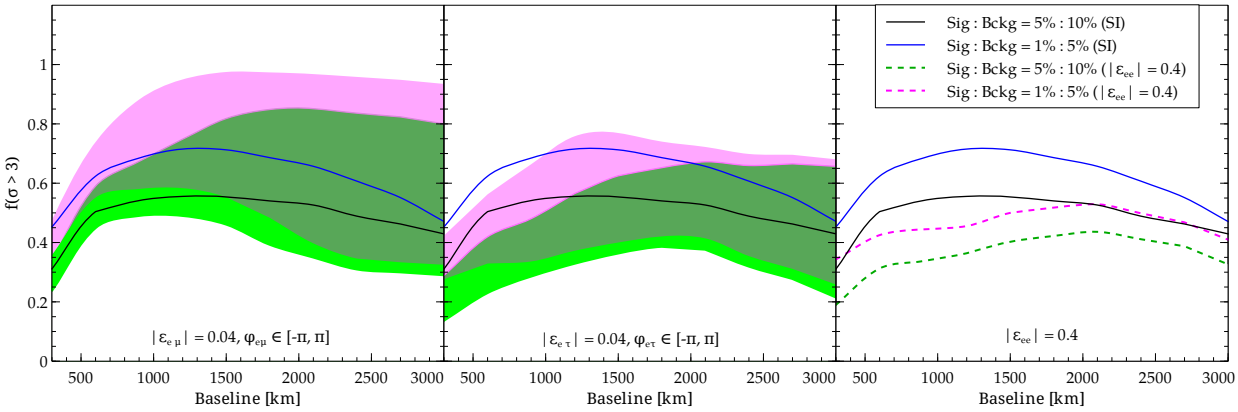

Figure 4.14: The CP fraction for which the sensitivity to CP violation is greater than 3σ as a function of baseline for SI and NSI case. The black and blue solid curves correspond to the different systematics assumed for SI. The three plots correspond to three NSI parameters taken one at a time. The green (magenta) band corresponds to the choice of nominal (optimal) systematics with full phase variation for the off-diagonal NSI parameters while the green (magenta) dashed line corresponds to ε_{ee} for nominal (optimal) systematics (also see table 4.3). NH is considered and the exposure taken is 350 kt.MW.yr.

is an overlap between them as well as with the SI values. *These aspects play a crucial role in altering the choice of best baseline for CP violation sensitivity.* However, in presence of NSI, for the choice of NSI phases representing the top (bottom) edge of the green or magenta band (we have used the dashed green or magenta lines to depict the diagonal NSI terms), the optimal choice of baseline (L_{opt}) that maximizes the CP fraction changes as a function of systematics (see Table 4.3).

NSI term	Nominal (sig:bckg=5% : 10%)		Optimal (sig:bckg=1% : 5%)	
	NSI	SI	NSI	SI
	$f(\sigma > 3)$ L_{opt} km	$f(\sigma > 3)$ L_{opt} km	$f(\sigma > 3)$ L_{opt} km	$f(\sigma > 3)$ L_{opt} km
$\lvert\varepsilon_{e\mu}\rvert = 0.04$	0.85 (1800 – 2500) 0.49 (800 – 1300)	0.52 (1300)	0.97 (1500 – 3000) 0.59 (800 – 1300)	0.71 (1300)
$\lvert\varepsilon_{e\tau}\rvert = 0.04$	0.65 (2000 – 3000) 0.37 (1800 – 2000)	0.52 (1300)	0.77 (1300 – 1500) 0.40 (1800 – 2000)	0.71 (1300)
$\varepsilon_{ee} = 0.04$	0.43 (1900 – 2100)	0.52 (1300)	0.52 (1900 – 2100)	0.71 (1300)

Table 4.3: Maximum $f(\sigma > 3)$ and optimal baseline range (L_{opt}) for the nominal and optimal choices of systematics (see Fig. 4.14) for NH. The values with larger (smaller) $f(\sigma > 3)$ correspond to upper (lower) edge of the respective bands.

4.4.6 Reconstruction of the CP phases

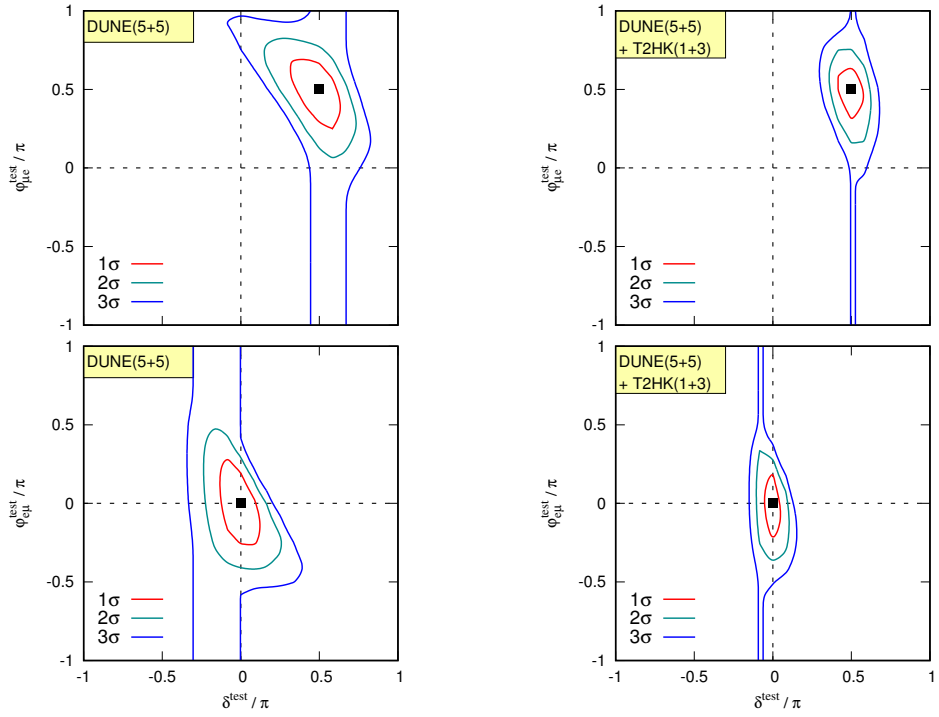

Figure 4.15: Regions in $\varphi_{e\mu}^{test} - \delta^{test}$ plane. The black dot represents the pair of true values $\{\varphi_{e\mu}^{true}, \delta^{true}\}$ which are taken to be $\{\pi/2, \pi/2\}$ (CP violating) in top row or $\{0, 0\}$ (CP conserving) in the bottom row. The value of NSI parameter is taken to be $|\varepsilon_{e\mu}| = 0.04$. The plots on the left are for DUNE and those on the right are for DUNE + T2HK.

Independent of the question of the CP violation sensitivity that we have addressed in the preceding subsections, one can explore the capability long baseline experiments to reconstruct the true values of the CP phases in presence of NSI. For the sake of simplicity, we assume that only one NSI parameter contributes at a time (let us assume that this is given by $\varphi_{e\mu}$)[9]. Let us now take some representative values of the true CP phases and discuss how well we are able to reconstruct those values among the allowed test ranges. In Fig. 4.15, for two possible choices of the pair of phases $\{\delta^{true}, \varphi_{e\mu}^{true}\} = \{\pi/2, \pi/2\}$ (maximal CP violation) and $\{\delta^{true}, \varphi_{e\mu}^{true}\} = \{0, 0\}$ (CP conservation), we show the ability of DUNE to reconstruct those phases assuming NH. For a comparison, we also show the

[9]For the other NSI parameter $\varphi_{e\tau}$, the results are similar.

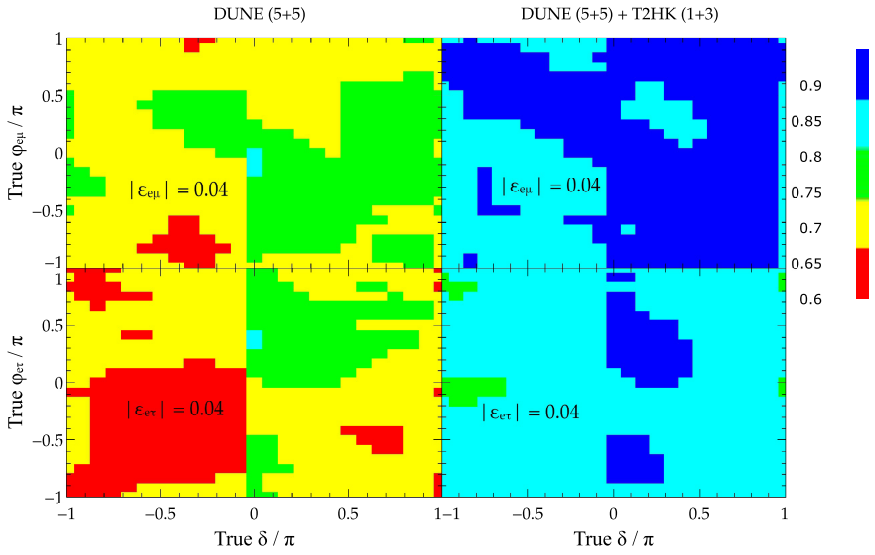

Figure 4.16: Oscillograms of generalized CP fraction in $\varphi_{e\mu}^{true} - \delta^{true}$ plane.

results for the combined case of DUNE +T2HK where we see that the regions enclosed by the contours become narrower.

The region outside the 3σ contour represents those values of the pair of test CP phases which can be safely discarded above 3σ while reconstructing their values for the specific choice of the true pair of CP phases. Smaller enclosed regions by the contours (see Fig. 4.15, right panel) imply better measurement ability.

Let us define a generalized CP fraction at a given confidence level [10] as the ratio of the area outside the contours to the full area. This quantity allows us to have an idea of how well a pair of CP phases can be reconstructed at any given confidence level. Large CP fraction implies better identification of the CP pair among the test values. To take into account all possible choices of the true pair of CP phases, we show in Fig. 4.16, oscillograms of generalized CP fraction in $\varphi_{e\mu}^{true} - \delta^{true}$ and $\varphi_{e\tau}^{true} - \delta^{true}$ plane. The colours represent values of the generalised CP fraction in the range $0.6-1$. For the case of DUNE, the range of generalised CP fraction is $\simeq 0.6 - 0.8$ while if we add T2HK to DUNE, the range of CP fraction increases to $\simeq 0.85 - 1$. This means that T2HK, when combined with DUNE allows us to measure the CP phases much better.

[10] This is different from the CP fraction that we have introduced earlier which involves only the Dirac CP phase (δ).

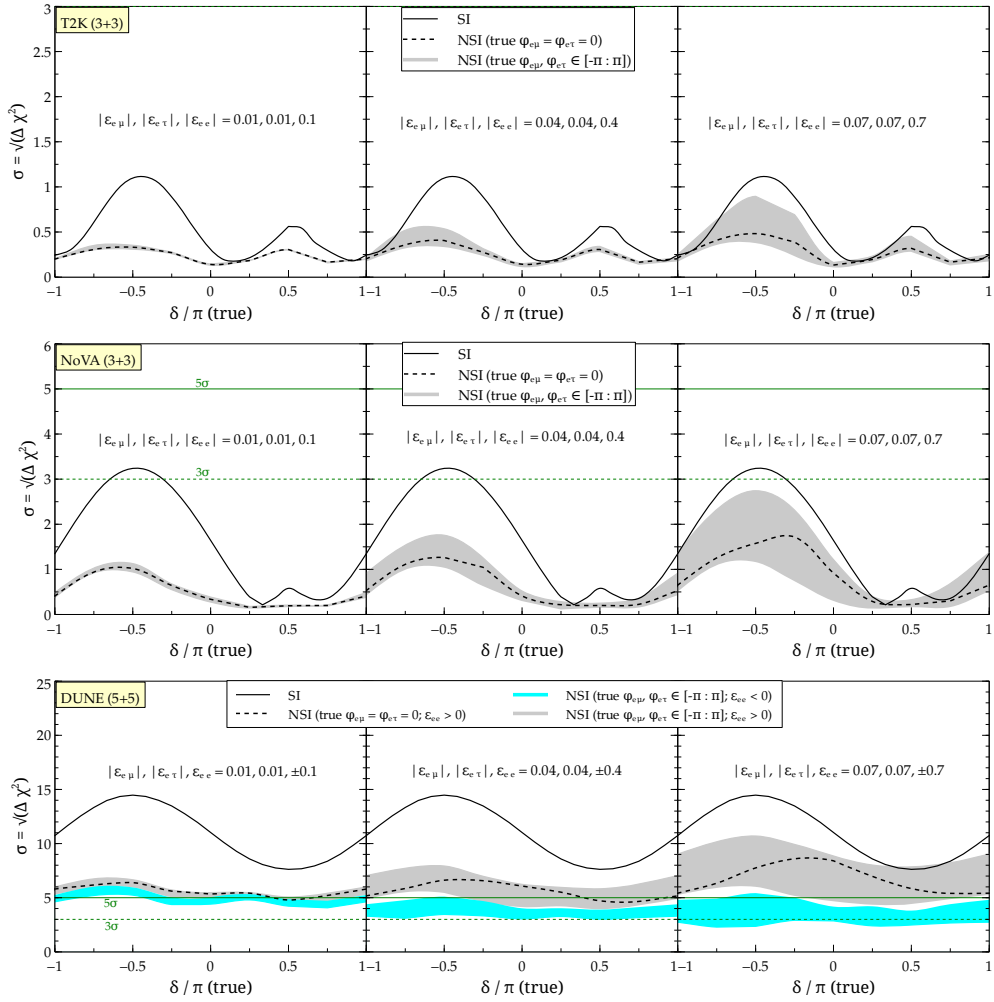

Figure 4.17: Mass ordering sensitivity at T2K, NOvA, and DUNE for collective NSI case and SI as a function of true δ (NH).

4.5 Results: Sensitivity to mass hierarchy

For the purpose of completing the analyses, we discuss a few important and relevant results on mass mass hierarchy in the context of long baseline experiments in presence of NSI [252]. Similar to the discussion of mass hierarchy in presence sterile neutrinos in chapter 3, we explore the sensitivity of the experiment to distinguish the true hierarchy from the test in the level of χ^2. The two similar competing effects discussed in subsection 4.4.1 also guide the value of χ^2 for mass hierarchy.

4.5.1 Comparison with other long baseline experiments

The expected mass ordering sensitivity offered by different experiments with and without NSI is illustrated in Figs. 4.17 and 4.18 for true NH and true NH respectively considering the relevant NSI parameters collectively. We can immediately notice that the (solid black) curves for SI resemble the characteristic shape based on the statistical definition of χ^2 described earlier (see Figs. 3.9 and 3.10.). In presence of NSI, the baseline-dependent characteristic shape of the χ^2 for mass ordering sensitivity is spoiled depending upon the baseline and the size of the NSI term. This distortion in shape is expectedly more for the longer baselines considered. In presence of NSI, there is a suppression in the value of χ^2 for all values of δ[11]. However for most values of δ, it stays above $\sim 5\sigma$ if the NSI parameter ε_{ee} is positive. If $\varepsilon_{ee} < 0$, the cyan band shows that the χ^2 can get further suppressed and can lie in the range $3 - 5\sigma$. As usual, for T2K and NOvA, because of the shorter baseline the mass hierarchy sensitivity is much smaller.

In Fig. 4.18, the mass ordering sensitivity is shown for the case of IH. The impact of NSI is similar to that for the case of NH.

4.5.2 Role of systematics

The impact of different assumptions on systematics can be seen in Fig. 4.19. The black solid curve represents our nominal choice of systematics while the blue solid curve is for an optimal choice mentioned in the legend [14]. The green (magenta) band corresponds to NSI case for off-diagonal parameters $\varepsilon_{e\mu}, \varepsilon_{e\tau}$ with full phase variation for nominal (optimal) choice of systematics. The green (magenta) dashed curve is for ε_{ee} for nominal (optimal) choice of systematics.

It can be seen that $f^{MO}(\sigma > 5)$ nearly reaches its maximum (~ 1) possible value at around 1150 km for SI (see Fig. 4.19). This implies that for the given configuration of the far detector planned for DUNE, the optimal distance to be able to infer the mass ordering for the largest fraction of the values of the CP phase is ≥ 1150 km. Clearly, in case of SI, better systematics does not significantly change the optimal baseline for mass ordering determination above 5σ. For the SI case, therefore the optimal baseline choice for mass ordering sensitivity remains the same for either choice of systematics. In case of

[11] In the χ^2 calculation for mass hierarchy, the test CP phases have been marginalized over their full allowed range $[-180°, 180°]$; whereas for CP violation sensitivity the marginalization was carried over the CP violating values - $0°$ and $180°$ only. This enhanced range of marginalization for mass hierarchy leads to a larger statistical effect (see effect (a) in the subsection 4.4.1), leading to a generally reduced χ^2 for NSI scenario, compared to the SI case.

NSI, the green (magenta) band shows the effect of two choices of systematics and there is an overlap between them as well as with the SI values. However, in presence of NSI, for the choice of NSI phases representing the top (bottom) edge of the green or magenta band (we have used the dashed green or magenta lines to depict the diagonal NSI terms), the optimal choice of baseline that maximizes the mass ordering fraction changes as a function of systematics.

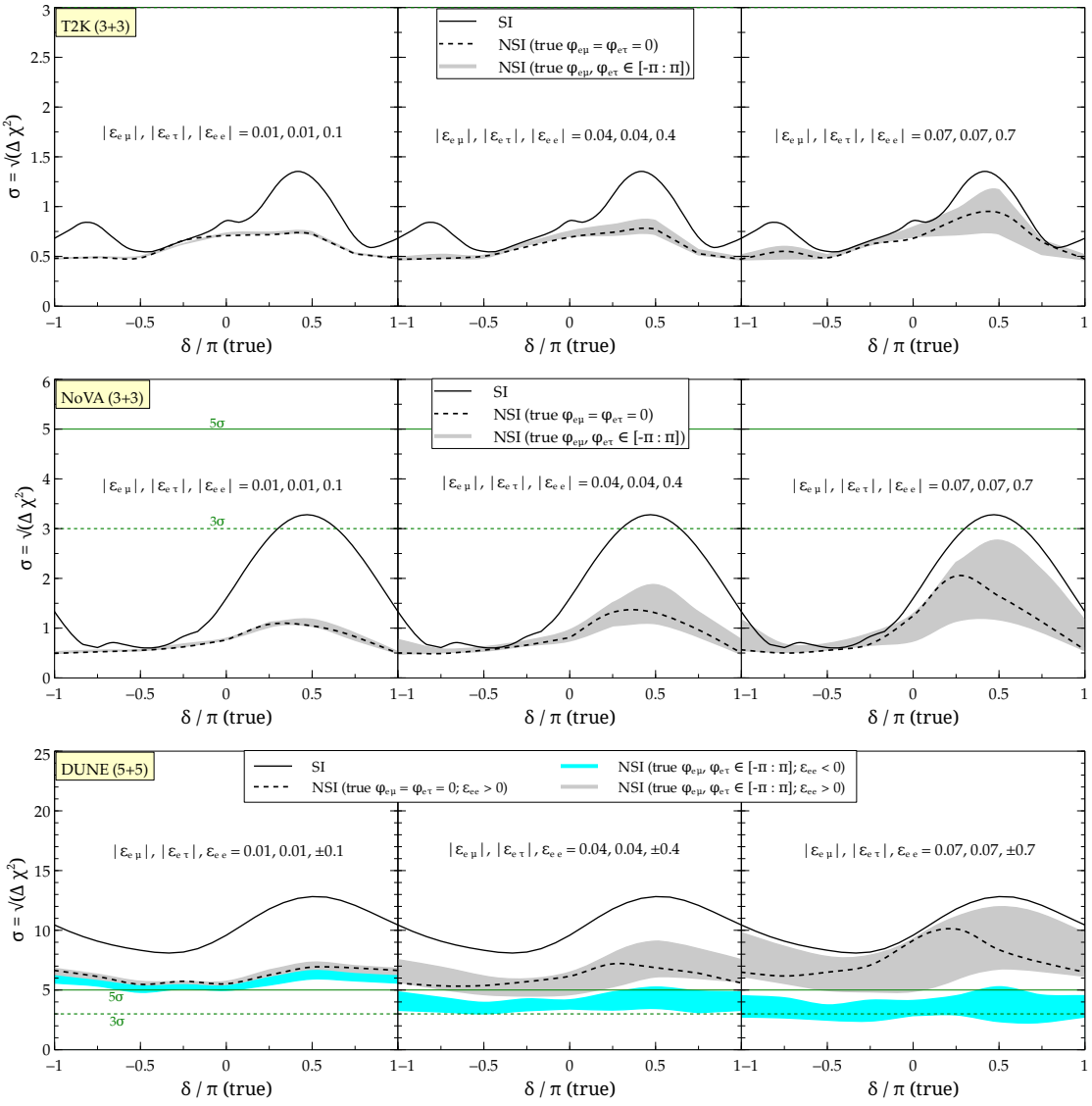

Figure 4.18: Mass ordering sensitivity at T2K, NOvA, and DUNE for collective NSI case and SI as a function of true δ (IH).

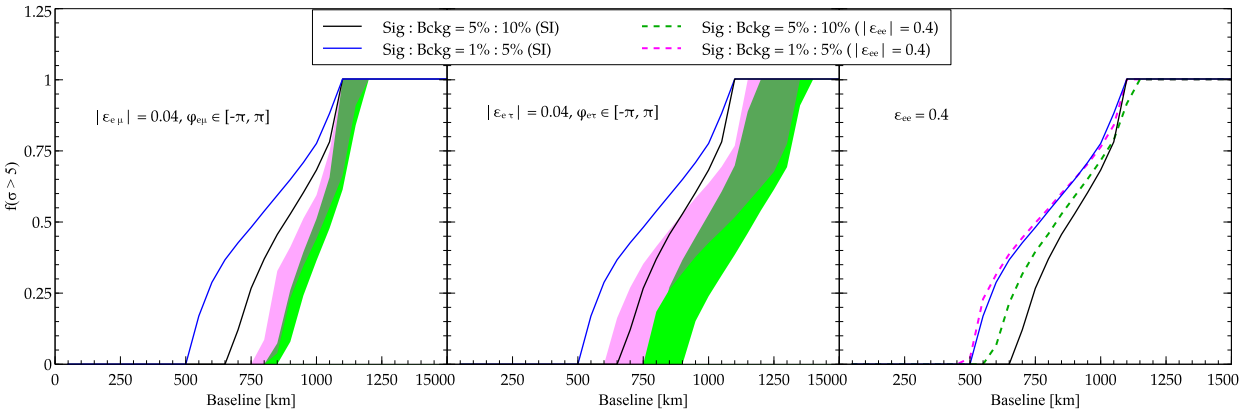

Figure 4.19: Mass ordering fraction $f^{MO}(\sigma > 5)$ plotted as a function of baseline for DUNE like detector configuration and NO.

Chapter 5

Conclusion

In this thesis, we have studied the capability of the long baseline experiments to resolve CP Violation and mass hierarchy ambiguities. Later, we have also illustrated the effects of new Beyond Standard Model physics such as the presence of a light sterile neutrino or the presence of nonstandard neutrino interactions (NSI) on the CPV and mass hierarchy measurements. The main conclusions from these various studies are summarized as follows.

5.1 Summary of CPV and mass hierarchy studies at long baselines for standard oscillation

We have done this study (chapter 2) by focusing especially on the upcoming Deep Underground Neutrino Experiment as either a 10 kt or 35 kt LAr far detector situated underground at the Homestake mine and taking data in a high intensity neutrino beam for 5 years and in an antineutrino beam for another 5 years. For the 35 kt detector, we find that reduced systematic uncertainties afforded by a near detector greatly benefit the sensitivity to CP violation. However, although a near detector provides some help in the determination of the mass hierarchy, the presence of it is redundant since the hierarchy sensitivity without a near detector is well above 5σ. While the sensitivity to the mass hierarchy from atmospheric neutrinos gets enhanced to almost 3σ, the combined beam and atmospheric data is not much affected by magnetization. Since magnetization is not currently feasible for a 35 kt detector, we only considered this possibility for a 10 kt detector. Also, magnetizing the detector does not help improve the sensitivity to CP violation or mass hierarchy significantly. Additionally, we have shown that adding the data from other long baseline experiments such as NOvA, T2K significantly help in breaking the

CPV degeneracy.

We have also attempted to give a semi quantitative explanation for the typical χ^2 shapes for CPV and mass hierarchy, connecting the χ^2 expressions and the relevant probabilities.

We can conclude from here that a 35 kt DUNE with a near detector augmented with a far one is likely to break the CPV and the hierarchy ambiguities that plague long-baseline beam experiments and will answer all the questions it is designed to address.

5.2 Summary of CPV and mass hierarchy studies at long baselines in presence of a sterile neutrino

We have studied the effects of the additional mixing angles and CP phases in the case of a 3+1 sterile sector on the determination and measurement of CPV at long baselines for the DUNE experiment in chapter 3. First, from a probability analysis, we show that the effects of the additional CP phases can be large at its chosen baseline of 1300 km. These effects, which arise from large interference terms (between the 3+0 and 3+1 sectors) in the appearance probability, are accentuated by the presence of matter, which additionally brings in contributions from sterile-sector mixings and phases which are dormant at short baselines. From event rate calculations, we show that the presence of a sterile sector manifests itself in measurably altered rates in energy bins across the spectrum, without significant distortion in the shape. This alteration in event rates increases, as expected, for larger values of the mixing angles connecting the active and sterile sectors.

We then translate our analyses to the level of χ^2 and illustrate that the sensitivities of long-baseline experiments to the mass hierarchy and CP Violation are affected and altered significantly in the presence of a sterile neutrino. While we use DUNE as our benchmark example, we study these sensitivities for T2K, T2HK, and NOvA also. Depending on the values of sterile mixing angles and phases, the sensitivities can be both significantly enhanced or suppressed compared to the 3+0 case. We explain qualitatively about the two competing effects that guide the value of χ^2.

If sterile neutrinos are indeed shown to exist, or if their existence cannot be conclusively ruled out by the short-baseline experiments, we ask how tightly one must then bound the sterile-active mixing angles to ensure that DUNE data can be safely interpreted without taking the possible existence of sterile neutrinos into account. In the process, we find that DUNE may exhibit signals hinting at the presence of a sterile sector even if the relevant mixing angles lie below the sensitivity of the planned short-baseline exper-

iments. However, the ability of long-baseline efforts like DUNE to signal the presence of this sector, while highly valuable, must remain complemenetary to an essential and primary short-baseline thrust aimed at discovering evidence of short-wavelength oscillations with convincing redundancy.

Importantly, the presence of a sterile sector obfuscates conclusive determinations of CP violation and mass hierarchy at the far detector, and makes uncertain the ability to ascribe any perceived CPV to a unique phase in the 3+0 sector. Thus, the linkage between the presently planned long and short baseline programs must be explored and strengthened. Until the presence of an $\sim$ eV^2 sector is conclusively ruled out, our work emphasizes the need for a complementary SBL sterile-search program and for a highly capable and versatile near detector for DUNE, enabling it to reduce systematics to low levels so that it may achieve its stated primary goals for CPV and hierarchy detection.

5.3 Impact of NSI on mass hierarchy and CPV studies at long baselines

In chapter 4, we study the role of neutral current nonstandard neutrino interactions (NSI) in determining CP Violation (CPV) and mass hierarchy in the context of long baseline experiments. We work with the most relevant channel $\nu_\mu \to \nu_e$ and discuss the impact of the NSI parameters both individually and collectively. We show that the additional moduli and CP phases of the NSI parameters can potentially lead to large changes in the probability and asymmetry curves near the peak of the $P(\nu_\mu \to \nu_e)$ and $P(\bar{\nu}_\mu \to \bar{\nu}_e)$ and at higher energies in comparison to the SI case.

From the event rate analysis, we show that the alteration in event rates is most significant near the peak but exists all across the spectrum. There is no significant distortion in the spectrum shape. However in terms of event rates, there is a certain wash out of effects seen in the higher energy range. This is because the flux falls off and hence the effects appearing in higher energy range are not cleanly observable. Interestingly, there are overlapping regions where SI and NSI results are consistent with one another due to a certain favourable choice of parameters. We refer to these as the NSI-SI degeneracies. Due to presence of these new degeneracies, it becomes hard to ascribe the signal to SI alone or to NSI.

We show the χ^2 sensitivities for CPV and mass hierarchy in presence of NSI for DUNE and compared that result with other experiments T2K, NOvA and T2HK. We illustrate that the longer baseline experiment DUNE gets much more affected by the presence of

NSI, while shorter baseline experiment T2HK is less affected, owing to less matter effect. T2HK with the high statistics thus can play a complementary role to the former in exploring leptonic CP Violation.

The relevant NSI parameters $\varepsilon_{e\mu}, \varepsilon_{e\tau}, \varepsilon_{ee}$ can change the value of χ^2 for CPV and mass hierarchy significantly depending on the interplay of two competing effects (similar to the case of sterile neutrinos). Consequently, if the effects of NSI are not considered in the interpretation of the DUNE data, one can potentially get completely misleading results. For *e.g.*, even in the case of CP conservation in the standard scenario, the χ^2 in presence of NSI can point to a $\gtrsim 3\sigma$ CP Violation sensitivity. The apparent increase/ decrease of mass hierarchy sensitivity in presence of NSI should also be carefully interpreted to avoid any wrong measurement.

Finally, it can be said that any conclusion regarding the CP phase/ hierarchy can not be arrived at without a thorough analysis of correlations and degeneracies that arise due to the extra parameters due to the presence of NSI, in addition to the standard three flavour parameters where the only source of CP violation is the Dirac phase. Thus in order to ascribe any result on the CP phase to the lone CP phase in the standard three neutrino paradigm, it is crucial to rule out/ constrain new physics scenarios that can also contribute to the signal.

Bibliography

[1] V. Barger, D. Marfatia, and K. Whisnant, Int. J. Mod. Phys. **E12**, 569 (2003), hep-ph/0308123.

[2] C. Giunti and C. W. Kim, *Fundamentals of Neutrino Physics and Astrophysics* (2007).

[3] S. R. Elliott and J. Engel, J. Phys. **G30**, R183 (2004), hep-ph/0405078.

[4] Elizabeth Worcester, private communication (2016).

[5] M. Gonzalez-Garcia, M. Maltoni, and T. Schwetz, JHEP **1411**, 052 (2014), 1409.5439.

[6] G. L. Fogli, E. Lisi, A. Marrone, D. Montanino, A. Palazzo, and A. M. Rotunno, Phys. Rev. **D86**, 013012 (2012), 1205.5254.

[7] T. Akiri *et al.* (LBNE) (2011), 1110.6249.

[8] Sanjib Mishra, private communication (2013).

[9] D. S. Ayres *et al.* (NOvA) (2004), hep-ex/0503053.

[10] Y. Itow *et al.* (T2K), in *Neutrino oscillations and their origin. Proceedings, 3rd International Workshop, NOON 2001, Kashiwa, Tokyo, Japan, December 508, 2001* (2001), pp. 239–248, hep-ex/0106019, URL http://alice.cern.ch/format/showfull?sysnb=2258620.

[11] V. Barger, R. Gandhi, P. Ghoshal, S. Goswami, D. Marfatia, *et al.*, Phys.Rev.Lett. **109**, 091801 (2012), 1203.6012.

[12] R. Gandhi, P. Ghoshal, S. Goswami, P. Mehta, S. U. Sankar, and S. Shalgar, Phys. Rev. **D76**, 073012 (2007), 0707.1723.

[13] R. Acciarri *et al.* (DUNE) (2015), 1512.06148.

[14] M. Bass *et al.* (LBNE), Phys. Rev. **D91**(5), 052015 (2015), 1311.0212.

[15] K. Abe *et al.* (Hyper-Kamiokande Proto-Collaboration), PTEP **2015**, 053C02 (2015), 1502.05199.

[16] M. C. Gonzalez-Garcia, M. Maltoni, and T. Schwetz (2015), 1512.06856.

[17] W. Pauli, Cambridge Monogr.Part.Phys.Nucl.Phys.Cosmol.,14,1 (2000).

[18] Solvay Conference, (1933).

[19] E. Fermi, Z. Phys. **88**, 161 (1934).

[20] E. Fermi, Nuovo Cim. **11**, 1 (1934), [,535(1934)].

[21] F. Reines, C. L. Cowan, F. B. Harrison, A. D. McGuire, and H. W. Kruse, Phys. Rev. **117**, 159 (1960).

[22] G. Danby, J. M. Gaillard, K. A. Goulianos, L. M. Lederman, N. B. Mistry, M. Schwartz, and J. Steinberger, Phys. Rev. Lett. **9**, 36 (1962).

[23] K. Kodama *et al.* (DONUT), Phys. Lett. **B504**, 218 (2001), hep-ex/0012035.

[24] B. Pontecorvo, Sov. Phys. JETP **6**, 429 (1957), [Zh. Eksp. Teor. Fiz.33,549(1957)].

[25] B. Pontecorvo, Sov. Phys. JETP **10**, 1236 (1960), [Zh. Eksp. Teor. Fiz.37,1751(1959)].

[26] Z. Maki, M. Nakagawa, and S. Sakata, Progress of Theoretical Physics **28**(5), 870 (1962).

[27] T. J. Haines *et al.*, Phys. Rev. Lett. **57**, 1986 (1986).

[28] M. Ambrosio *et al.* (MACRO), Phys. Lett. **B434**, 451 (1998), hep-ex/9807005.

[29] K. S. Hirata *et al.* (Kamiokande-II), Phys. Lett. **B205**, 416 (1988), [,447(1988)].

[30] Y. Ashie *et al.* (Super-Kamiokande), Phys. Rev. **D71**, 112005 (2005), hep-ex/0501064.

[31] Y. Fukuda *et al.* (Super-Kamiokande), Phys. Rev. Lett. **81**, 1562 (1998), hep-ex/9807003.

[32] B. Aharmim *et al.* (SNO), Phys. Rev. **C72**, 055502 (2005), nucl-ex/0502021.

[33] L. Wolfenstein, Phys. Rev. **D17**, 2369 (1978).

[34] S. P. Mikheev and A. Y. Smirnov, Sov. Phys. Usp. **30**, 759 (1987).

[35] T. Kajita and A. B. McDonald, *For the discovery of neutrino oscillations, which shows that neutrinos have mass*, the Nobel Prize in Physics 2015.

[36] J. N. Bahcall, M. H. Pinsonneault, and S. Basu, Astrophys. J. **555**, 990 (2001), astro-ph/0010346.

[37] J. N. Bahcall and A. M. Serenelli, Astrophys. J. **626**, 530 (2005), astro-ph/0412096.

[38] J. N. Bahcall, A. M. Serenelli, and S. Basu, Astrophys. J. **621**, L85 (2005), astro-ph/0412440.

[39] J. N. Bahcall and R. K. Ulrich, Rev. Mod. Phys. **60**, 297 (1988).

[40] T. K. Gaisser and M. Honda, Ann. Rev. Nucl. Part. Sci. **52**, 153 (2002), hep-ph/0203272.

[41] V. Barger, D. Marfatia, and K. Whisnant, *The physics of neutrinos* (Princeton Univ. Pr., Princeton, USA, 2012), ISBN 9780691128535, URL http://press.princeton.edu/titles/9913.html.

[42] L. A. Mikaelyan, Phys. Atom. Nucl. **65**, 1173 (2002), [Yad. Fiz.65,1206(2002)], hep-ph/0210047.

[43] C. Bemporad, G. Gratta, and P. Vogel, Rev. Mod. Phys. **74**, 297 (2002), hep-ph/0107277.

[44] S. Nussinov, Phys. Lett. **B63**, 201 (1976).

[45] B. Kayser, Phys. Rev. **D24**, 110 (1981).

[46] K. Kiers, S. Nussinov, and N. Weiss, Phys. Rev. **D53**, 537 (1996), hep-ph/9506271.

[47] C. Giunti, C. W. Kim, and U. W. Lee, Phys. Rev. **D44**, 3635 (1991).

[48] C. Giunti and C. W. Kim, Phys. Rev. **D58**, 017301 (1998), hep-ph/9711363.

[49] B. Pontecorvo, Sov. Phys. JETP **26**, 984 (1968), [Zh. Eksp. Teor. Fiz.53,1717(1967)].

[50] E. K. Akhmedov, R. Johansson, M. Lindner, T. Ohlsson, and T. Schwetz, JHEP **0404**, 078 (2004), hep-ph/0402175.

[51] T. Araki *et al.* (KamLAND), Phys. Rev. Lett. **94**, 081801 (2005), hep-ex/0406035.

[52] A. Gago, M. Guzzo, P. de Holanda, H. Nunokawa, O. Peres, *et al.*, Phys.Rev. **D65**, 073012 (2002), hep-ph/0112060.

[53] P. Adamson *et al.* (MINOS), Phys.Rev.Lett. **112**, 191801 (2014), 1403.0867.

[54] F. P. An *et al.* (Daya Bay), Phys. Rev. Lett. **108**, 171803 (2012), 1203.1669.

[55] J. K. Ahn *et al.* (RENO), Phys. Rev. Lett. **108**, 191802 (2012), 1204.0626.

[56] Y. Abe *et al.* (Double Chooz Collaboration), JHEP **1410**, 086 (2014), 1406.7763.

[57] P. Adamson *et al.* (NOvA) (2016), 1601.05022.

[58] S. T. Petcov, Phys. Lett. **B110**, 245 (1982).

[59] C. H. Albright and S. M. Barr, Phys. Rev. **D58**, 013002 (1998), hep-ph/9712488.

[60] M.-C. Chen and K. T. Mahanthappa, Phys. Rev. **D62**, 113007 (2000), hep-ph/0005292.

[61] R. Kitano and Y. Mimura, Phys. Rev. **D63**, 016008 (2001), hep-ph/0008269.

[62] S. F. King and G. G. Ross, Phys. Lett. **B574**, 239 (2003), hep-ph/0307190.

[63] M. Bando, S. Kaneko, M. Obara, and M. Tanimoto, Phys. Lett. **B580**, 229 (2004), hep-ph/0309310.

[64] C. H. Albright, Phys. Lett. **B599**, 285 (2004), hep-ph/0407155.

[65] A. D. Sakharov, Pisma Zh. Eksp. Teor. Fiz. **5**, 32 (1967), [Usp. Fiz. Nauk161,61(1991)].

[66] M. Fukugita and T. Yanagida, Phys. Lett. **B174**, 45 (1986).

[67] W. Buchmuller, P. Di Bari, and M. Plumacher, Annals Phys. **315**, 305 (2005), hep-ph/0401240.

[68] S. Davidson, E. Nardi, and Y. Nir, Phys. Rept. **466**, 105 (2008), 0802.2962.

[69] R. Barbieri, P. Creminelli, A. Strumia, and N. Tetradis, Nucl. Phys. **B575**, 61 (2000), hep-ph/9911315.

[70] A. Abada, S. Davidson, A. Ibarra, F. X. Josse-Michaux, M. Losada, and A. Riotto, JHEP **09**, 010 (2006), hep-ph/0605281.

[71] G. F. Giudice, A. Notari, M. Raidal, A. Riotto, and A. Strumia, Nucl. Phys. **B685**, 89 (2004), hep-ph/0310123.

[72] W. Buchmuller and M. Plumacher, Phys. Lett. **B389**, 73 (1996), hep-ph/9608308.

[73] G. C. Branco, T. Morozumi, B. M. Nobre, and M. N. Rebelo, Nucl. Phys. **B617**, 475 (2001), hep-ph/0107164.

[74] G. C. Branco, R. Gonzalez Felipe, F. R. Joaquim, and M. N. Rebelo, Nucl. Phys. **B640**, 202 (2002), hep-ph/0202030.

[75] M. N. Rebelo, Phys. Rev. **D67**, 013008 (2003), hep-ph/0207236.

[76] A. Aguilar-Arevalo *et al.* (LSND), Phys.Rev. **D64**, 112007 (2001), hep-ex/0104049.

[77] S. Schael *et al.* (SLD Electroweak Group, DELPHI, ALEPH, SLD, SLD Heavy Flavour Group, OPAL, LEP Electroweak Working Group, L3), Phys. Rept. **427**, 257 (2006), hep-ex/0509008.

[78] V. D. Barger, P. Langacker, J. P. Leveille, and S. Pakvasa, Phys. Rev. Lett. **45**, 692 (1980).

[79] A. Aguilar-Arevalo *et al.* (MiniBooNE), Phys.Rev.Lett. **110**, 161801 (2013), 1207.4809.

[80] M. A. Acero, C. Giunti, and M. Laveder, Phys. Rev. **D78**, 073009 (2008), 0711.4222.

[81] C. Giunti and M. Laveder, Phys. Rev. **C83**, 065504 (2011), 1006.3244.

[82] G. Mention, M. Fechner, T. Lasserre, T. Mueller, D. Lhuillier, *et al.*, Phys.Rev. **D83**, 073006 (2011), 1101.2755.

[83] T. Ota and J. Sato, Phys. Rev. **D71**, 096004 (2005), hep-ph/0502124.

[84] R. Adhikari, S. K. Agarwalla, and A. Raychaudhuri, Phys. Lett. **B642**, 111 (2006), hep-ph/0608034.

[85] Y. Grossman, Phys.Lett. **B359**, 141 (1995), hep-ph/9507344.

[86] S. Davidson, C. Pena-Garay, N. Rius, and A. Santamaria, JHEP **0303**, 011 (2003), hep-ph/0302093.

[87] G. Mitsuka *et al.* (Super-Kamiokande Collaboration), Phys.Rev. **D84**, 113008 (2011), 1109.1889.

[88] P. Adamson *et al.* (MINOS Collaboration), Phys.Rev. **D88**(7), 072011 (2013), 1303.5314.

[89] O. W. Greenberg, Phys. Rev. Lett. **89**, 231602 (2002), hep-ph/0201258.

[90] J. D. Bjorken and S. D. Drell (1965).

[91] S. R. Coleman and S. L. Glashow, Phys. Rev. **D59**, 116008 (1999), hep-ph/9812418.

[92] G. Barenboim and J. D. Lykken, Phys. Lett. **B554**, 73 (2003), hep-ph/0210411.

[93] N. Arkani-Hamed, S. Dimopoulos, G. R. Dvali, and J. March-Russell, Phys. Rev. **D65**, 024032 (2002), hep-ph/9811448.

[94] S. J. Huber and Q. Shafi, Phys. Lett. **B512**, 365 (2001), hep-ph/0104293.

[95] J. S. Diaz (2015), 1506.01936.

[96] B. Kayser and J. Kopp (2010), 1005.4081.

[97] S. W. Hawking, Phys. Rev. **D14**, 2460 (1976).

[98] Y. Liu, L.-z. Hu, and M.-L. Ge, Phys. Rev. **D56**, 6648 (1997).

[99] C.-H. Chang, W.-S. Dai, X.-Q. Li, Y. Liu, F.-C. Ma, and Z.-j. Tao, Phys. Rev. **D60**, 033006 (1999), hep-ph/9809371.

[100] M. Blennow, T. Ohlsson, and W. Winter, JHEP **06**, 049 (2005), hep-ph/0502147.

[101] F. Benatti and R. Floreanini, JHEP **02**, 032 (2000), hep-ph/0002221.

[102] P. B. Pal and L. Wolfenstein, Phys. Rev. **D25**, 766 (1982).

[103] V. D. Barger, W.-Y. Keung, and S. Pakvasa, Phys. Rev. **D25**, 907 (1982).

[104] G. B. Gelmini and M. Roncadelli, Phys. Lett. **B99**, 411 (1981).

[105] H. M. Georgi, S. L. Glashow, and S. Nussinov, Nucl. Phys. **B193**, 297 (1981).

[106] J. Schechter and J. W. F. Valle, Phys. Rev. **D25**, 774 (1982).

[107] F. Wilczek, Phys. Rev. Lett. **49**, 1549 (1982).

[108] G. B. Gelmini and J. W. F. Valle, Phys. Lett. **B142**, 181 (1984).

[109] M. Lindner, T. Ohlsson, and W. Winter, Nucl. Phys. **B607**, 326 (2001), hep-ph/0103170.

[110] E. Majorana, Nuovo Cim. **14**, 171 (1937).

[111] S. M. Bilenky, J. Hosek, and S. T. Petcov, Phys. Lett. **B94**, 495 (1980).

[112] M. Doi, T. Kotani, H. Nishiura, K. Okuda, and E. Takasugi, Phys. Lett. **B102**, 323 (1981).

[113] L. Wolfenstein, Phys. Lett. **B107**, 77 (1981).

[114] W. C. Haxton and G. J. Stephenson, Prog. Part. Nucl. Phys. **12**, 409 (1984).

[115] C. Aalseth *et al.* (2004), hep-ph/0412300.

[116] P. Minkowski, Phys. Lett. **B67**, 421 (1977).

[117] R. N. Mohapatra and G. Senjanovic, Phys. Rev. Lett. **44**, 912 (1980).

[118] T. Yanagida, Conf. Proc. **C7902131**, 95 (1979).

[119] M. Gell-Mann, P. Ramond, and R. Slansky, Conf. Proc. **C790927**, 315 (1979), 1306.4669.

[120] W. Konetschny and W. Kummer, Phys. Lett. **B70**, 433 (1977).

[121] T. P. Cheng and L.-F. Li, Phys. Rev. **D22**, 2860 (1980).

[122] G. Lazarides, Q. Shafi, and C. Wetterich, Nucl. Phys. **B181**, 287 (1981).

[123] J. Schechter and J. W. F. Valle, Phys. Rev. **D22**, 2227 (1980).

[124] R. N. Mohapatra and G. Senjanovic, Phys. Rev. **D23**, 165 (1981).

[125] R. Foot, H. Lew, X. G. He, and G. C. Joshi, Z. Phys. **C44**, 441 (1989).

[126] S. M. Barr, Phys. Rev. Lett. **92**, 101601 (2004), hep-ph/0309152.

[127] A. Zee, Phys. Lett. **B93**, 389 (1980), [Erratum: Phys. Lett.B95,461(1980)].

[128] C. S. Lam, Phys. Lett. **B507**, 214 (2001), hep-ph/0104116.

[129] W. Grimus and L. Lavoura, JHEP **07**, 045 (2001), hep-ph/0105212.

[130] E. Ma, Phys. Rev. **D66**, 117301 (2002), hep-ph/0207352.

[131] Z.-z. Xing, Phys. Lett. **B530**, 159 (2002), hep-ph/0201151.

[132] B. R. Desai, D. P. Roy, and A. R. Vaucher, Mod. Phys. Lett. **A18**, 1355 (2003), hep-ph/0209035.

[133] W. Grimus and L. Lavoura, J. Phys. **G31**, 693 (2005), hep-ph/0412283.

[134] C. S. Aulakh and R. N. Mohapatra, Phys. Lett. **B119**, 136 (1982).

[135] L. J. Hall and M. Suzuki, Nucl. Phys. **B231**, 419 (1984).

[136] J. R. Ellis, G. Gelmini, C. Jarlskog, G. G. Ross, and J. W. F. Valle, Phys. Lett. **B150**, 142 (1985).

[137] K. R. Dienes, E. Dudas, and T. Gherghetta, Nucl. Phys. **B557**, 25 (1999), hep-ph/9811428.

[138] R. N. Mohapatra, S. Nandi, and A. Perez-Lorenzana, Phys. Lett. **B466**, 115 (1999), hep-ph/9907520.

[139] Y. Grossman and M. Neubert, Phys. Lett. **B474**, 361 (2000), hep-ph/9912408.

[140] V. M. Lobashev *et al.*, Nucl. Phys. Proc. Suppl. **91**, 280 (2001).

[141] C. Kraus *et al.*, Eur. Phys. J. **C40**, 447 (2005), hep-ex/0412056.

[142] A. Osipowicz *et al.* (KATRIN) (2001), hep-ex/0109033.

[143] F. T. Avignone, III, S. R. Elliott, and J. Engel, Rev. Mod. Phys. **80**, 481 (2008), 0708.1033.

[144] H. V. Klapdor-Kleingrothaus *et al.*, in *Proceedings, 3rd International Heidelberg Conference on Dark matter in astro- and particle physics (DARK 2000)* (2000), pp. 520–533.

[145] Y. Huang and B.-Q. Ma, The Universe **2**, 65 (2014), 1407.4357.

[146] J. Tauber, M. Bersanelli, J. M. Lamarre, G. Efstathiou, C. Lawrence, F. Bouchet, E. Martinez-Gonzalez, S. Matarrese, D. Scott, M. White, *et al.* (Planck) (2006), astro-ph/0604069.

[147] M. Lattanzi (Planck), J. Phys. Conf. Ser. **718**(3), 032008 (2016).

[148] F. P. An *et al.* (Daya Bay), Chin. Phys. **C37**, 011001 (2013), 1210.6327.

[149] Y. Abe *et al.* (Double Chooz), Phys. Rev. **D86**, 052008 (2012), 1207.6632.

[150] K. Abe *et al.* (T2K), Phys. Rev. **D88**(3), 032002 (2013), 1304.0841.

[151] J. Arafune and J. Sato, Phys. Rev. **D55**, 1653 (1997), hep-ph/9607437.

[152] M. Tanimoto, Phys. Rev. **D55**, 322 (1997), hep-ph/9605413.

[153] S. M. Bilenky, C. Giunti, and W. Grimus, Phys. Rev. **D58**, 033001 (1998), hep-ph/9712537.

[154] V. D. Barger, K. Whisnant, and R. J. N. Phillips, Phys. Rev. Lett. **45**, 2084 (1980).

[155] M. V. Diwan *et al.*, Phys. Rev. **D68**, 012002 (2003), hep-ph/0303081.

[156] B. Brahmachari, S. Choubey, and P. Roy, Nucl. Phys. **B671**, 483 (2003), hep-ph/0303078.

[157] E. K. Akhmedov, Phys. Scripta **T121**, 65 (2005), hep-ph/0412029.

[158] W. Marciano and Z. Parsa, Nucl. Phys. Proc. Suppl. **221**, 166 (2011), hep-ph/0610258.

[159] S. Pakvasa, Journal of Physics: Conference Series **556**(1), 012060 (2014).

[160] M. Thomson, talk at WINP at Brookhaven, February 2015. "https://indico.bnl.gov/conferenceDisplay.py?confId=918" (2015).

[161] A. Norman (NOνA), AIP Conf. Proc. **1666**, 110001 (2015).

[162] C. Farnese, AIP Conf. Proc. **1666**, 110002 (2015).

[163] S. Dusini (OPERA), AIP Conf. Proc. **1666**, 110003 (2015).

[164] A. B. Sousa (MINOS+, MINOS), AIP Conf. Proc. **1666**, 110004 (2015), 1502.07715.

[165] A. K. Ichikawa, AIP Conf. Proc. **1666**, 130001 (2015).

[166] F. J. P. Soler, AIP Conf. Proc. **1666**, 130002 (2015).

[167] Y. Hayato, AIP Conf. Proc. **1666**, 130003 (2015).

[168] R. J. Wilson (LBNE), AIP Conf. Proc. **1666**, 130004 (2015).

[169] T. Patzak, AIP Conf. Proc. **1666**, 130005 (2015).

[170] K. Long (ICFA Neutrino Panel), AIP Conf. Proc. **1666**, 130006 (2015).

[171] A. de Gouvea *et al.* (Intensity Frontier Neutrino Working Group) (2013), 1310.4340.

[172] J. Strait *et al.* (DUNE) (2016), 1601.05823.

[173] R. Acciarri *et al.* (DUNE) (2016), 1601.05471.

[174] R. Acciarri *et al.* (DUNE) (2016), 1601.02984.

[175] C. Adams *et al.* (LBNE) (2013), 1307.7335.

[176] V. Barger, A. Bhattacharya, A. Chatterjee, R. Gandhi, D. Marfatia, and M. Masud, Phys. Rev. **D89**(1), 011302 (2014), 1307.2519.

[177] V. Barger, A. Bhattacharya, A. Chatterjee, R. Gandhi, D. Marfatia, and M. Masud, Int. J. Mod. Phys. **A31**(07), 1650020 (2016), 1405.1054.

[178] M. Bass, D. Cherdack, and R. J. Wilson, in *Meeting of the APS Division of Particles and Fields (DPF 2013) Santa Cruz, California, USA, August 13-17, 2013* (2013), 1310.6812, URL http://inspirehep.net/record/1262111/files/arXiv:1310.6812.pdf.

[179] M. Goodman, Adv. High Energy Phys. **2015**, 256351 (2015).

[180] K. Bora and D. Dutta, J. Phys. Conf. Ser. **481**, 012019 (2014), 1209.1870.

[181] S. K. Agarwalla, Adv. High Energy Phys. **2014**, 457803 (2014), 1401.4705.

[182] S. K. Agarwalla, S. Prakash, and S. Uma Sankar, JHEP **03**, 087 (2014), 1304.3251.

[183] C. Bromberg, PoS **DSU2012**, 036 (2012).

[184] N. Nath, M. Ghosh, and S. Goswami (2015), 1511.07496.

[185] M. Ghosh, S. Goswami, and S. K. Raut, Eur. Phys. J. **C76**(3), 114 (2016), 1412.1744.

[186] K. N. Deepthi, C. Soumya, and R. Mohanta, New J. Phys. **17**(2), 023035 (2015), 1409.2343.

[187] J. Beringer *et al.* (Particle Data Group), Phys. Rev. **D86**, 010001 (2012).

[188] T. Ohlsson, H. Zhang, and S. Zhou, Phys. Rev. **D87**(5), 053006 (2013), 1301.4333.

[189] P. Huber, M. Lindner, and W. Winter, Comput. Phys. Commun. **167**, 195 (2005), hep-ph/0407333.

[190] P. Huber, J. Kopp, M. Lindner, M. Rolinec, and W. Winter, Comput. Phys. Commun. **177**, 432 (2007), hep-ph/0701187.

[191] S. K. Agarwalla, S. Prakash, S. K. Raut, and S. U. Sankar, JHEP **12**, 075 (2012), 1208.3644.

[192] Mary Bishai, private communication (2014).

[193] M. D. P. t. Messier UMI-99-23965.

[194] E. A. Paschos and J. Y. Yu, Phys. Rev. **D65**, 033002 (2002), hep-ph/0107261.

[195] A. M. Dziewonski and D. L. Anderson, Phys. Earth Planet. Interiors **25**, 297 (1981).

[196] P. Huber, M. Lindner, and W. Winter, Nucl. Phys. **B645**, 3 (2002), hep-ph/0204352.

[197] M. Ishitsuka, T. Kajita, H. Minakata, and H. Nunokawa, Phys. Rev. **D72**, 033003 (2005), hep-ph/0504026.

[198] M. Honda, T. Kajita, K. Kasahara, and S. Midorikawa, Phys. Rev. **D70**, 043008 (2004), astro-ph/0404457.

[199] M. Ghosh, P. Ghoshal, S. Goswami, and S. K. Raut, Nucl. Phys. **B884**, 274 (2014), 1401.7243.

[200] X. Qian, A. Tan, W. Wang, J. J. Ling, R. D. McKeown, and C. Zhang, Phys. Rev. **D86**, 113011 (2012), 1210.3651.

[201] M. Blennow, P. Coloma, P. Huber, and T. Schwetz, JHEP **03**, 028 (2014), 1311.1822.

[202] E. Ciuffoli, J. Evslin, and X. Zhang, JHEP **01**, 095 (2014), 1305.5150.

[203] T. Schwetz, Phys. Lett. **B648**, 54 (2007), hep-ph/0612223.

[204] M. Blennow, JHEP **01**, 139 (2014), 1311.3183.

[205] R. Gandhi, P. Ghoshal, S. Goswami, and S. U. Sankar, Phys. Rev. **D78**, 073001 (2008), 0807.2759.

[206] M. Gonzalez-Garcia and M. Maltoni, Phys.Rev. **D70**, 033010 (2004), hep-ph/0404085.

[207] Steven G. Johnson, *The NLopt nonlinear-optimization package*(http://ab-initio.mit.edu/nlopt).

[208] J. A. Nelder and R. Mead, Comput. J. **7**, 308 (1965).

[209] V. Barger, D. Marfatia, and K. Whisnant, Phys. Rev. **D65**, 073023 (2002), hep-ph/0112119.

[210] K. Kimura, A. Takamura, and H. Yokomakura, Phys. Rev. **D66**, 073005 (2002), hep-ph/0205295.

[211] A. Aguilar-Arevalo *et al.* (MiniBooNE), Phys.Rev.Lett. **102**, 101802 (2009), 0812.2243.

[212] T. Mueller, D. Lhuillier, M. Fallot, A. Letourneau, S. Cormon, *et al.*, Phys.Rev. **C83**, 054615 (2011), 1101.2663.

[213] R. Gandhi, B. Kayser, M. Masud, and S. Prakash, JHEP **11**, 039 (2015), 1508.06275.

[214] D. Dutta, R. Gandhi, B. Kayser, M. Masud, and S. Prakash (2016), 1607.02152.

[215] J. Bian (NOvA), in *Proceedings, Meeting of the APS Division of Particles and Fields (DPF 2015)* (2015), 1510.05708, URL https://inspirehep.net/record/1399048/files/arXiv:1510.05708.pdf.

[216] E. Kearns *et al.* (Hyper-Kamiokande Working Group), in *Community Summer Study 2013: Snowmass on the Mississippi (CSS2013) Minneapolis, MN, USA, July 29-August 6, 2013* (2013), 1309.0184, URL https://inspirehep.net/record/1252067/files/arXiv:1309.0184.pdf.

[217] A. Donini, M. Lusignoli, and D. Meloni, Nucl.Phys. **B624**, 405 (2002), hep-ph/0107231.

[218] A. Dighe and S. Ray, Phys.Rev. **D76**, 113001 (2007), 0709.0383.

[219] A. Donini, K.-i. Fuki, J. Lopez-Pavon, D. Meloni, and O. Yasuda, JHEP **0908**, 041 (2009), 0812.3703.

[220] O. Yasuda, in *Physics beyond the standard models of particles, cosmology and astrophysics. Proceedings, 5th International Conference, Beyond 2010, Cape Town, South Africa, February 1-6, 2010* (2011), pp. 300–313, 1004.2388, URL http://inspirehep.net/record/851933/files/arXiv:1004.2388.pdf.

[221] D. Meloni, J. Tang, and W. Winter, Phys.Rev. **D82**, 093008 (2010), 1007.2419.

[222] N. Klop and A. Palazzo, Phys. Rev. **D91**(7), 073017 (2015), 1412.7524.

[223] K. Abe *et al.* (T2K), Phys. Rev. Lett. **112**, 061802 (2014), 1311.4750.

[224] B. Bhattacharya, A. M. Thalapillil, and C. E. Wagner, Phys.Rev. **D85**, 073004 (2012), 1111.4225.

[225] D. Hollander and I. Mocioiu, Phys.Rev. **D91**(1), 013002 (2015), 1408.1749.

[226] J. M. Berryman, A. de Gouvêa, K. J. Kelly, and A. Kobach, Phys. Rev. **D92**(7), 073012 (2015), 1507.03986.

[227] S. K. Agarwalla, S. S. Chatterjee, A. Dasgupta, and A. Palazzo, JHEP **02**, 111 (2016), 1601.05995.

[228] S. K. Agarwalla, S. S. Chatterjee, and A. Palazzo, JHEP **09**, 016 (2016), 1603.03759.

[229] J. Kopp, Sterile neutrinos and non-standard neutrino interactions in GLoBES, November 2010. https://www.mpi-hd.mpg.de/personalhomes/globes/tools/snu-1.0.pdf (2010).

[230] F. Capozzi, G. Fogli, E. Lisi, A. Marrone, D. Montanino, *et al.*, Phys.Rev. **D89**(9), 093018 (2014), 1312.2878.

[231] D. V. Forero, M. Tortola, and J. W. F. Valle, Phys. Rev. **D90**(9), 093006 (2014), 1405.7540.

[232] A. Esmaili, E. Kemp, O. Peres, and Z. Tabrizi, Phys.Rev. **D88**, 073012 (2013), 1308.6218.

[233] F. P. An *et al.* (Daya Bay), Phys. Rev. Lett. **113**, 141802 (2014), 1407.7259.

[234] P. Adamson *et al.* (MINOS), Phys. Rev. Lett. **107**, 011802 (2011), 1104.3922.

[235] B. Jones, *Results of the Search for Sterile Neutrinos with IceCube*, talk at FermiLab, February 12, 2016. "https://hep.uchicago.edu/seminars/semwin2016/BenJones1.pdf" (2016).

[236] L. Camilleri, AIP Conference Proceedings **1680**, 020004 (2015), URL http://scitation.aip.org/content/aip/proceeding/aipcp/10.1063/1.4931863.

[237] S. M. Bilenky, N. P. Nedelcheva, and S. T. Petcov, Nucl. Phys. **B247**, 61 (1984).

[238] J. Arafune, M. Koike, and J. Sato, Phys. Rev. **D56**, 3093 (1997), [Erratum: Phys. Rev.D60,119905(1999)], hep-ph/9703351.

[239] A. Datta, R. Gandhi, P. Mehta, and S. U. Sankar, Physics Letters B **597**(3âĂŞ4), 356 (2004).

[240] A. Chatterjee, R. Gandhi, and J. Singh, JHEP **1406**, 045 (2014), 1402.6265.

[241] M. Masud, A. Chatterjee, and P. Mehta, J. Phys. **G43**(9), 095005 (2016), 1510.08261.

[242] P. Coloma, JHEP **03**, 016 (2016), 1511.06357.

[243] A. de Gouvêa and K. J. Kelly, Nucl. Phys. **B908**, 318 (2016), 1511.05562.

[244] D. V. Forero and P. Huber, Phys. Rev. Lett. **117**(3), 031801 (2016), 1601.03736.

[245] J. Liao, D. Marfatia, and K. Whisnant, Phys. Rev. **D93**(9), 093016 (2016), 1601.00927.

[246] K. Huitu, T. J. Kärkkäinen, J. Maalampi, and S. Vihonen, Phys. Rev. **D93**(5), 053016 (2016), 1601.07730.

[247] P. Bakhti and Y. Farzan, JHEP **07**, 109 (2016), 1602.07099.

[248] M. Masud and P. Mehta, Phys. Rev. **D94**, 013014 (2016), 1603.01380.

[249] A. Rashed and A. Datta (2016), 1603.09031.

[250] P. Coloma and T. Schwetz, Phys. Rev. **D94**(5), 055005 (2016), 1604.05772.

[251] A. de Gouvea and K. J. Kelly (2016), 1605.09376.

[252] M. Masud and P. Mehta, Phys. Rev. **D94**(5), 053007 (2016), 1606.05662.

[253] M. Blennow, S. Choubey, T. Ohlsson, D. Pramanik, and S. K. Raut, JHEP **08**, 090 (2016), 1606.08851.

[254] M. C. Gonzalez-Garcia, Y. Grossman, A. Gusso, and Y. Nir, Phys. Rev. **D64**, 096006 (2001), hep-ph/0105159.

[255] J. Kopp, M. Lindner, T. Ota, and J. Sato, Phys.Rev. **D77**, 013007 (2008), 0708.0152.

[256] H. Minakata, in *Fourth NO-VE International Workshop on Neutrino Oscillations in Venice : Ten years after the neutrino oscillations!! : Venezia, April 15-18, 2008, Istituto Veneto di Scienze, Lettere ed Arti, Campo Santo Stefano* (2008), pp. 361–380, 0805.2435, URL http://inspirehep.net/record/785901/files/arXiv:0805.2435.pdf.

[257] Y. Farzan, Phys. Lett. **B748**, 311 (2015), 1505.06906.

[258] S. M. Bilenky and C. Giunti, Phys. Lett. **B300**, 137 (1993), hep-ph/9211269.

[259] D. Meloni, T. Ohlsson, W. Winter, and H. Zhang, JHEP **04**, 041 (2010), 0912.2735.

[260] P. Langacker and D. London, Phys. Rev. **D38**, 907 (1988).

[261] T. Ohlsson, Rept. Prog. Phys. **76**, 044201 (2013), 1209.2710.

[262] J. W. F. Valle, Phys. Lett. **B199**, 432 (1987).

[263] E. Roulet, Phys. Rev. **D44**, 935 (1991).

[264] D. Meloni, T. Ohlsson, and H. Zhang, JHEP **04**, 033 (2009), 0901.1784.

[265] C. Biggio, M. Blennow, and E. Fernandez-Martinez, JHEP **0908**, 090 (2009), 0907.0097.

[266] J. Kopp, P. A. Machado, and S. J. Parke, Phys.Rev. **D82**, 113002 (2010), 1009.0014.

[267] S. Choubey, A. Ghosh, T. Ohlsson, and D. Tiwari, JHEP **12**, 126 (2015), 1507.02211.

[268] K. Kimura, A. Takamura, and H. Yokomakura, Phys. Lett. **B537**, 86 (2002), hep-ph/0203099.

[269] T. Kikuchi, H. Minakata, and S. Uchinami, JHEP **0903**, 114 (2009), 0809.3312.